The PHILOSOPHICAL MAGAZINE

FIRST PUBLISHED IN 1798

L. 45 SEVENTH SERIES No. 367 August 1954

A Journal of Theoretical Experimental and Applied Physics

PRICE 15s. 0d.
Annual Subscription £8 0s. 0d. payable in advance

ED AND PUBLISHED BY TAYLOR & FRANCIS LTD., RED LION COURT, FLEET ST., LONDON, E.C.4.

LXXXVII. *Theory of Dislocations in Germanium*

By W. T. Read, Jr.
Bell Telephone Laboratories*

[Received March 29, 1954]

Abstract

Dislocations have a large effect on the electrical properties of germanium. Experiments show that dislocations act as acceptor centres. This paper discusses a simple model (due to W. Shockley) which identifies dislocation acceptors with the dangling unpaired electrons on the edge of the extra atomic plane of a dislocation having some edge component. In n-type germanium the line of acceptors along a dislocation accepts electrons and becomes negatively charged. The electrostatic energy in the resulting space charge region is found and shown to be a dominant factor in determining the occupation of dislocation acceptors. Formulas are given for the temperature variation of the average electron concentration in n-type material that has been lightly deformed by plastic bending. Experiments are suggested to test the theory and determine exactly the energy level of the dislocation acceptors.

§ 1. Introduction

Dislocations have pronounced effects on the electrical properties of semiconductors. Associated with dislocations are energy states lying in the energy gap. The observations of Gallagher (1952) and Pearson, Read and Morin (1954) on lightly deformed germanium show that the dislocation energy levels are acceptor type ; that is, when dislocations are introduced, by controlled plastic deformation at high temperatures, the number of conduction electrons decreases. Also, the dislocations scatter conduction electrons and thereby reduce the mobility. R. Logan (private communication) has found that even very slight plastic deformation—such as bending into a curvature of one (metre)$^{-1}$—may reduce the lifetime measurably. This paper makes a start toward a quantitative theory of the electrical effects of dislocations in semiconductors and suggests several promising lines of combined experimental-theoretical attack.

It is possible to produce simple and controlled arrays of dislocations by plastic twisting or bending. When the sample is sufficiently well annealed or deformed at sufficiently high temperature that there are no macroscopic internal stresses, then the dislocation array can be predicted from the geometry of the deformation. The etch pits of Vogel, Pfann, Corey and Thomas (1953) provide an experimental tool for knowing accurately the

* Communicated by the Author.

distribution of dislocations. By making measurements both before and after a known array of dislocations have been introduced, the effect of dislocations on mobility, carrier concentration and lifetime can be studied with a high degree of accuracy. Such studies are important not only because dislocations affect the electrical properties of semiconductors, which are of practical importance, but also because the electrical effects of dislocations provide a powerful tool for studying the mechanism of plastic flow. Although it has been recognized since the early 1930's that plastic deformation in crystals takes place by the generation and motion of dislocations, the techniques for investigating dislocations and their role in deformation have been limited, particularly in the case of metals, and the experimental observations (such as stress-strain or creep curves) have been too macroscopic in scale to throw much light on the basic atomic mechanism. In semiconductors, however, the pronounced electrical effects of dislocations provide a powerful tool not available for metals.

Finally the study of dislocations may throw light on the basic structural and electronic properties of semiconductors.

The acceptor centres associated with dislocations differ from other acceptor centres, such as group III impurities or the centres introduced by heat treatment, in that they are not uniformly distributed through the specimen but form a line of acceptors spaced only a few Ångströms apart. As these acceptors accept electrons, the line becomes negatively charged and a space charge region develops around the dislocation. If we imagine that a dislocation is suddenly introduced into n-type material where the Fermi level lies above the energy level of the dislocation acceptors, then the acceptors will begin to fill up. Initially the decrease in the free energy of the system will be proportional to the number of electrons that have dropped from the conduction band into the dislocation-acceptors. The electrostatic energy of the negatively charged line is proportional to the *square* of the number of accepted electrons on the line. Thus eventually the acceptors become filled to a point where the increase in electrostatic energy makes it unfavorable, from the viewpoint of free energy, to add any more electrons to the dislocation. For example, in the 15 ohm cm n-type specimen studied by Pearson, Read and Morin (1954) the dislocation-acceptors appear to be about one-tenth filled at the lowest temperatures (around 10°K). The fraction filled decreases as the temperature increases and is almost unmeasurable at room temperature. The data are consistent with the idea that the dislocation acceptors are a line of discrete acceptors having a single energy lying about 0·2 electron volts below the conduction band. In this paper we treat the electrical properties of dislocations using the model of a dislocation as a row of closely spaced acceptors having a single energy level (rather than a band of levels).

The following is the general plan of the paper: First, the geometry and crystallography of dislocations in the diamond structure is discussed,

and it is shown why dislocations introduce additional energy levels. The space charge and electrostatic energy are calculated. As in the theory of an abrupt p-n junctions, we neglect the carriers inside the space charge region. The statistics of occupation of dislocation energy levels at low temperatures is found by minimizing the energy. Two approximations are discussed for temperatures up to the intrinsic range (above about 300°K in germanium). Finally some experiments are proposed and further theoretical studies outlined.

§ 2. Geometry of Dislocations in the Diamond Structure

Figure 1 (*a*) shows the diamond cubic structure. Plastic deformation occurs by slip on {111} planes. Figure 1 (*b*) shows a dislocation which could have been formed either by slip or in crystallization, but in any case can be visualized as the boundary within the crystal of a slipped area. This dislocation runs in the [01$\bar{1}$] direction and on the (111) plane ; the slip, or Burgers, vector is in the [1$\bar{1}$0] direction. Above the slip plane is a row of atoms that have no neighbours in the plane below. These atoms form the edge of an atomic plane that ends on the slip plane. For each atom that has no neighbour below there is a dangling unpaired electron. Such dangling electrons are believed to be the basis of the electrical effects discussed in the following sections.

In fig. 1 (*b*) the spacing between dangling bonds is equal to the spacing b of neighbouring atoms in a (111) plane ; b is also the lattice translation vector of minimum length. In germanium $b=4$ Å.

We now derive a general expression for the spacing c between dangling bonds as a function of the arbitrary angle α between the dislocation and its Burgers vector. In fig. 1 (*b*) the slip that could form the dislocation takes place between two atomic planes connected by covalent bonds that are normal to those planes ; that is, the slip plane is (111), and [111] bonds connect the atoms on the two sides of the slip plane. Consider rows of atoms parallel to the slip vector. Each row above the slip plane lies *directly* above a row below. When unit slip occurs, the upper row moves over the lower row one interatomic spacing b. At the boundary between slipped and unslipped areas on the slip plane there must be an extra atom in the row on one side of the slip plane. The spacing c between dangling bonds will therefore be the distance between points where the dislocation crosses rows of atoms parallel to the slip vector. Thus c is proportional to cosec α. Since $c=b$ when $\alpha=60°$ (as in fig. 1 (*b*)), we have

$$c=\frac{b \sin 60°}{\sin \alpha}=0{\cdot}866\, b \operatorname{cosec} \alpha. \quad . \quad . \quad . \quad . \quad . \quad (2.1)$$

The spacing c is a minimum for the edge ($\alpha=90°$) orientation, and is infinite (no dangling bonds) for the screw orientation ($\alpha=0$). Equation (2.1) applies only when the dislocation and its slip vector lie in the same {111} plane. This will probably be the case for most of the dislocations formed in plastic deformation. In general it will not be the case for dislocations in low-angle-of-misfit grain boundaries. However, c can

Fig. 1

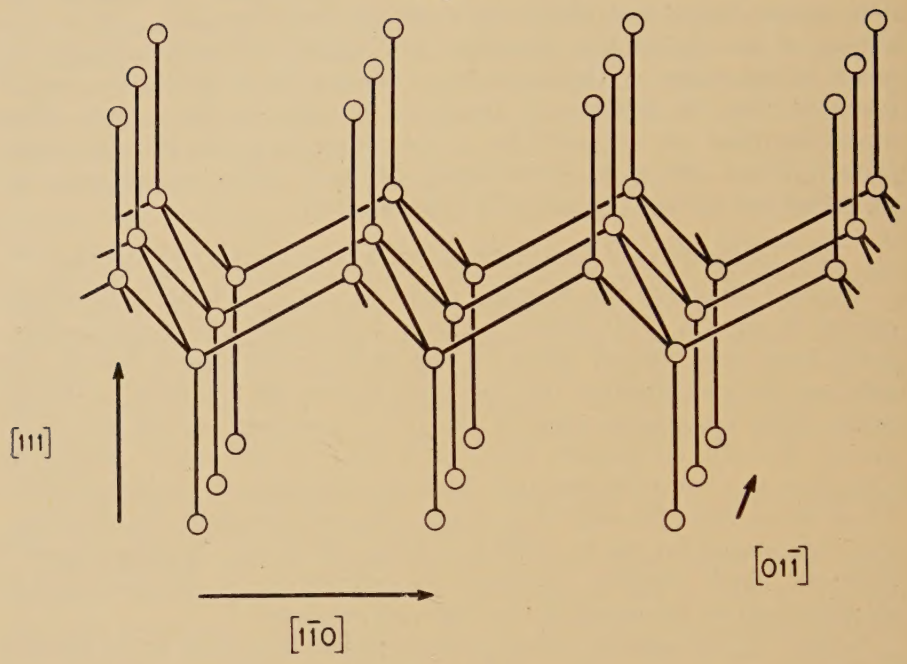

(*a*)

The diamond cubic structure (*after* W. Shockley).

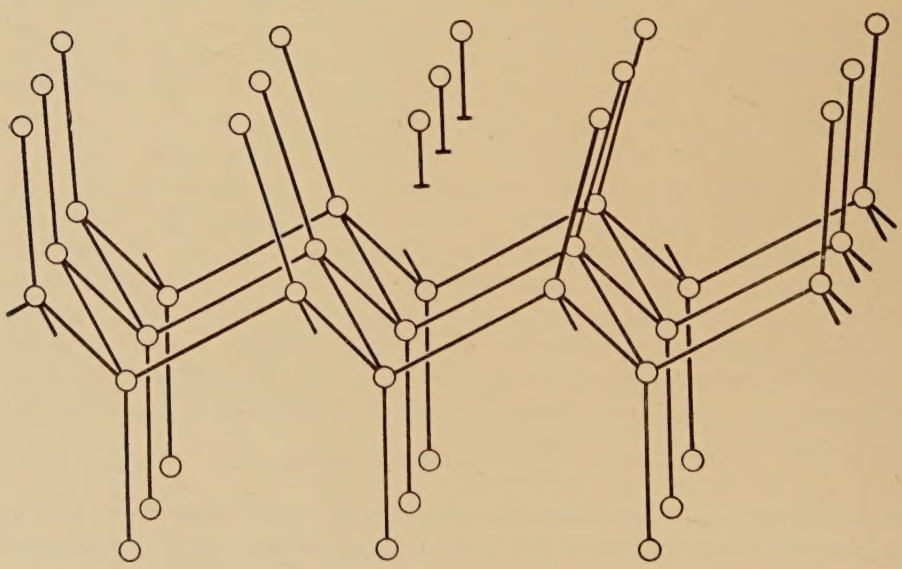

(*b*)

A dislocation lying in a (111) and running at 60° to its slip vector. Note the dangling unpaired electrons (*after* Shockley).

readily be worked out for any particular orientation of the dislocation by the reasoning given above.

In fig. 1 (*b*) the dislocation is formed by slip between the top two atomic planes shown. W. Shockley (1953) has pointed out that the nature of the dislocation would be quite different if slip occurred between the 2nd and 3rd planes, which are connected by three times as many bonds per atom as the 1st and 2nd. In this case the dislocation could reduce its elastic energy by splitting into two partial dislocations connected by a strip of stacking fault, as in the face-centred cubic structure. The two partials and connecting fault are known as an extended dislocation. It seems doubtful, however, whether the lower elastic energy of an extended dislocation could compensate for the fact that in the diamond structure it requires three times as many covalent bonds to be broken. We shall therefore deal with the case illustrated in fig. 1 (*b*), although the analysis will apply with only minor changes to the case of an extended dislocation.

§ 3. Electronic Energy Levels Associated with Dislocations

As mentioned in § 1, experiments show that dislocations in germanium act as acceptor centres. This section gives a simple explanation—due to W. Shockley (1953)—that accounts for the acceptor type behaviour in terms of the dangling bonds discussed in § 2.

The single dangling electrons in fig. 1 (*b*) are unpaired. It is reasonable to expect that an electron paired with one of these dangling electrons would have less energy than a single, free electron in the conduction band. It would, however, probably have more energy than an electron in a complete valence bond. We shall define $\mathscr{E}_2$ as the energy of an electron that has been accepted by the dislocation to form a dangling pair. Then we expect that $\mathscr{E}_2$ lies somewhere in the energy gap. In an n-type sample with the Fermi level above $\mathscr{E}_2$ we would expect the dislocation to accept electrons and the sample to become less n-type. The model also predicts that there will be more acceptor centres per dislocation in a bent specimen, where the dislocations are mainly edge-type, than in a twisted sample, where the dislocations are largely screw-type. Pearson (unpublished) has found this to be the case.

In theory the dislocation could also act as a donor. Let $\mathscr{E}_c - \mathscr{E}_1$ be the energy required for a single dangling electron to jump into the conduction band; then a single dangling electron lies at an energy level $\mathscr{E}_1$. It might be thought that a single unpaired dangling electron would be less tightly bound than a valence electron, so that $\mathscr{E}_1$ would also lie in the energy gap. However, experiments on germanium seem to contradict this. Even with the Fermi level nearly as low as the chemical acceptors there is no evidence of donor-type behaviour. In silicon, with a larger gap, the dislocation donor level might lie in the gap; the question could be studied by measurements on plastically deformed p-type silicon at low temperature.

W. Shockley (1953) has suggested that a line of dangling electrons forms a continuous band of energy levels and that the band is normally half full because the spin of each electron can have either of two values. A consequence of such a view is that dislocations in or near the edge orientation would be highly conducting—the electrons in the half-filled band could be accelerated by an electric field and carry current. There are two sets of experimental data that throw doubt on this idea:

(1) The observations of Gallagher (1952) and of Pearson, Read and Morin (1954) of lightly deformed germanium show that dislocations make a specimen less, rather than more, conducting.

(2) C. S. Smith (unpublished) found that a small-angle-of misfit grain boundary made up of edge dislocations did not have any measurable effect on conductivity. If the dislocations were conducting at all, their conductance was less than 0·01 of the conductance of copper wire extrapolated to a diameter of one atomic diameter.

On the basis of these two lines of experimental evidence we conclude that the picture of a continuous band of states, normally half full, does not apply to germanium. We shall treat a dislocation as a row of acceptor centres, closely spaced but having a single level $\mathscr{E}_2$. The analysis will apply if there are dislocation donor levels provided they are always full, that is not ionized.

We now define some terms that will be used throughout the paper:

An acceptor centre on a dislocation is defined as a *site*. Following Shockley, we think of a site as a dangling bond and calculate the line density of sites from the spacing between dangling bonds. An *empty site*, or unoccupied acceptor, is then identified with a single dangling electron, and a *full site*, or occupied acceptor, is thought of as a dangling double bond, or pair of dangling electrons.

We shall call f the fraction of sites that are full; a fraction $1-f$ are therefore empty.

§ 4. Case of No Space Charge

Section 5 and the following sections will deal with the case where the added electrons on the dislocation are sufficiently closely spaced that the dislocation acts like a charged line and repels other electrons, thus creating a space charge. This section considers briefly the much simpler but probably rather rare case where the spacing between added electrons on a dislocation is no smaller than the average distance between dislocations in the specimen. The charge of the added electrons is then uniform over the volume and there is no space charge. Since dislocations are line imperfections, their density is expressed as a flux density, that is as the number cutting a unit area normal to their direction. If N is the density of dislocations then the volume density of sites N_s is N/c. The fraction f of sites that are full is given by the Fermi function

$$f=\frac{1}{1+\exp\{(\mathscr{E}_2-\mathscr{E}_F)/kT\}}, \quad \ldots\ldots \quad (4.1)$$

where k is Boltzmann's constant ($8{\cdot}63\times10^{-5}$ electron volts per degree), T is the absolute temperature and $\mathscr{E}_F$ is the Fermi level.

Both N_s and $\mathscr{E}_2$ can be determined in a straightforward way by fitting curves of measured carrier concentration vs. T. Measurements should be made both before and after dislocations are introduced by deformation.

To give a uniform volume density of sites the dislocations produced by deformation should be almost pure screw (parallel to their slip vectors) so that c is as large as possible. Plastic twist about the normal to a slip plane would be the deformation most likely to produce dislocations in the screw orientation. However, it seems unlikely that the average angle α between dislocation and slip vector could ever be made small enough in actual samples. For example, suppose we want $N_s=10^{15}$ cm^{-3}. For uniformly spaced sites this requires that c be no smaller than 10^{-5} cm. For small α (2.1) becomes $\alpha=0{\cdot}866\,b/c$. In germanium $b=4$ Å. Thus we need $\alpha<3{\cdot}5\times10^{-3}$ radians, which is probably much too small to be realized in practice.

If the Fermi function (4.1) is used in the standard way to interpret electrical measurements on deformed samples, the results might be quite misleading. For example, a single energy level associated with the dislocation would appear as a continuous distribution of levels. An accurate analysis must consider the space charge around a dislocation that has accepted electrons.

§ 5. Space Charge Around a Dislocation

Let a dislocation be introduced into an n-type sample where the Fermi level lies above the dislocation-acceptor levels. That is, $\mathscr{E}_F>\mathscr{E}_2$ when $\mathscr{E}_2$ is measured upward from the top of the valence band and $\mathscr{E}_F$, from the top of the valence band in the normal, electrically neutral, n-type material. The dislocation accepts electrons to form double dangling bonds. Let a be the spacing between added electrons or occupied sites. The fraction of sites that are occupied is $f=c/a$. In this section we consider the case where a is small compared to the mean spacing between chemical donors and acceptors. Then the dislocation will act like a charged line with charge q/a per unit length. The negatively charged line repels conduction electrons and a cylindrical space charge region forms around the dislocation, the average (positive) charge per unit volume in the cylinder being $q(N_d-N_a)$. We can define a radius R such that a cylinder of radius R contains an amount of fixed poitive charge equal to the negative charge on the dislocation. Then R is defined in terms of a by

$$\pi R^2(N_d-N_a)=1/a=f/c. \quad . \quad . \quad . \quad . \quad . \quad . \quad (5.1)$$

Near the absolute zero of temperature, where there are no carriers, the negative charge on the dislocation is neutralized entirely by the fixed charge $q(N_d-N_a)$ of the ions. (In the space charge region the impurities are ionized at all temperatures.) Therefore the boundary of the space charge cylinder is sharp and its radius is R. That is, inside

of the cylinder the space charge density is $q(N_d - N_a)$ and outside the cylinder the space charge is zero. As the temperature is raised and the impurities become fully ionized, the boundary of the space charge cylinder becomes smeared out. The net charge density

$$\rho = q(N_d - N_a - \mathrm{n} + \mathrm{p}) \quad . \quad . \quad . \quad . \quad . \quad . \quad (5.2)$$

varies from zero well away from the dislocation to $q(N_d - N_a)$ close to the dislocation. It may also happen that very close to the dislocation there is a small cylinder of p-type material. *The following sections will deal with the case where the contribution of the carriers to space charge is negligible*—as will always be the case at low enough temperatures. It is hoped to treat the more general case in a later paper.

Inside the space charge region the electrostatic potential decreases (electrostatic energy of an electron increases) in going toward the dislocation. When the carrier charge is negligible and R is large compared to a, we can regard the potential ψ as that due to a continuous line charge lying along the axis of a cylinder of uniformly distributed poitive charge and we have

$$\psi = \frac{-q^2}{\kappa a}\left[\ln \frac{R^2}{r^2} + 1 - \frac{r^2}{R^2}\right], \quad . \quad . \quad . \quad . \quad . \quad (5.3)$$

where $a < r \leqslant R$ is distance from the dislocation and κ is the dielectric constant. Outside of the space charge cylinder $\psi = 0$. The equation is exact only when r is large compared to a. For r smaller than a it is necessary to take account of the discrete nature of the charges on the line. For $r \to 0$ the formula gives $\psi \to -\infty$. In the Appendix we find the electrostatic energy taking into account the discrete nature of the charges on the dislocation.

The following section finds f at the absolute zero of temperature in terms of the electrostatic energy.

§ 6. Absolute Zero of Temperature

This section illustrates the general method of finding f by minimizing the free energy. At $T = 0°\mathrm{K}$ the analysis is simplified by the fact that free energy is equal to energy.

Let $\mathscr{E}_2$ be measured upward from the top of the valence band *at the dislocation*. (The top of the valence band $\mathscr{E}_v$ will vary with the electrostatic potential in the space charge region.) Let $\mathscr{E}_\mathrm{F}$ be measured upward from the top of the valence band *in the normal n-type material*. Thus both $\mathscr{E}_2$ and $\mathscr{E}_\mathrm{F}$ are constants for a given material and temperature and are *not* functions of position. The situation is illustrated in fig. 2. The fact that the Fermi level is shown lying above the dislocation acceptor level does not necessarily mean that $f > 1/2$ since, as we shall see later, Fermi statistics does not govern the occupation of the closely spaced line of acceptors on a dislocation except when f is very low—of the order of 10^{-4} or 10^{-5} in typical cases.

If we imagine that the dislocation is suddenly introduced into a sample with $\mathscr{E}_F > \mathscr{E}_2$, then the conduction electrons will begin to drop into the empty sites on the dislocation. As the sites fill, the potential energy of an electron on the dislocation rises and the total electrostatic energy increases until nothing is gained energywise by transferring electrons from the normal n-type material to the dislocation. Define $\mathscr{E}_s = \mathscr{E}_s(f)$ as the electrostatic energy per added electron. The Appendix derives $\mathscr{E}_s$ as a function of f. $\mathscr{E}_s$ is the total work done in forming the space

Fig. 2

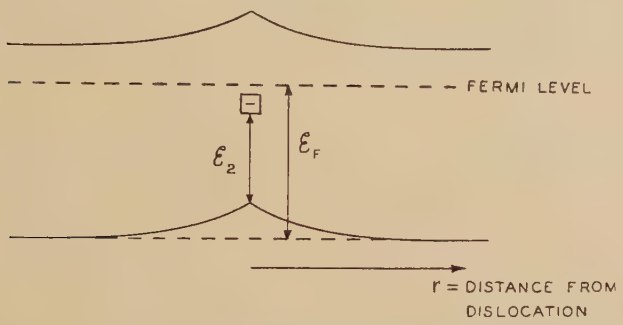

Variation of energy bands with distance r from the dislocation and the meaning of $\mathscr{E}_2$ and $\mathscr{E}_F$.

charge cylinder with the line of evenly spaced electrons along its axis starting with normal (electrically neutral) n-type material. Each electron on the dislocation comes from the normal n-type material, where the free energy per electron is $\mathscr{E}_F$ (by definition of $\mathscr{E}_F$). Let F be the total increase in free energy of the system (due to the presence of the dislocation) divided by the number of electrons on the dislocation. Then

$$F(f) = \mathscr{E}_2 - \mathscr{E}_F + \mathscr{E}_s(f). \quad . \quad . \quad . \quad . \quad . \quad . \quad (6.1)$$

We now find an expression for f by minimizing the energy per unit length or per site. For a given f the minimum energy configuration is the one in which the added electrons are evenly spaced. Thus $\mathscr{E}_s$ refers to the configuration of constant spacing $a = c/f$ between added electrons. The free energy per site is fF,

$$fF(f) = f[\mathscr{E}_2 - \mathscr{E}_F + \mathscr{E}_s(f)]. \quad . \quad . \quad . \quad . \quad . \quad (6.2)$$

Minimizing fF with respect to f, we have

$$\mathscr{E}_F - \mathscr{E}_2 = \mathscr{E}^*(f), \quad . \quad . \quad . \quad . \quad . \quad . \quad . \quad (6.3)$$

where

$$\mathscr{E}^* = \frac{d}{df} f\mathscr{E}_s(f). \quad . \quad . \quad . \quad . \quad . \quad . \quad . \quad (6.4)$$

Thus when the temperature $T = 0$ we can find f if we know $\mathscr{E}_s$ as a function of f. It will turn out that eqn. (6.3) may be a good approximation not only at low temperature but almost up to the intrinsic range.

As the temperature T increases the Fermi level $\mathscr{E}_F$ drops; therefore $\mathscr{E}^*(f)$ must drop as T increases. We shall find that $\mathscr{E}^*$ is a monotonically increasing function of f. Thus f decreases as T increases, as would be expected.

§ 7. Electrostatic Energy and $\mathscr{E}^*$

Formula for $\mathscr{E}_s(f)$

The Appendix derives $\mathscr{E}_s$ as a function of f for a given arbitrary material and orientation of the dislocation. $\mathscr{E}_s$ is the work done per added electron in forming the space charge distribution starting with electrically neutral n-type material. $\mathscr{E}_s$ includes the energy of the electrons and the energy stored in the surrounding field of positive charge. The formula

$$\mathscr{E}_s=\frac{q^2}{\kappa a}\left(\ln\frac{R}{a}-0{\cdot}866\right), \quad . \quad . \quad . \quad . \quad . \quad . \quad . \quad (7.1)$$

derived in the Appendix, is seen to be physically reasonable. It is convenient to define the parameters

$$\left.\begin{aligned}\mathscr{E}_0&=q^2/\kappa c,\\ f_c&=c\sqrt[3]{\{\pi(N_d-N_a)\}}.\end{aligned}\right\} \quad . \quad . \quad . \quad . \quad . \quad . \quad . \quad (7.2)$$

Then $\mathscr{E}_s(f)$ can be written in the form

$$\mathscr{E}_s=f\mathscr{E}_0\left(\frac{3}{2}\ln\frac{f}{f_c}-0{\cdot}866\right). \quad . \quad . \quad . \quad . \quad . \quad . \quad (7.3)$$

$\mathscr{E}_0$ is the energy of interaction of two electrons in adjacent sites. For germanium, with dielectric constant $\kappa=16$, $\mathscr{E}_0=0{\cdot}90/c$, where $\mathscr{E}_0$ is in electron volts and c is in Ångströms. The parameter f_c is so defined that $R=a$ when $f=f_c$. When $f=f_c/\sqrt[3]{\pi}=0{\cdot}68f_c$ the spacing a between charges on the dislocation equals the mean spacing $L=(N_d-N_a)^{-1/3}$ between excess donors.

Limitations of the Formula at Small f

The following two assumptions made in deriving eqn (7.3) limit the range of its validity to values of f that are not too small:

(1) The radius R of the space charge cylinder is assumed to be large compared to a. From the neutrality condition (eqn 5.1), $f=\pi R^2c(N_d-N_a)$ and the definition of f_c we have

$$R/a=(f/f_c)^{3/2}. \quad . \quad . \quad . \quad . \quad . \quad . \quad . \quad . \quad . \quad (7.4)$$

Thus the formula for $\mathscr{E}_s(f)$ is valid only when f is large compared to f_c. In this range $\mathscr{E}_s(f)$ is positive and increases monotonically with f.

(2) The positive space charge is assumed to be uniformly distributed. This will become exact as R becomes large compared to the mean spacing L between excess donors. Again using the neutrality condition, we have

$$R/L=\sqrt{(fL/\pi c)}. \quad . \quad . \quad . \quad . \quad . \quad . \quad . \quad . \quad (7.5)$$

This assumption is usually more stringent than (2). However, we can probably come closer to violating it without serious error in $\mathscr{E}_s$.

$\mathscr{E}^*$ *and its Physical Meaning*

In the range where (7.3) is valid, $\mathscr{E}_s$ is roughly a linear function of f (since the ln term changes relatively slowly). Therefore the electrostatic energy $f\mathscr{E}_s$ per site varies roughly as f^2; so $\mathscr{E}^*=(d/df)f\mathscr{E}_s$ has the same form as $\mathscr{E}_s$. From (7.3)

$$\mathscr{E}^*=\mathscr{E}_0 f[3\ln(f/f_c)-0{\cdot}232]. \quad . \quad . \quad . \quad . \quad . \quad (7.6)$$

Figure 3 is a plot of $\mathscr{E}^*$ vs. f for the dislocation shown in fig. 1 (*b*) in germanium with $N_d-N_a=10^{15}$ cm^{-3}, which corresponds to about

Fig. 3

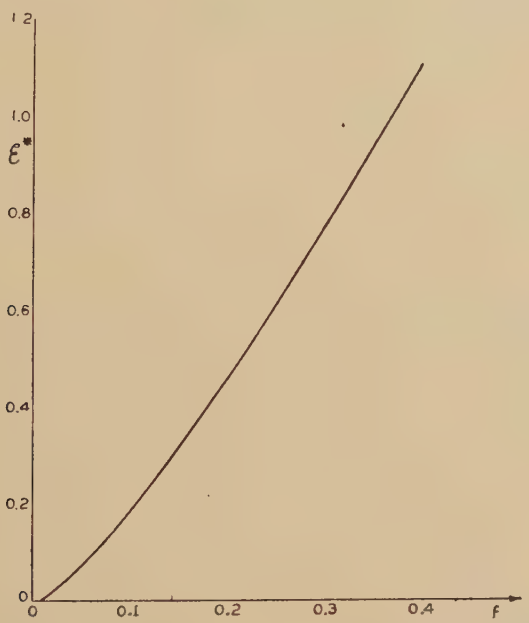

Variation of $\mathscr{E}^*$ with f for $N_d-N_a=10^{15}$ cm^{-3} and the dislocation shown in fig. 1 (*b*) in germanium.

1·7 ohm cm at room temperature. In fig. 1 (*b*), $c=b=$interatomic spacing in a ⟨110⟩ direction, which in germanium is 4 Å. Thus

$$f_c=4\times\pi^{1/3}\times10^{-3}=0{\cdot}00586 \qquad \text{and} \qquad \mathscr{E}_0=0{\cdot}255 \text{ ev.}$$

To bring out the physical meaning of $\mathscr{E}^*$ let us compare it with $-q\psi_0$, where ψ_0 is the potential at an electron due to the other electrons and the positive space charge. From eqn. (A.12) of the Appendix

$$-q\psi_0=\mathscr{E}_0 f[3\ln(f/f_c)-1{\cdot}232]. \quad . \quad . \quad . \quad . \quad . \quad (7)$$

$\mathscr{E}^*$ exceeds $-q\psi_0$ by $\mathscr{E}_0 f=$energy of interaction of neighbouring added electrons. That $\mathscr{E}^*$ must exceed $-q\psi_0$ by roughly this amount can be shown by the following physical argument.

Consider N electrons in electrostatic equilibrium in a space charge region. Let the total electrostatic energy be $\mathscr{E}_N = N\mathscr{E}_s$, and let the potential at each electron be ψ_0. Remove one electron from the array, keeping the others fixed. By definition of electrostatic potential the work done in removing the electron is $q\psi_0$. In the present case ψ_0 is negative (an electron has a higher energy on the dislocation than in the normal n-type material, where $\psi = 0$). Thus in removing the electron we get a positive amount of work $-q\psi_0$ out of the system. Now the remaining $N-1$ electrons are no longer in electrostatic equilibrium. They want to fill in the gap left by the missing electron and re-establish a uniform spacing. Therefore, by allowing the remaining electrons to relax, we get still more work out of the system. However, the work done by the system when one is removed and the others allowed to relax is

$$\frac{d\mathscr{E}_N}{dN} = \frac{df}{d}(f\mathscr{E}_s) = \mathscr{E}^*.$$

Thus $\mathscr{E}^*$ is greater than $-q\psi_0$. The difference should be of the order of the enegy $f\mathscr{E}_0$ of interactions of neighbouring electrons.

Example

To conclude this section we find f at $T=0$ for the particular example discussed earlier in the section. At $T=0$ the Fermi level in the normal n-type material goes through the energy level $\mathscr{E}_d$ of chemical donors. For P, A_s or S_b donor impurities in germanium $\mathscr{E}_d$ is 0·01 ev below the conduction band. If $\mathscr{E}_c$ is the bottom of the conduction band, we have $\mathscr{E}_F(0) = \mathscr{E}_d = \mathscr{E}_c - 0{\cdot}01$. Thus the relation $\mathscr{E}^*(f) = \mathscr{E}_F(T) - \mathscr{E}_2$ becomes, at $T=0$, $\mathscr{E}^*(f) = (\mathscr{E}_c - \mathscr{E}_2) - 0{\cdot}01$. This, together with the $\mathscr{E}^*$ vs. f curve in fig. 2, gives f for any chosen value of $\mathscr{E}_c - \mathscr{E}_2$. For example, if the dislocation acceptor level lies 0·225 ev below the conduction band, $f = 0{\cdot}11$ at $T=0$. For this case $R = 2820$ Å as compared with $L = 1000$ Å.

§ 8. The Minimum Energy Approximation

This section deals with the possibility of extending the formula

$$\mathscr{E}_F(T) - \mathscr{E}_2 = \mathscr{E}^*(f)$$

to higher temperatures. We shall refer to this formula as *the minimum energy approximation*. We first discuss the sources of error for $T>0$ and conclude that the approximation may be good over a range of temperature in which experimental measurements could be made and compared with the theory. The predicted f vs. T relation is discussed and illustrated for a particular example.

In the minimum energy distribution the added electrons are evenly spaced; hence the entropy vanishes, there being only one configuration of even spacing. As the temperature increases some of the electrons acquire enough thermal energy to jump into neighbouring sites, thus

disturbing the even spacing. The non-uniformity has the following two effects on free energy:

(1) Since the even spacing gives minimum energy for a given f, the non-uniformity must raise the energy. We continue to let $\mathscr{E}_s(f)$ refer to the uniform distribution and define $\delta\mathscr{E}_s$ as the average increase in energy per electron. Since $\delta\mathscr{E}_s$ arises from thermal energy it will not be greater than the order of $\boldsymbol{k}T$ and can be neglected for $\mathscr{E}_s \gg \boldsymbol{k}T$.

(2) The entropy S per electron vanishes for the uniform distribution, which can be realized in only one way. A statistically specified non-uniform distribution, however, can be realized in a number of ways. The greater the departures from uniformity, the greater the entropy S. At low temperatures, where $\boldsymbol{k}T$ is small compared to the energy $f\mathscr{E}_0$ of interaction of neighbouring electrons, thermal energy will not be able to overcome the strong coulomb forces between electrons that tend to maintain the uniform spacing. For $f=0{\cdot}11$, as in the example in § 9, the spacing between electrons is only 36 Å, which corresponds to $f\mathscr{E}_0=0{\cdot}025$ ev.

The total change in free energy per electron due to the non-uniformity is $\delta\mathscr{E}_s - TS$. Since both terms are positive they tend to cancel. However, the entropy term will always be at least a little larger, since the value of $\delta\mathscr{E}_s - TS$ will be such as to minimize the free energy. Thus the minimum energy approximation overestimates the free energy. It will be a good approximation at low temperatures and will become increasingly bad as $f\mathscr{E}_0$ becomes comparable to $\boldsymbol{k}T$. Section 9 will discuss an approximation that underestimates the free energy by neglecting $\delta\mathscr{E}_s$ and representing S by an upper limit that becomes an increasingly good approximation at higher temperature.

We now consider the f vs. T relation as given by the minimum energy approximation

$$\mathscr{E}_F(T) - \mathscr{E}_2 = \mathscr{E}^*(f). \quad . \quad . \quad . \quad . \quad . \quad . \quad (8.1)$$

We have already found $\mathscr{E}^*(f)$. $\mathscr{E}_F(T)$ can be calculated for given values of N_d and N_a. In the saturation range, where the donors and acceptors are completely ionized, $\mathscr{E}_F(T)$ depends only on the difference $N_d - N_a$ and is given by the simple relation†

$$\mathscr{E}_c - \mathscr{E}_F = \boldsymbol{k}T \ln\{N_c/(N_d - N_a)\}, \quad . \quad . \quad . \quad . \quad . \quad (8.2)$$

where

$$N_c = 4{\cdot}82 \times 10^{15} T^{3/2}, \quad . \quad . \quad . \quad . \quad . \quad . \quad (8.3)$$

is the effective number of states per cm³ in the conduction band. In typical germanium crystals (8.2) is a good approximation down to about 50°K. At lower temperatures, where the impurities are partially ionized, we replace $N_d - N_a$ in (8.2) by the density $n < N_d - N_a$ of conduction electrons in the normal n-type material; n depends on both $N_d - N_a$

† Formulas (8·2) to (8·4) are derived in *Electrons and Holes in Semiconductors* by W. Shockley (New York: D. Van Nostrand Co., 1950), Chap. 16.

and N_a, and is not given by a simple expression. However, in the bound range, where most of the impurities are *not* ionized and $n \ll N_d - N_a$, $\mathscr{E}_F$ again has a simple form:

$$\mathscr{E}_F'(T) = \mathscr{E}_d + \boldsymbol{k}T \ln \{(N_d - N_a)/N_a\}. \quad . \quad . \quad . \quad . \quad (8.4)$$

Figure 4 is a plot of $\mathscr{E}_c - \mathscr{E}_F$ from 0° to 300°K for the case

$$N_d - N_a = N_a = 10^{15} \text{ cm}^{-3} \quad \text{and} \quad \mathscr{E}_c - \mathscr{E}_d = 0{\cdot}01 \text{ ev}.$$

From the known functions $\mathscr{E}^*(f)$ and $\mathscr{E}_F(T)$ we can find the f vs. T curve for any value of $\mathscr{E}_2$. The lower (minimum energy) curve in fig. 5 is a plot of f vs. T for the dislocation shown in fig. 1 (b) in germanium with $N_d - N_a = N_a = 10^{15}$ and $\mathscr{E}_c - \mathscr{E}_2 = 0{\cdot}225$ ev.

Above about 50°K, and also at $T=0$, the curve depends only on the difference $N_d - N_a$. The effect of the actual values of N_d and N_a can be illustrated by the slope at the origin. From (8.1)

$$\frac{df}{dT} = \frac{d\mathscr{E}_F/dT}{d\mathscr{E}^*/df}.$$

Using (8.4), which holds near $T=0$, and (7.4),

$$\frac{df}{dT} = \frac{\boldsymbol{k} \ln \{(N_d - N_a)/N_a\}}{\{(\mathscr{E}^*/f) + 3\mathscr{E}_0\}}. \quad . \quad . \quad . \quad . \quad . \quad . \quad . \quad (8.5)$$

Thus throughout the bound range, where (8.4) is valid, the f vs. T curve slopes up if $N_d > 2N_a$ and down if $N_d < 2N_a$. In figs. 4 and 5 we have taken $N_d = 2N_a$ so that $\mathscr{E}_F$ vs. T and the f vs. T curves are flat in the bound range.

The high temperature (low f) range of the f vs. T curve in fig. 5 is inaccurate. The effect of non-uniformity on free energy becomes significant when $f\mathscr{E}_0$ is near $\boldsymbol{k}T$; also the whole calculation becomes meaningless when f becomes comparable to f_c.

Curves similar to the one in fig. 5 can readily be constructed for other values of $\mathscr{E}_2$. As $\mathscr{E}_2$ increases, the f vs. T curves move up and approach $f=0$ at higher temperatures. The curves, however, will not be accurate in the intrinsic range (above about 300°K in germanium), where the hole concentration becomes comparable to the electron concentration and both become large compared to $N_d - N_a$. Even below the intrinsic range the hole concentration near the dislocation may begin to affect the space charge if $\mathscr{E}_2$ is below the middle of the gap. The potential near a line of charges varies so rapidly that a quantum mechanical calculation is required to find the carrier concentrations; the classical Boltzmann expression does not hold.

§ 9. Fermi Statistics

This section derives another approximate f vs. T relation by minimizing the free energy $fF(f)$ per site. In the preceding section F was approximated by an upper limit (the minimum energy for given f). Now we

Fig. 4

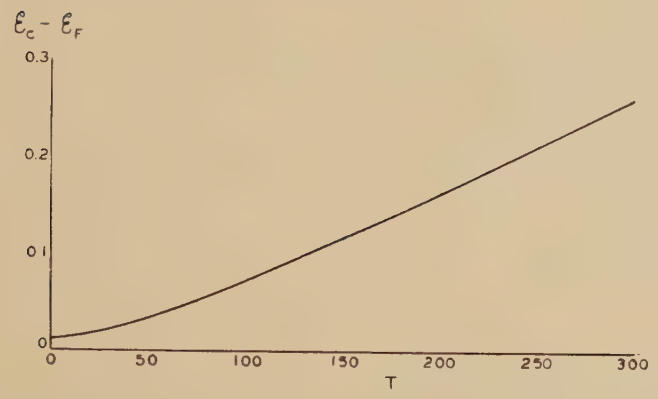

Variation of $\mathscr{E}_C - \mathscr{E}_F$ with T for $N_d - N_a = N_a = 10^{15}\,\mathrm{cm}^{-3}$ in germanium.

Fig. 5

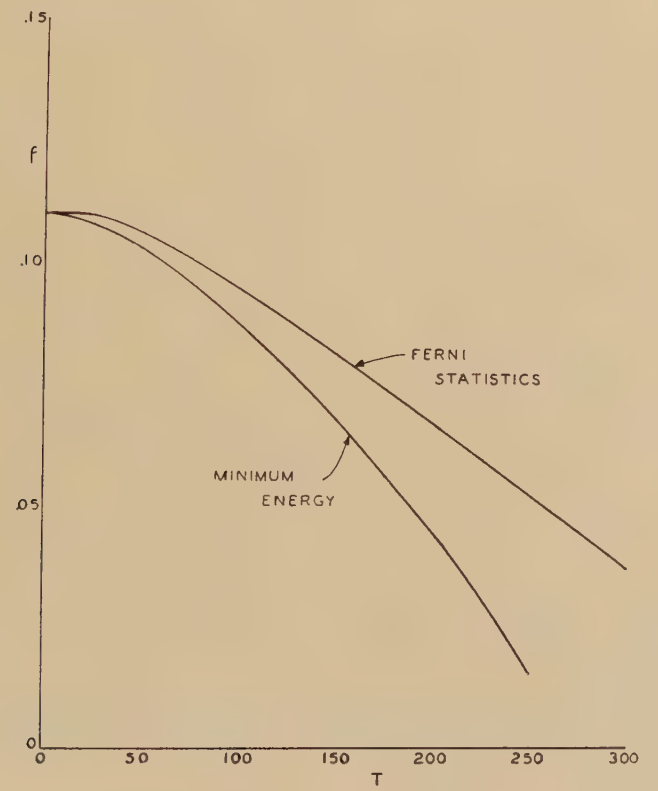

The minimum energy and Fermi approximations to the f vs. T curve. $\mathscr{E}^*$ and $\mathscr{E}_F$ found from figs. 3 and 4.

represent $F(f)$ by a lower limit. The result will be exact at $T=0$ and will be a good approximation at sufficiently high temperature or low f that $f\mathscr{E}_0 \ll \boldsymbol{k}T$.

$\mathscr{E}_s(f)$ is a lower limit on the electrostatic energy. We now find an upper limit for the entropy S per electron. Then $\mathscr{E}_2+\mathscr{E}_s-\mathscr{E}_F-TS$ will be a lower limit for F.

The maximum entropy for N electrons occupying N different sites (out of M possible sites) corresponds to uncorrelated occupation, where the probability of finding an electron in a site is independent of the occupation of neighbouring sites; or, in other words, the energy of the system is the same for all $W=(M!/N!(M-N)!)$ ways of putting N electrons in M sites with no more than one electron per site. This condition forms the basis of Fermi statistics as applied to semiconductors. It is seldom fulfilled exactly in any physical system. For example, if the sites in question were donors uniformly distributed throughout the volume and a fraction f of the donors were charged, that is ionized, then the energy would be a maximum if all the charged donors were in one corner of the sample, and would be a minimum if they were uniformly distributed. However, most of the W ways of filling donors correspond to sufficiently uniform distributions that the energy differs from the minimum by a negligible fraction of $\boldsymbol{k}T$. The added electrons on a dislocation, however, may be only about 30 Å apart. Thus the coulomb forces between electrons are much stronger than is usually the case for charges in semiconductors. When the interaction energy between neighbouring electrons $f\mathscr{E}_0$ is small compared to thermal energy $\boldsymbol{k}T$, then it is reasonable to assume that the electron distribution deviates only slightly from uniformity and the minimum energy approximation is good, as discussed in § 8. However, when $f\mathscr{E}_0 \ll \boldsymbol{k}T$, most of the W ways of arranging N electrons in M sites have approximately the same energy, and Fermi statistics applies.

The entropy *per site* is

$$fS(f)=-(\boldsymbol{k}/M)\ln W=-\boldsymbol{k}[f\ln f+(1-f)\ln(1-f)],$$

which is symmetrical about the maximum, at $f=\frac{1}{2}$, and vanishes at $f=0$ and $f=1$. Adding $-fTS$ to $f(\mathscr{E}_2-\mathscr{E}_F+\mathscr{E}_s)$ and minimizing we have the following equation relating f to T:

$$\mathscr{E}^*(f)=\mathscr{E}_F(T)-\mathscr{E}_2+\boldsymbol{k}T\ln\{1-f/f\}. \quad . \quad . \quad . \quad . \quad (9.1)$$

We have seen that Fermi statistics apply when $f\mathscr{E}_0 \ll \boldsymbol{k}T$. However, as discussed in § 7, $f\mathscr{E}_0$ is the difference between $\mathscr{E}^*$ and $-q\psi$, where ψ is the potential at an electron. Thus, where the formula is valid, we can take $\mathscr{E}_2+\mathscr{E}^*=\mathscr{E}_2-q\psi=\mathscr{E}$=energy of an electron added to the dislocation at a point where the potential is ψ. Now (9.1) becomes the familiar Fermi function

$$f=\frac{1}{1+\exp\{(\mathscr{E}-\mathscr{E}_F)/\boldsymbol{k}T\}}, \quad . \quad . \quad . \quad . \quad . \quad . \quad (9.2)$$

with $\mathscr{E}$ being an explicit function of f: $\mathscr{E}(f)=\mathscr{E}_2-q\psi(f)=\mathscr{E}_2+\mathscr{E}^*(f)$.

We conclude this section by considering the f vs. T relation as given by (9.1). When $f<\frac{1}{2}$, which will usually be the case, the f vs. T curve given by (9.1) will lie above the curve for the minimum energy approximation, which is the lower curve in fig. 5. The upper curve is the Fermi-statistics approximation for the same conditions. In the region where the two curves differ appreciably the correct curve probably lies between the two approximations. Over much of the temperature range $f\mathscr{E}_0$ and $\boldsymbol{k}T$ are comparable; so neither approximation is accurate. However, the two curves together give a picture of the f vs. T relation, which could be compared with experimental data to see whether the basic ideas of the theory are sound. The following section discusses possible experimental measurements and their interpretation.

§ 10. Further Theoretical and Experimental Studies

This section outlines a number of the remaining problems and suggests experimental and theoretical attacks.

Simple Plastic Bending

The simplest case to study both experimentally and theoretically is an array of parallel dislocations. This array can be produced by plastic deformation in pure bending as reported by Gallagher (1952) and Pearson, Read and Morin (1954). Nye (1953) and Read (1953, p. 39) give general formulas for finding the array of dislocations for any specified case of plastic deformation where the specimen is free of macroscopic internal stress, that is, where the average internal stress vanishes over any element of volume containing many dislocations. For simple bending all the dislocations are parallel to the axis of bending, and the resultant Burgers (or slip) vector of all the dislocations is normal to the planes that (1) contain the axis of bending and (2) remain plane during bending. The sum of the slip vectors of all the dislocations that cut unit area normal to the axis of bending is equal to the curvature. In the simple case where the dislocations are all alike, the density of dislocations per cm^2 is $N=K/b$, where K is the curvature in cm^{-1} and b the slip distance. In general there are several sets of parallel dislocations, each set corresponding to a favorably oriented slip system.

Conductivity Parallel to Dislocations

When the dislocations are all parallel we would expect the electrical conductivity to be highly anisotropic, with maximum conductivity parallel to the dislocations and minimum conductivity at right angles to the dislocations. The scattering due to dislocations will have a small effect on mobility when the current is flowing parallel to the dislocations, since the dislocations would be relatively ineffective in scattering the component of momentum parallel to their length. Such scattering would not occur at all if the boundary of the space charge cylinder were perfectly smooth. However, because of the discrete nature of the fixed charge, there will be some roughness in the boundary of the space charge.

In other words, the electric field in the space charge region may not be exactly radial near the outer boundary. This would cause some scattering —although, perhaps, a negligible amount—of the current parallel to the dislocations. The mobility parallel to the dislocations could be found from measurement of the Hall angle (with current parallel to the dislocations and normal to the magnetic field and Hall field).

If the only contribution to the conductivity comes from the conduction electrons in the normal n-type material, then the conductivity is $\sigma_n = q\mu_n \langle n \rangle$, where μ_n is the electron mobility and $\langle n \rangle$ is the average conduction electron density in the sample. There are no conduction electrons inside a cylinder of cross-sectional area πR^2 around each dislocation. Thus if there are N dislocations per cm^2, $\langle n \rangle$ is related to the electron concentration n in the normal n-type material by $\langle n \rangle = n(1 - \pi R^2 N)$. Since $\pi R^2 (N_d - N_a) = 1/a = f/c$, we have

$$\langle n \rangle = n\left[1 - \frac{fN}{c(N_d - N_a)}\right]$$

In the general case of simple bending the parallel dislocations will be of several different types—each type, or set, corresponding to a different slip system and having different values of N and c. In this case the number of sites N_s per cm^3 is the sum of the N/c for each set, and

$$\langle n \rangle = n[1 - \{fN_s/(N_d - N_a)\}]. \quad . \quad . \quad . \quad . \quad . \quad (10.1)$$

In the saturation range of temperature, where $n = N_d - N_a$, (10.1) becomes $\langle n \rangle = n - fN_s$. That is, the decrease in the number of conduction electrons is equal to the number of electrons accepted by dislocations. In the range where the donors are not fully ionized, some of the electrons on the dislocations come from non-ionized donors.

If $\sigma_n = q\mu_n \langle n \rangle$ is the only contribution to conductivity and N_s is known from the curvature or the density of etch pits, then f can be found from the measured conductivity σ_n and Hall angle. The Hall angle gives μ_n; so $\langle n \rangle$ can be calculated from σ_n. Then f is found from (10.1). Thus the f vs. T relation can be measured and compared with the theoretical predictions, the parameter $\mathscr{E}_2$ being adjustable.

It is possible that the dislocation itself has an electrical conductivity. As discussed in § 3, there is evidence that single dangling electrons do not conduct. However, it is possible that the added electrons may move along the dislocation and carry current. Their mobility would probably be less than that of a conduction electron in n-type material. If μ_2 is the mobility of an added electron on a dislocation the conductivity due to the dislocations is $\sigma_2 = q\mu_2 f N_s$.

A Crucial Experiment

At low temperatures the conductivity σ_n decreases with decreasing temperature because $\langle n \rangle$ and n decrease and approach zero as the

donors become full. However, σ_2 should be a maximum in the bound range. As we have seen, f is a maximum in the bound range. The mobility μ_2 should also be a maximum in the low temperature range when thermal scattering is small. Thus a crucial experiment would be to measure conductivity vs. temperature for an n-type sample both before and after dislocations have been introduced by deformation. Near room temperature the deformed sample should have a lower conductivity since we expect that $\mu_2<\mu_n$. However, at low enough temperatures the deformed sample should have a higher conductivity. Thus σ_2 could be measured in the range of temperature where it is large compared to σ_n. To measure σ_2 where σ_n is not negligible would be more of a problem.

Mobility Normal to the Dislocations

When the current flows normal to the dislocations, the dislocations will have a large effect on mobility because (1) the conduction electrons are deflected (that is, scattered) by the dislocations; so the mean free time is reduced. (2) Even when the mean free time is not appreciably affected, the mobility may be considerably reduced because the conduction electrons cannot drift in straight lines but have to follow a tortuous path winding between the space charge cylinders. A later paper will deal with both of these effects and will derive the drift mobility for combined dislocation and thermal scattering. The Hall mobility will also be found when the magnetic field is (1) parallel to the dislocations and (2) normal to the dislocations.

Acknowledgments

The author wishes to thank W. Shockley, R. C. Fletcher, W. L. Brown, C. Herring and S. P. Morgan of the Bell Laboratories for valuable discussion. The theoretical analysis was stimulated and guided throughout by the experimental work of G. L. Pearson and F. J. Morin.

APPENDIX

Electrostatic Energy $\mathscr{E}_s$ of Evenly Spaced Electrons

In this Appendix we derive $\mathscr{E}_s=\mathscr{E}_s(f)$ for a row of evenly spaced electrons running along the axis of a cylinder of positive space charge. We shall consider the positive space charge to have a continuous uniform distribution with density $\rho=q(N_d-N_a)$. The radius R of the cylinder is related to the spacing a between electrons by the neutrality condition

$$\pi R^2\rho=q/a. \quad . \quad . \quad . \quad . \quad . \quad . \quad . \quad . \quad . \quad \text{(A.1)}$$

$\mathscr{E}_s$ is the work done per electron in forming the space charge starting with electrically neutral n-type material, for which $\mathscr{E}_s=0$. It is more convenient, however, to start with all the charges at infinite distances from one another, for which $\mathscr{E}_s$ also vanishes. Then, in the final distribution, the total electrostatic energy is

$$\tfrac{1}{2}\Sigma\psi_i q_i$$

where q_i is the charge (in coulombs) of the ith charge and ψ_i, the potential at the ith charge due to all the other charges, is, by Coulomb's law,

$$\psi_i=\Sigma\frac{q_j}{\kappa r_{ij}}$$

where r_{ij} is the distance between the ith and jth charges and the sum is over all j's except $j=i$. In the continuous charge distribution the sums become integrals. We shall find the electrostatic energy $\mathscr{E}_N$ of the electrons and surrounding positive charge for N electrons in the row. $\mathscr{E}_s$ is then the limit of $\mathscr{E}_N/N$ as $N\to\infty$.

The potential ψ varies with distance r from the dislocation and distance z measured along the dislocation. ψ is periodic in z with period a. $\mathscr{E}_s$ is the energy inside of a section of cylinder of length a with an electron at the centre. The potential $\psi=\psi(r, z)$ is the same in all such cylinders except those within a distance of the order of R from the ends. In the limit for a cylinder of infinite length the end effects are negligible.

It will considerably simplify the calculation to set ψ equal to $\psi_e+\psi_c$, where ψ_e is the potential of the row of electrons and ψ_c the potential of the positive space charge. We shall make the calculation for the section of cylinder in the middle of the length aN of the cylinder. The energy and the potential are the same in all cyclinders, but ψ_e and ψ_c have a simpler form in the central section. For example, the field $\nabla\psi_c$ is radial in the central section.

By using the conservation of energy, we can find $\mathscr{E}_s$ without evaluating $\psi_e=\psi_e(r, z)$. Instead we need know only the potential at one electron due to all the other electrons, which is easily found by summation. ψ_c is a function of r only and is found by integrating Poisson's equation. The two potentials ψ_e and ψ_c and the two charge distributions give four terms in the energy $\mathscr{E}_s$. Two terms are self-energies and involve the potentials and corresponding charge distributions; the other two terms involve the potential of one distribution and the charge of the other. We now consider the four terms in order.

$\mathscr{E}_e$ is the energy of interaction per electron of the electrons with one another. It is equal to one-half the electronic charge q times the potential ψ_{e0} at one electron due to the other electrons:

$$\psi_{e0}=-\frac{2q}{\kappa a}\sum_{n=1}^{N/2}\frac{1}{n}.$$

The limit of the sum as $N \to \infty$ is $\ln (N/2)$ plus Euler's constant 0·577. Thus

$$\psi_{e0} = -\frac{2q}{\kappa a}\{\ln (N/2) + 0{\cdot}577\}. \quad . \quad . \quad . \quad . \quad . \quad . \quad (A.2)$$

and

$$\mathscr{E}_e = \frac{q^2}{\kappa a}\{\ln (N/2) + 0{\cdot}577\}. \quad . \quad . \quad . \quad . \quad . \quad . \quad (A.3)$$

We shall find that all four terms in the energy approach $+\infty$ or $-\infty$ as $\ln N$ when N approaches ∞. However, the $\ln N$ terms cancel in the expression for $\mathscr{E}_s$.

$\mathscr{E}_c$ is the energy of the positive space charge alone; that is, both the charge distribution and the potential refer to the positive space charge. Thus

$$\mathscr{E}_c = \frac{a}{2}\int_0^R \rho\psi_c(r) 2\pi r \, dr. \quad . \quad . \quad . \quad . \quad . \quad . \quad (A.4)$$

$\psi_c(r)$ is found by integrating Poisson's equation. For $r \leqslant R$

$$\psi_c(r) = \frac{\pi\rho}{\kappa}(R_0^2 - r^2),$$

where R_0 is a constant of integration determined by the continuity of $\psi_c(r)$ at $r=R$. Outside of the cylinder the potential is the same as if all the charge were concentrated along the axis of the cylinder. Thus for $r \geqslant R$

$$\psi_c(r) = \frac{\pi\rho R^2}{\kappa}\int_{-Na/2}^{Na/2} \frac{dz}{\sqrt{(r^2+z^2)}}$$

$$= \frac{2\pi\rho R^2}{\kappa}\ln\frac{Na}{r}.$$

Joining the two solutions at $r=R$ gives $R_0^2 = R^2[1+2\ln(Na/R)]$, from which

$$\psi_c(r) = \frac{q}{\kappa a}\left[1 + 2\ln\frac{Na}{R} - \frac{r^2}{R^2}\right], \quad . \quad . \quad . \quad . \quad (A.5)$$

where a and R are related by $\pi\rho R^2 a = q$, eqn (A.1), and $r \leqslant R$. Substituting (A.5) in (A.4) and integrating, we have

$$\mathscr{E}_c = \frac{q^2}{\kappa a}\left(\ln\frac{Na}{R} + \frac{1}{4}\right). \quad . \quad . \quad . \quad . \quad . \quad . \quad (A.6)$$

$\mathscr{E}_{ec}$ is the interaction energy of the electrons and the positive charge. The charge distribution is that of the electrons and the potential that of the positive charge. Thus $\mathscr{E}_{ec} = -\frac{1}{2}q\psi_c(0)$. From (A.5) we have

$$\mathscr{E}_{ec} = \frac{-q^2}{2\kappa a}\{1 + 2\ln(Na/R)\}. \quad . \quad . \quad . \quad . \quad . \quad (A.7)$$

$\mathscr{E}_{ee}$ is the other interaction term. It is equal to the integral of $\frac{1}{2}\rho\psi_e(r, z)$ integrated (with respect to both r and z) over a section of the

cylinder of length a in the z direction. We can avoid the laborious calculation and double integration of $\psi_e(r,z)$ by using the relation $\mathscr{E}_{ce}=\mathscr{E}_{ec}$, which follows from the conservation of energy.

$\mathscr{E}_s$ is the total electrostatic energy.

$\mathscr{E}_s=\mathscr{E}_e+\mathscr{E}_c+\mathscr{E}_{ce}+\mathscr{E}_{ec}=\mathscr{E}_e+\mathscr{E}_0+2\mathscr{E}_{ec}$ is found from (A.3), (A.6) and (A.7) and is

$$\mathscr{E}_s=\frac{q^2}{\kappa a}\{\ln(R/a)-0{\cdot}866\}. \quad . \quad . \quad . \quad . \quad . \quad . \quad (A.8)$$

It will be convenient to define a value f_c of f such that $f=f_c$ when $R=a$. From $\pi R^2a(N_d-N_a)=1$ and $af=c$ we have

$$f_c=c\pi^{1/3}(N_d-N_a)^{1/3}. \quad . \quad . \quad . \quad . \quad . \quad . \quad . \quad (A.9)$$

It will also be convenient to define

$$\mathscr{E}_0=q^2/\kappa c. \quad . \quad . \quad . \quad . \quad . \quad . \quad . \quad . \quad (A.10)$$

Then

$$\mathscr{E}_s=f\mathscr{E}_0[\tfrac{3}{2}\ln(f/f_c)-0{\cdot}866], \quad . \quad . \quad . \quad . \quad . \quad . \quad (A.11)$$

which is eqn (7.3) of the text.

We shall also want to know the potential $\psi_0=\psi_{0e}+\psi_c(0)$ at one electron due to the other electrons and the positive space charge. From (A.2) and (A. 5)

$$\psi_0=-\frac{q}{\kappa c}f[3\ln(f/f_c)-1{\cdot}232], \quad . \quad . \quad . \quad . \quad (A.12)$$

from which we have eqn (7.7) of the text.

References

Gallagher, C. J., 1952, *Phys. Rev.*, **88,** 721.

Pearson, G. L., Read, W. T., Jr., and Morin, F. J., 1954, *Phys. Rev.* (in press).

Nye, J. F., 1953, *Acta Metallurgica*, **1,** 153.

Read, W. T., Jr., 1953, *Dislocations in Crystals* (New York: McGraw-Hill).

Shockley, W., 1953, *Phys. Rev.*, **91,** 228.

Vogel, F. L., Pfann, W. G., Corey, H. F., and Thomas, E. E., 1953, *Phys. Rev.*, **90,** 489.

LXXXVIII. *The Lattice Spacings of Dilute Solid Solutions of Zirconium, Niobium, Molybdenum, Rhodium, and Palladium in Ruthenium*

By A. Hellawell and W. Hume-Rothery
Inorganic Chemistry Laboratory, Oxford*

[Received March 29, 1954]

Abstract

Measurements have been made of the lattice spacings of pure ruthenium, and of dilute solid solutions of zirconium, niobium, molybdenum, rhodium, and palladium in ruthenium. In all cases the c lattice spacings and axial ratios of the c.p. hexagonal cell are increased by the formation of a solid solution, and at equiatomic percentages of solute the increases are in the order Rh<Pd<Mo<Nb<Zr. The a lattice spacings are diminished by Zr and Rh, and increased by Pd, Nb, and Mo. With Rh as solute, the increase in c and decrease in a counterbalance so that the mean volume per atom is unaltered, whereas Zr decreases, and Nb and Mo increase the mean volume per atom. The theoretical significance of these results is discussed.

§ 1. Introduction

It is well known that, in the region of Group VIA–VIII, the lattice spacings and some physical properties of the elements of the First Long Period do not follow exactly the same sequences as those in the later Periods. The object of the present work was to measure the distortion of the lattice of ruthenium by the adjacent elements of the Second Long Period, in order to see whether the effects were simply related to the lattice spacings of the solute elements concerned.

§ 2. Experimental

The ruthenium used in the present work was supplied by Messrs. Johnson Matthey and Co. Ltd., and the authors must express their thanks to Mr. A. R. Powell for his interest, and for his help in the preparation of the alloys. The metal was doubly distilled as RuO_4, which by means of pure HCl was converted into $RuCl_3$, and from this the ammine $(NH_4)_2$ $RuCl_5$ was prepared by precipitation with pure ammonium chloride. The ammine was converted into metal by ignition in air, followed by heating at 1200°C in an atmosphere of hydrogen in order

* Communicated by the Authors.

to remove traces of oxygen. The spectrographic report of this ruthenium sponge showed that it was highly pure with gold, silver, copper, manganese, nickel, and palladium as the chief impurities. Some of the sponge was melted on a copper hearth in an argon arc furnace, and a spectrographic test of this material showed that, on the whole, the proportion of the impurity elements was diminished by the melting process, although there was a slight increase in the proportion of copper and silver. The alloys of ruthenium were prepared from sponge metal of the type referrred to above. Apart from this, a small quantity of specially pure 'spectrographic ruthenium' was available for lattice spacing measurements, and is referred to on p. 799, § 3.

The alloys in the form of buttons of from 5–10 g in weight were prepared by Messrs. Johnson Matthey and Co. Ltd., in an argon arc furnace. Each button was melted two or three times, and was then partly homogenized by heating in the arc for about 5 minutes as near to the melting point (2550°C) as was practicable. The resulting ingots were then ground to powder in a tungsten carbide percussion mortar, and the powder was strain annealed for 12 hours at 1050°C in sealed evacuated silica tubes; no change in the quality of the x-ray powder diffraction photographs could be detected between specimens annealed for 6 and 12 hours respectively.

Debye–Scherrer photographs were taken with unfiltered copper Kα radiation in a 19 cm diameter Unicam camera, and the lattice spacings determined by standard extrapolation methods. With this radiation, the six highest angle lines are from reflections with the following indices: ((210) at approximately 58·3° (211), (114), (212), (105), (204)), and ((300) at approximately 80·4°). The occurrence of the (300) reflection at the highest angle enabled the a parameter of the close packed hexagonal structure to be obtained with certainty, and the occurrence of high and low values of l enabled the axial ratio to be determined accurately. The films for pure ruthenium were of the highest quality, and the lattice spacings could be determined to within $\pm 0{\cdot}00003$ kx so far as measurement and extrapolation were concerned. For the alloys, the diffraction lines were not absolutely sharp, but the doublets were clearly resolved down to low angles; and repeat measurements gave results agreeing within $\pm 0{\cdot}00005$ kx. The slightly diffuse nature of the lines increased in the order Rh<Pd<Mo<Nb<Zr, and was due to slight lack of homogenity of the ingots, because the high melting points of the alloys made it impossible to obtain complete uniformity with the apparatus available. It is thought that no appreciable error can have resulted from this source, because the measurements were reproducible, and a chemical analysis was always made of the annealed powder, so that slight variations of composition and lattice spacing would tend to give average values to both sets of figures.

All results in the present paper are expressed in kx units at 25°C and are uncorrected for refractive index. The temperature during an x-ray exposure was followed by a thermometer inside the camera (see Axon,

Poole, Hellawell, and Hume-Rothery 1953), and the results were corrected to 25°C by assuming that the coefficient of expansion of the alloys is the same as that of ruthenium ; the corrections were negligible.

§ 3. Results for Pure Ruthenium

The results obtained for pure ruthenium are summarized in table 1, from which it will be seen that the remelting produced a slight change in the axial ratio, but that the results for the remelted sponge agreed well

Table 1. Results for Pure Ruthenium

a	c	c/a	Notes
2·7000(4)	4·2730(9)	1·5826	Annealed sponge. Mean of two films of the same specimen
2·7003(0)	4·2728(7)	1·5824	Remelted sponge. Mean of values for three specimens
2·7004(3)	4·2730(2)	1·5823	Annealed spectroscopically pure sponge. Mean of values for two specimens

with those for the annealed spectroscopically pure sponge. The above values may be compared with those of Owen, Roberts and Pickup (1937) who obtained $a=2{\cdot}6984(4)$ kx, $c=4{\cdot}2730(5)$ kx, and $c/a=1{\cdot}5335(3)$ for metal described as ' chemically pure '.

In the present paper, the values assumed in drawing the diagrams are $a=2{\cdot}7003$, $c=4{\cdot}2730$, $c/a=1{\cdot}5824$.

§ 4. Discussion

The results obtained for the alloys are summarized in table 2, whilst figs. 1, 2, 3, and 4 show the effects of solutes with composition on the axial ratio c/a, the a and c parameters, and the volume per atom respectively. The last quantity is calculated on the assumption that all the lattice points are occupied.

In all cases the formation of a solid solution is accompanied by an increase in the axial ratio, and this effect decreases continuously on passing from Zr→Nb→Mo→Rh, after which there is an increase on passing to Pd (fig. 1). The c lattice spacing is increased by all the solutes, and the sequence is the same as for the axial ratios (fig. 3). The behaviour of the a spacing is quite different. In spite of the much larger atomic diameter of zirconium, the solution of this element in ruthenium produces

a decrease in the a spacing (fig. 2); although the solubility is less than 1 atomic per cent, the effect is clear, and the a spacings for the 2-phase alloys are less than that of pure ruthenium. In dilute solutions, Nb and Mo produce nearly the same expansion of the a spacing of ruthenium, whilst Rh produces a slight contraction, and Pd a considerable expansion.

Table 2. Results for Ruthenium Alloys

Solute Element	Atomic % Solute	a	c	c/a	Notes
Zr	0·25	2·6999(6)	4·2732(5)	1·5827	
	0·35	2·6999(7)	4·2736(5)	1·5828(5)	
	0·50	2·6994(7)	4·2746(4)	1·5835	2 phase alloy.
	2	2·6995(1)	4·2744(0)	1·5834	Synthetic composition 2 phase alloy
	4	2·6994(5)	4·2745(8)	1·5835	
	6	2·6994(5)	4·2745(8)	1·5835	
Nb	1·15	2·7009(6)	4·2753(6)	1·5829	average of two films
	1·45	2·7016(5)	4·27725	1·5832	
	2·15	2·7021(7)	4·2802(8)	1·5840	
	2·41	2·7031(9)	4·2818(5)	1·5840	
Mo	0·99	2·7014(0)	4·2752(4)	1·5826	
	1·07	2·7011(9)	4·2746(3)	1·5825	
	2·32	2·7023(9)	4·2773(4)	1·5828	
	3·07	2·7032(9)	4·2793(1)	1·5830	
Rh	1·93	2·7003(2)	4·2736(8)	1·5826(5)	average of two films
	3·12	2·7000(5)	4·2736(4)	1·5828	
	5·30	2·6999(3)	4·2739(9)	1·5830	
Pd	1·96	2·70095	4·27590	1·5831	average of two films
	2·05	2·70084	4·27560	1·5831	
	2·52	2·70108	4·27680	1·5834	
	2·61	2·70110	4·27695	1·5834	

The mean volume per atom is equal to 13·498 kx^3, and is diminished by solution of Zr, and unaltered by Rh. Pd increases the mean volume per atom, whilst a larger and roughly equal increase is produced by niobium and molybdenum.

The axial ratio of ruthenium (1·5824) is considerably less than that (1·633) for close-packed spheres, and the distance between the atoms in the basal plane (2·70 kx) is greater than the distance (2·64 kx) between an atom and its nearest neighbour in the plane above or below. This distance (2·64 kx) is the minimum distance of approach between atoms in the crystals of the elements of the Second Long Period, the values for

the adjacent elements being Nb (b.c.cube 2·85 kx), Mo (b.c.cube 2·72 kx), Re (c.p.hex. 2·73, 2·76 kx), Rh (f.c.cube 2·68 kx), Pd (f.c.cube 2·75 kx). It is possible, therefore, that geometrical considerations may to some extent explain the general increase in axial ratio resulting from the

Fig. 1

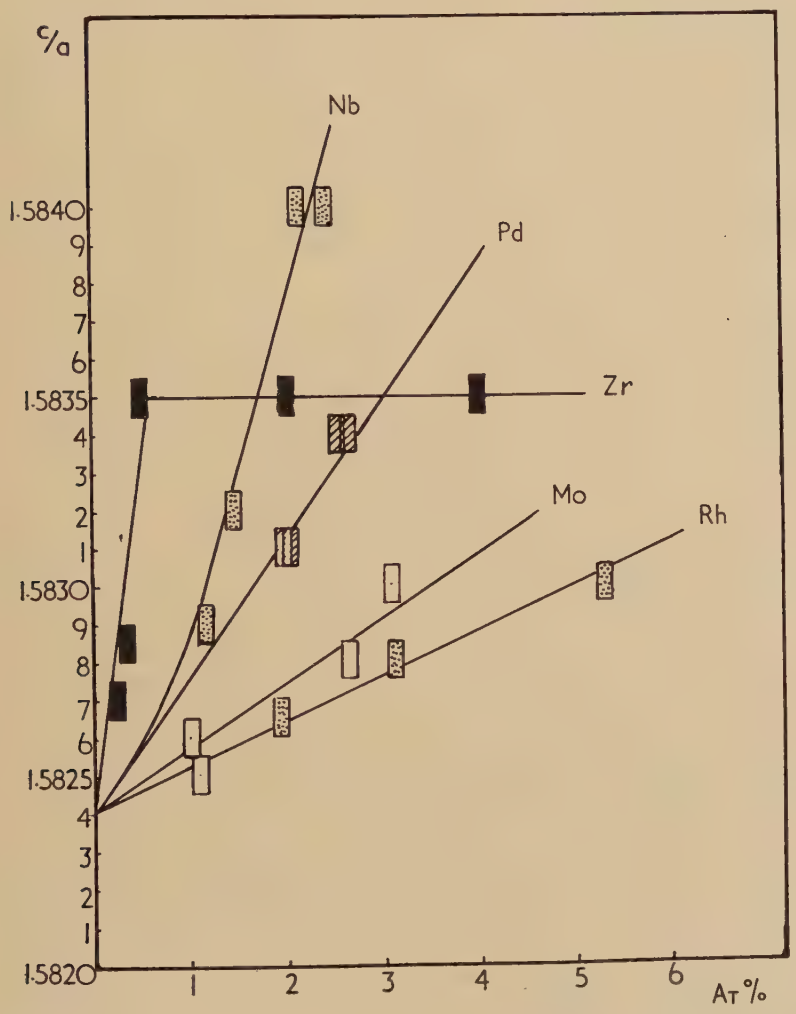

formation of a solid solution. In so far as we are justified in regarding the atoms in a crystal of ruthenium as being held apart by the repulsion resulting from the overlapping electron clouds of the atomic core, it is clear that the structure is one of close-packed spheroids, and not one of close packed spheres. If, therefore, the atomic core of rhodium is spherical and of radius 2·68 kx, as suggested by the interatomic distances in the face-centred cubic metal, an atom of rhodium, when dissolved in

ruthenium, will not be ' in contact ' with ruthenium atoms in its own basal plane (for which the characteristic distance is 2·70 kx), but will displace the nearest neighbours in the planes above and below, whose interatomic distance in pure ruthenium is only 2·64 kx. We can thus

Fig. 2

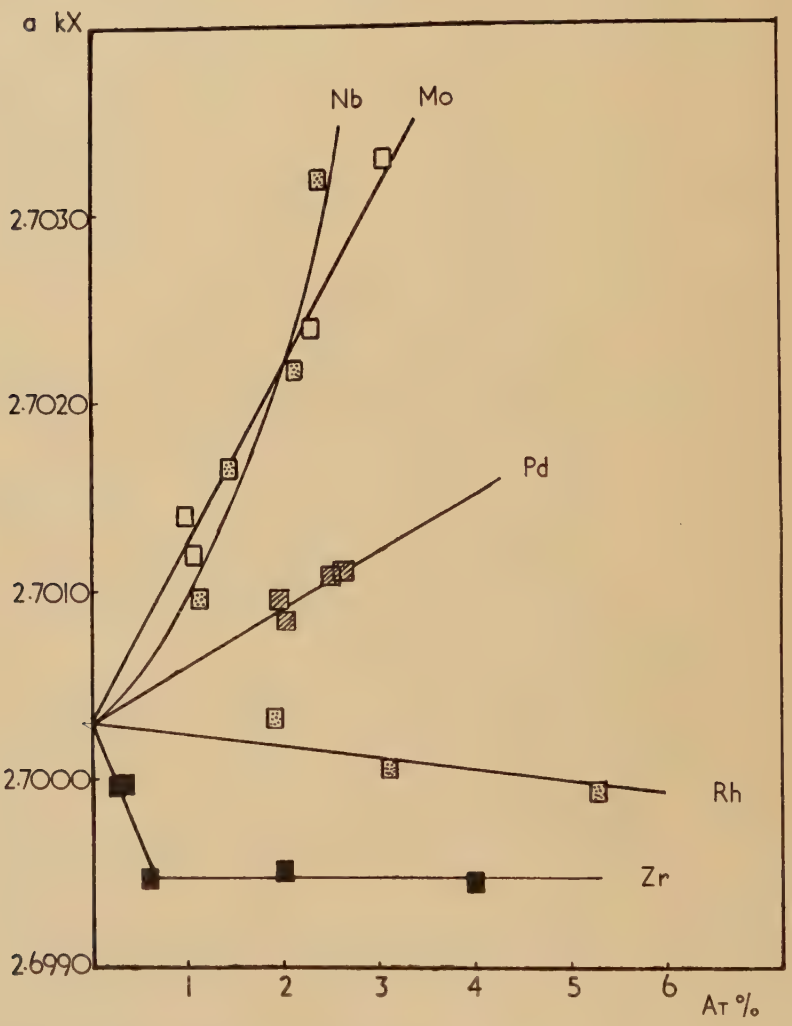

understand why rhodium expands the c parameter and contracts the a parameter of ruthenium. The way in which the two effects neutralize one another so as to preserve an exactly constant atomic volume is striking. With a solute element whose electron cloud is spherical with an atomic diameter greater than either close distance of approach in ruthenium, there will still be relatively more free space in the direction

of the basal plane, and the general effect of increasing axial ratio can be understood.

If the mean volume per atom (V_a) were a linear function of the values for the solvent and solute elements, we should expect the V_a value of ruthenium to be increased by all the solute elements concerned, and the

Fig. 3

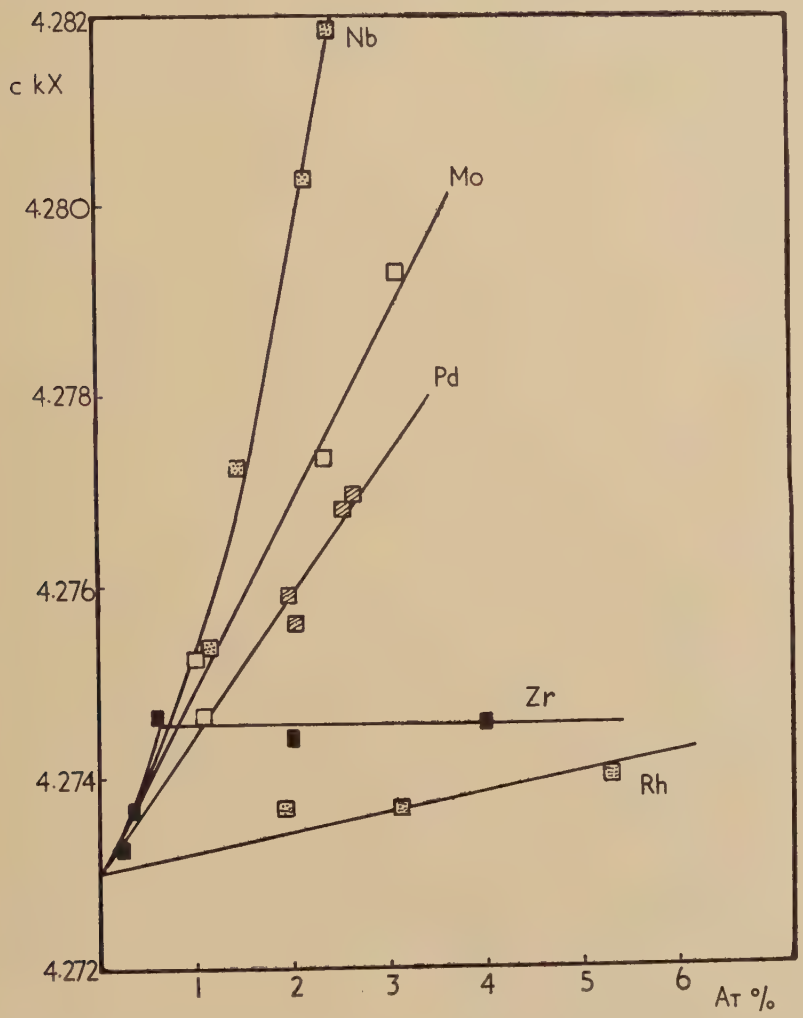

effects would be in the order Rh<Pd<Mo<Nb<Zr. Except for Zr, the order of curves in fig. 4 agrees with expectation, but in all cases the increase in V_a is less than that expected for a linear relation between solvent and solute. The differences are comparatively slight for Mo, and not very great for Rh. Zirconium clearly behaves abnormally, but the effects for the remaining elements may be related to those found

by Axon and Hume-Rothery (1948) for solid solutions in aluminium. These workers showed that if V_e were the mean volume per electron in the crystal of a metal, the lattice spacing of a solid solution, where a solute of high V_e was dissolved in a solute of relatively low V_e, tended

Fig. 4

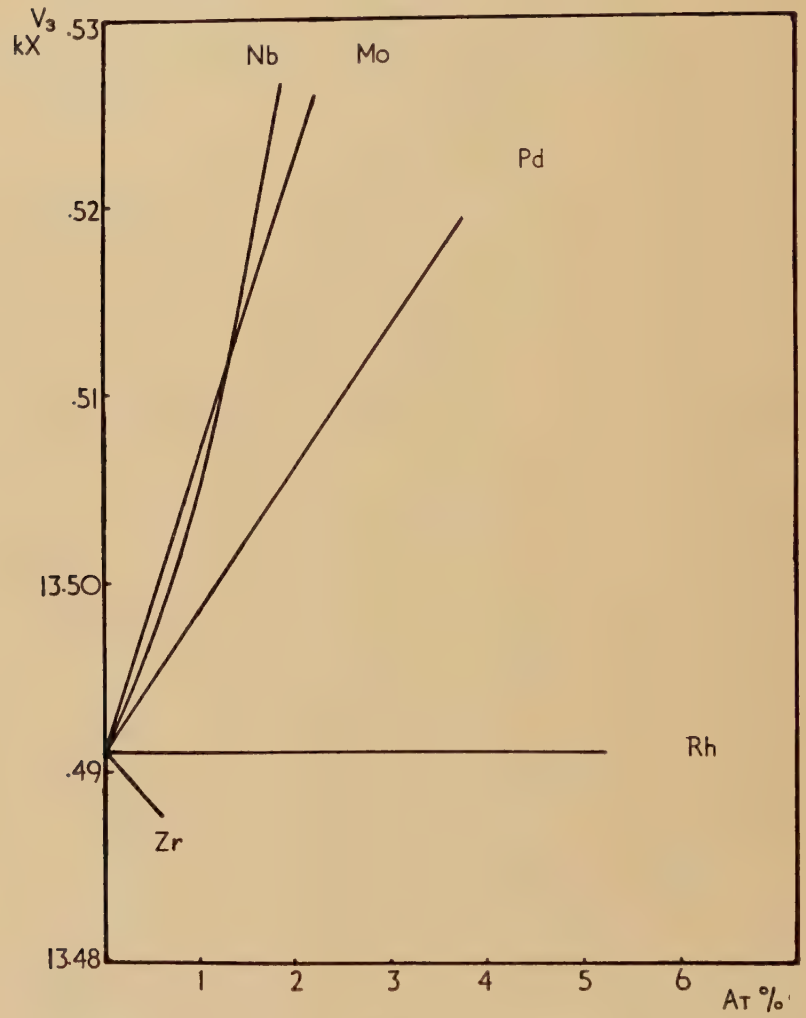

to be smaller than would otherwise be expected. In the transition metals of the present paper there is general agreement that the valencies of Zr, Nb, and Mo are 4, 5 and about 6* respectively. For Ru, Rh, and Pd the position is less certain. According to the Pauling hypothesis the valency in all these elements is about 6*, but as emphasized elsewhere

* For abbreviation in the present discussion the Pauling valency of 5·78 has been smoothed off to 6 ; the difference does not affect the argument.

(Hume-Rothery, Irving and Williams 1951, Hume-Rothery and Coles 1954) this is not in agreement with the physical properties. The melting point of Ru is markedly lower than that of Mo, but the compressibilities and interatomic distances do not suggest any diminution in the strength of bonding on passing from Mo→Ru, and for the latter element we think that the valency is probably still about 6—this agrees with the Pauling views. On passing to Rh, the physical properties all indicate a slight diminution in the strength of bonding, with a further and more marked fall on passing to Pd. According to Sidgwick (1951), the chemical valencies of these elements are as follows, where the degree of underlining indicates the importance of the valency state concerned:

Ru	2	3	4	5	6	7	8
Rh	(2)	3	4	5			
Pd	(1)	2	3	4			

For Pd, therefore, it seems probable that in the metal the effective valency is between 2 and 4, and for Rh between 3 and 5. The following table shows the V_a values for the elements concerned, and also the V_e values for different assumed valencies.

Element	Zr	Nb	Mo	Ru	Rh	Pd
V_a in $(kx)^3$	23·0	17·9	15·5	13·5	13·7	14·6
V_e for valency stated	(4) 5·8	(5) 3·6	(6) 2·6	(6) 2·3	(5) 2·7	(4) 3·7
					(4) 3·4	(3) 4·9
					(3) 4·6	(2) 7·3

These figures clearly support the views outlined above. The V_e value for Ru is only slightly less than that for Mo, in agreement with the relatively small difference between the observed V_a values and those expected for a linear relation between the values for Mo and Ru. With any reasonable scheme of effective valencies, the V_e values increase on passing from Mo→Nb→Zr, and from Ru→Rh→Pd, and these effects run parallel to the difference between the observed V_a values and those expected from a linear relation between solvent and solute.

It remains to consider the curious effect of Zr in contracting the a spacing of Ru. It is perhaps significant that both Zr(c/a=1·59) and Ru(c/a=1·58) possess close-packed hexagonal structures with axial ratios which are nearly the same, and are markedly less than those for close packed spheres. It is possible that in the case of Ru this corresponds with a condition resembling hybrid trigonal prism bonding and that an atom of Zr has the same characteristic. In this case the fact that, in Zr there are only 4 valency electrons per atom, may mean that when an atom of Zr is in solid solution in Ru with 6 valency electrons* per atom, so much of the electron cloud of a Zr atom is used in bonding to the nearest neighbours (in the planes above and below) that the electron

* If the effective valency is more than 6, the effect will be even greater.

cloud is drained away from the basal plane to such an extent that it can here no longer exert an influence corresponding to its normal size. It is perhaps significant that Nb shows slight signs of a similar effect, for although in fig. 3 the c spacing is expanded much more by Nb than by Mo, there is relatively little difference between the effects of those elements on the a spacing.

The above interpretation of the effect of Zr on the spacings of Ru depends on (1) the low axial ratio of Ru, and (2) on the much higher V_e value for Zr as solute. We should therefore not expect the same effect for Zr dissolved in Pd, because the lattice is face-centred cubic, and as shown above the V_e values for Zr and for the probable effective valency state of Pd are more nearly equal than are those for Zr and Ru. It has not been possible to make an extensive examination of palladium alloys, but preliminary experiments have shown that the lattice of palladium is expanded by zirconium in agreement with the suggested interpretation.

Acknowledgments

The authors must express their gratitude to Professor Sir Cyril Hinshelwood, F.R.S., for laboratory accommodation, and to Dr. F. M. Brewer for many other facilities which have greatly assisted the present research. Grateful acknowledgment of financial assistance is made to the Council of the Royal Society and the British Non-Ferrous Metals Research Association.

References

Axon, H. J., and Hume-Rothery, W., 1948, *Proc. Roy. Soc.* A, **193,** 1.

Axon, H. J., Poole, M. J., Hellawell, A., and Hume-Rothery, W., 1953, *J. Appl. Phys.*, **4,** 188.

Hume-Rothery, W., and Coles, B. R., 1954, *Advances in Physics*, **3,** 149.

Hume-Rothery, W., Irving, H. M., and Williams, E. J. P., 1951, *Proc. Roy. Soc.* A, **208,** 431.

Owen, E. A., Roberts, I. O., and Pickup, L., 1937, *Z. Kristallogr.*, **96,** 496.

Sidgwick, N. V., 1951, *Chemical Elements and Compounds* (Oxford : O.U.P.).

LXXXIX. *Angular Correlations in Deuteron Reactions*

By A. G. Stanley
Cavendish Laboratory, Cambridge*

[Received April 14, 1954]

Abstract

The angular correlations have been measured between the charged particles and gamma-rays in the $^{14}N(d, \alpha\gamma)^{12}C$, $^{14}N(d, p\gamma)^{15}N$, and $^{9}Be(d, p\gamma)^{10}Be$ reactions. In the first two reactions the angular distributions of the charged particles leading to the ground state and first excited state of the final nucleus have also been observed. The results agree with the assignments 2^+ for the first excited levels of ^{12}C and ^{10}Be, and suggest spins 1/2 or 3/2 for the close doublet of ^{15}N at 5·3 Mev.

§ 1. Introduction

We have measured the angular correlation between the charged particles and gamma-rays emitted in the reactions $^{14}N(d, \alpha\gamma)^{12}C$, $^{14}N(d, p\gamma)^{15}N$, and $^{9}Be(d, p\gamma)^{10}Be$ in which the first excited state of the final nucleus is formed. Our main aim has been to obtain more information about the spins of these states. In the two reactions with a nitrogen target we have also measured the angular distributions of the charged particles leading to the ground state and first excited state of the final nucleus. These had not previously been studied at very low deuteron energies.

Gibson and Thomas (1952) have studied the angular distributions of the ground state and 4·4 Mev state groups of alpha-particles produced in the $^{14}N(d, \alpha)^{12}C$ reaction by 7·9 Mev deuterons. Both distributions are complex and show a minimum at an angle of 77°. The angular distributions of the proton groups in the $^{14}N(d, p)^{15}N$ reaction have been measured by Wily (1949) at deuteron energies between 1·5 and 3 Mev and by Gibson and Thomas (1952) using 7·9 Mev deuterons. Their results are discussed in § 4.2. A magnetic analysis of the proton groups by Malm and Buechner (1950) showed that the first excited level of ^{15}N at 5·3 Mev is a close doublet with a separation of 30 kev. Terrell and Phillips (1951) have observed 4·4 and 5·3 Mev gamma-rays from the first excited states of ^{12}C and ^{15}N produced by the deuteron bombardment of ^{14}N.

In the $^{9}Be(d, p)^{10}Be$ reaction the angular distributions of the ground state and 3·4 Mev state proton groups have been studied by several experimenters over a wide range of deuteron energies from 0·3 to 14·5 Mev (Ajzenberg and Lauritsen 1952). Rasmussen *et al.* (1949) have observed a 3·38 Mev gamma-ray corresponding to the decay of the first excited state of ^{10}Be.

* Communicated by E. S. Shire.

§ 2. Experimental Method

In the experiments with ^{14}N a thick target, prepared by heating melamine on a thin copper backing, was bombarded by 630 kev deuterons from the 1 MeV high tension apparatus of the Cavendish Laboratory. For the $^{9}Be(d, p\gamma)^{10}Be$ reaction we used an evaporated target of beryllium, 50 $\mu g\ cm^{-2}$, on a thin copper backing and an energy of the deuteron beam of 480 kev.

We measured the angular correlations both in the horizontal plane containing the incident deuteron beam and in the vertical plane perpendicular to the incident beam. We detected the gamma-rays by means of a sodium iodide crystal with a photomultiplier, and charged particles with a proportional counter fixed in the horizontal plane at right angles to the incident beam. We used a conventional circuit with a resolving time of 0·2 μsecs to detect coincidences between the charged particles and the gamma-rays. In order to record the true and accidental coincidences concurrently, we delayed the pulses from one of the two channels by 2·5 μsecs before passing them into a second coincidence unit together with the undelayed pulses from the other channel (Littauer 1950). We succeeded in removing all true coincidences due to competing reactions by placing suitable absorber foils in front of the proportional counter and by adjusting the discriminator bias, so as not to record long-range charged particles and gamma-rays of lower energy. By using a well focused deuteron beam producing a current of about 0·5 μA at the target, we were able to increase the ratio of true to accidental coincidences to about 1·5 : 1.

The apparatus used in the angular distribution experiments is described in a paper by Thomson *et al.* (1952). The target and deuteron energy were the same as for the angular correlations.

§ 3. Experimental Results

We have used the method of least squares to fit curves to the experimental points. The experimental results obtained after correcting for the finite geometry of the detectors and for the motion of the emitted particles in centre-of-mass coordinates are shown in tables 1 and 2.

Table 1. Angular Correlations of Charged Particles and Gamma-Rays

Reaction	Direction of plane of correlation with respect to incident beam	Correlation
$^{14}N(d, \alpha\gamma)^{12}C$	Perpendicular	$1+(2{\cdot}19\pm0{\cdot}35)\cos^2\phi-(1{\cdot}63\pm0{\cdot}35)\cos^4\phi$
$^{14}N(d, \alpha\gamma)^{12}C$	Parallel	Isotropic
$^{14}N(d, p\gamma)^{15}N$	Perpendicular	$1+(0{\cdot}44\pm0{\cdot}08)\cos^2\phi$
$^{14}N(d, p\gamma)^{15}N$	Parallel	$1+(0{\cdot}15\pm0{\cdot}02)\cos^2\theta$
$^{9}Be(d, p\gamma)^{10}Be$	Perpendicular	Isotropic
$^{9}Be(d, p\gamma)^{10}Be$	Parallel	$1-(1{\cdot}75\pm0{\cdot}22)\cos^2\theta+(1{\cdot}81\pm0{\cdot}22)\cos^4\theta$

Table 2. Angular Distributions of Charged Particles

Reaction	Particles	Distribution
$^{14}N(d, \alpha)^{12}C$	long-range α-particles	$1+(1{\cdot}39\pm0{\cdot}08)\cos\theta+(2{\cdot}93\pm0{\cdot}18)\cos^2\theta$
$^{14}N(d, \alpha)^{12}C^*$	short-range α-particles	$1-(0{\cdot}55\pm0{\cdot}02)\cos\theta+(0{\cdot}17\pm0{\cdot}04)\cos^2\theta$
$^{14}N(d, p)^{15}N$	long-range protons	$1+(0{\cdot}76\pm0{\cdot}01)\cos\theta+(1{\cdot}15\pm0{\cdot}03)\cos^2\theta$
$^{14}N(d, p)^{15}N^*$	short-range protons	$1+(0{\cdot}27\pm0{\cdot}05)\cos^2\theta$

§ 4. Interpretation of Experimental Results

The processes involved in deuteron reactions are very complicated, and the compound nucleus is formed in a highly excited state ; it is therefore not possible to compare the experimental correlations and distributions with theoretical expressions.

4.1. $^{14}N(d, \alpha\gamma)^{12}C$ *Reaction*

The $\cos^4\theta$ term in the angular correlation in the plane perpendicular to the deuteron beam suggests that the 4·4 MeV gamma-rays produce a quadrupole transition to the 0^+ ground level of ^{12}C, in agreement with the assignment of 2^+ for the first excited level, obtained from the study of several other reactions also forming this level (Ajzenberg and Lauritsen 1952) and predicted by both the alpha-particle and independent particle models. The angular distributions of the alpha-particles in this reaction contain odd powers of $\cos\theta$, indicating interference between states of opposite parity in the compound nucleus, ^{16}O.

4.2. $^{14}N(d, p\gamma)^{15}N$ *Reaction*

The close doublet formed by the first excited state of ^{15}N complicates the interpretation of our results. Gibson and Thomas (1952) observed that at a deuteron energy of 7·9 MeV the angular distribution of the protons forming this state was roughly isotropic showing no peak in the forward direction. This rather unexpected result led Butler (1951) to suggest that both members of the doublet might require a large angular momentum transfer causing the magnitude of the stripping effect to fall below the background due to compound nucleus formation : thus both members of the doublet must have large spins, i.e. spins $\geqslant 5/2$ and even parity, or $\geqslant 7/2$ and odd parity. However, these assignments cannot be regarded as certain, for the absence of stripping may well be due to other causes, e.g. the preferential formation of the compound nucleus of ^{16}O even at high bombarding energies. From a measurement of the relative intensities of the gamma-rays produced by the slow neutron capture of ^{14}N Kinsey *et al.* (1951) conclude that one of the members of the doublet should have odd parity and spin 1/2, 3/2 or 5/2. This assignment is also very uncertain and does not agree with that of Butler.

From the results of our angular correlation experiments we may postulate that the transition to the $1/2^-$ ground level of ^{15}N proceeds by dipole emission, so that the spins of the doublet are 1/2 or 3/2, with odd

or even parity. Inglis (1953) has tried to explain the formation of the close doublet in terms of the individual particle model. He suggests that an excited s nucleon is coupled to the angular momentum vector of an almost filled p-shell; this coupling is very weak for some reason associated with the inadequacy of the phenomenological Hamiltonian. This leads to the formation of two states with spins and parities $3/2^+$ and $1/2^+$. These assignments, though rather tentative, are in excellent agreement with our experimental results.

We have compared our proton distributions with those obtained by Wyly (1949) with 1·5 to 3 MEV deuterons. Despite the increased effect of the Coulomb barrier at lower bombarding energies the distributions are very similar. The angular distributions of the short-range protons are very nearly isotropic. In the distributions of the long-range protons the angle of minimum yield is displaced in the forward direction with increasing deuteron energy.

4.3. ^{9}Be(d, pγ)^{10}Be *Reaction*

The angular correlation in the plane containing the incident beam suggests that the transition to the 0^+ ground level proceeds by quadrupole emission. The same result was obtained by Cohen *et al.* (Ajzenberg and Lauritsen 1952) with deuterons of higher energy. From these experiments and from the deuteron stripping reactions studied by El–Bedewi (1952) one obtains the assignment 2^+ for the first excited state of ^{10}Be in agreement with the general rule (Goldhaber and Sunyar 1951) that the first excited state of an even–even nucleus has spin 2 and even parity.

Acknowledgments

The author wishes to express his thanks to Dr. A. P. French for assistance with the experiments and to Mr. E. S. Shire for advice in preparing this paper. He is indebted to Trinity College, Cambridge, for a Research Scholarship and to the Department of Scientific and Industrial Research for financial assistance.

References

Ajzenberg, F., and Lauritsen, T., 1952, *Rev. Mod. Phys.*, **24,** 321.
Butler, S. T., 1951, *Proc. Roy. Soc.* A, **208,** 559.
El-Bedewi, F. A., 1952, *Proc. Phys. Soc.* A, **65,** 64.
Gibson, W. M., and Thomas, E. E., 1952, *Proc. Roy. Soc.* A, **210,** 543.
Goldhaber, M., and Sunyar, A. W., 1951, *Phys. Rev.*, **83,** 906.
Inglis, D. R., 1953, *Rev. Mod. Phys.*, **25,** 390.
Kinsey, B. B., Bartholomew, G. A., and Walker, W. H., 1951, *Can. J. Phys.*, **29,** 1.
Littauer, R. M., 1950, *Rev. Sci. Instrum.*, **21,** 750.
Malm, R., and Buechner, W. W., 1950, *Phys. Rev.*, **80,** 771.
Rasmussen, V. K., Hornyak, W. F., and Lauritsen, T., 1949, *Phys. Rev.*, **76,** 581.
Terrell, J., and Phillips, G. C., 1951, *Phys. Rev.*, **83,** 703.
Thomson, D. M., Cohen, A. V., French, A. P., and Hutchinson, G. W., 1952, *Proc. Phys. Soc.* A, **65,** 745.
Wyly, L. D., 1949, *Phys. Rev.*, **76,** 104.

XC. *The Influence of Zero-Point Energy on the Thermodynamic Properties of the Low Boiling Point Elements*

By J. S. Dugdale and D. K. C. MacDonald
Division of Physics, National Research Council, Ottawa, Canada*

[Received April 8, 1954]

Abstract

The internal energy and molar volume at absolute zero and the characteristic temperature of the inert gas solids, together with solid hydrogen and deuterium, are calculated taking account of zero-point energy. It is found that to a good approximation a law of corresponding states is valid and the consequences of this are discussed.

§ 1. Introduction

The inert gas solids are in many ways the simplest examples of the solid state which exist. Because the interatomic attractive forces, of the van der Waals type, are comparatively weak, these solids under normal pressures melt at relatively low temperatures. For the same reason the influence of zero-point energy on their properties is most evident. Consequently these elements together with the hydrogen isotopes are the primary subject of this paper.

The importance of zero-point energy as a governing factor in the behaviour of condensed helium was pointed out by Simon (1934) who showed that this energy compensates (at the lowest pressures at which solid helium can exist) for nearly 90% of the expected lattice energy of the crystal. The zero-point energy is also responsible for the large molar volume of condensed helium (about twice that to be expected from the gas kinetic properties of helium atoms).

Nevertheless, in spite of these remarkable changes in the properties of the lighter inert elements (neon is also considerably influenced) it is found that, for example, their melting curves (apart from deviations in the neighbourhood of and below the λ-point in helium) can all be represented rather well by a reduced equation

$$\pi = \tau^c - 1, \quad . \quad . \quad . \quad . \quad . \quad . \quad . \quad . \quad . \quad (1)$$

where π and τ are the reduced melting pressure and temperature and c is approximately constant for all the low boiling point elements.

It is therefore desirable to understand (*a*) how the general influence of zero-point energy on these solids can be taken into account; (*b*) how the marked change in the thermodynamic properties can be reconciled with the continued existence of a law of corresponding states in the solid phase.

It is the object of this paper to try to answer these questions.

* Communicated by the Authors.

§ 2. The General Method and Assumptions

(*a*) There are good theoretical reasons for believing that the forces acting between inert gas atoms are symmetrical, central, short range forces representable by a potential (London 1937) of which the attractive part varies, to a first good approximation, inversely as the sixth power of their mutual separation. Furthermore, gas kinetic considerations (e.g. Lennard-Jones 1924) have shown that the important features of the gas phase may be accounted for on the basis of a classical potential of the form $\epsilon[(\sigma/r)^n-(\sigma/r)^6]$ where n is an integer between 9 and 14. In the present discussion we shall assume an intermolecular potential of this form, using values of ϵ, σ and n which are consistent with gas kinetic data. We wish to take as our starting-point a completely 'classical' intermolecular potential. Since, however, even in the gas phase some residual quantum effects still exist (particularly in the lighter elements) we shall use data which have been corrected (de Boer and Michels 1938) for these deviations. The intermolecular potential so derived is thus the limiting classical value from which quantal aggregation effects have been eliminated.

(*b*) In a classical lattice we may assume that the characteristic frequency (which may be interpreted as a characteristic temperature, θ) is proportional to $(d^2V/dr^2)^{1/2}$ where $V(r)$ is the lattice potential energy per atom, the derivative being taken of course at the value of r appropriate to the volume considered. In an actual solid where $E(r)$ is the *total* lattice energy per atom at the absolute zero (i.e. $E(r)=V(r)+ZPE$), we assume that the effective characteristic frequency, which will essentially determine the zero-point energy, is now proportional to $(d^2E/dr^2)^{1/2}$. This assumption has been shown by Domb (1952) to provide a sound basis for correlating the experimental data on solid helium (cf. Dugdale and Simon 1953).

(*c*) Although in a single harmonic oscillator, of frequency ν, the zero-point energy is given by $\frac{1}{2}h\nu$, in a *lattice* an appropriate average over the frequency-spectrum is necessary. Domb and Salter (1952) have shown for a variety of crystal structures that the zero-point energy, assuming harmonic vibrations, is given closely by $(9/8)k\theta_\infty$ per atom where θ_∞ is the limiting high temperature value of the Debye θ. We shall use this result, and assume that θ is given by

$$\frac{k\theta}{h}=\frac{\beta}{2\pi}\left(\frac{1}{m}\frac{d^2E}{dr^2}\right)^{1/2}, \quad \ldots\ldots\ldots \quad (2)$$

where β is a parameter of the order of unity dependent on the particular lattice structure and character of the intermolecular forces. For all of the substances we consider, which have close-packed structures and van der Waals interaction, β will be a constant.

(*d*) We shall assume that to a first approximation the influence of anharmonicity is to add a term $9h^2E^{\mathrm{IV}}/4.4!\,(2\pi)^2mE''$ to the zero-point energy (cf. Pauling and Wilson (1935, p. 161, eqn. (23–30)). In this

anharmonic correction term we have replaced the lattice by a single oscillator of frequency $\tilde{\nu}$ such that $\frac{3}{2}h\tilde{\nu}=\frac{9}{8}k\theta$ and therefore

$$\tilde{\nu}=\frac{3\beta}{8\pi}\left(\frac{E''}{m}\right)^{1/2}.$$

§ 3. The Analysis

On the foregoing assumptions, we have thus to find an acceptable solution of the following equation:

$$(9h^2E^{\mathrm{IV}}/4.4!\,(2\pi)^2mE'')+(9\beta h(E'')^{1/2}/8.2\pi\sqrt{m})-E(r)=-V(r). \quad . \quad (3)$$

We consider as acceptable only that solution which, as $r\to 0$, approaches asymptotically the solution obtained when zero-point energy is neglected.

It is found convenient in solving eqn. (3) to take for $V(r)$ the 6, 10 form of the Lennard-Jones potential

$$V(r)=\epsilon\left\{\left(\frac{\sigma}{r}\right)^{10}-\left(\frac{\sigma}{r}\right)^{6}\right\} \quad . \quad . \quad . \quad . \quad . \quad . \quad . \quad . \quad (4)$$

where the values of ϵ and σ are those appropriate to a face-centred cubic lattice (Lennard-Jones and Ingham 1926). Since, however, we wish to use the molecular parameters of de Boer and Michels which are already corrected for quantum aggregation effects, we have so chosen ϵ and σ that the position of the classical minimum, and value of the energy there, agree with those of de Boer and Michels using the 6, 12 Lennard-Jones potential. We introduce also the dimensionless parameter $\Lambda=h/2\pi\sigma\sqrt{m\epsilon}$ which is similar to that used by de Boer (1948). (The overall correction factors are then $\Lambda=3{\cdot}2_0\times10^{-2}\Lambda^*$; $\epsilon=46{\cdot}4\epsilon^*$; $\sigma=0{\cdot}96_0\sigma^*$, the starred parameters being those quoted by de Boer.) Then in reduced form the equation reads

$$y=v(x)+a\left(\frac{d^2y}{dx^2}\right)^{1/2}+0{\cdot}054a^2\left(\frac{d^4y}{dx^4}\right)\Big/\frac{d^2y}{dx^2} \quad . \quad . \quad . \quad . \quad (5)$$

where $y=(E/\epsilon)$, $v=(V/\epsilon)$, $x=(r/\sigma)$ and $a=(9/8)\beta\Lambda$, and in the anharmonic term we have set $\beta=1{\cdot}17$, the appropriate value determined later (following eqn. (18)).

Thus finally, inserting

$$v(x)=\frac{1}{x^{10}}-\frac{1}{x^6} \quad . \quad . \quad . \quad . \quad . \quad . \quad . \quad . \quad . \quad (6)$$

we have

$$y=\frac{1}{x^{10}}-\frac{1}{x^6}+a\left(\frac{d^2y}{dx^2}\right)^{1/2}+0{\cdot}054a^2\left(\frac{d^4y}{dx^4}\right)\Big/\frac{d^2y}{dx^2}. \quad . \quad . \quad . \quad . \quad (7)$$

The appropriate solution of eqn. (7) is

$$y=\frac{1}{x^{10}}-\frac{1-10{\cdot}5a}{x^6}-\frac{2a(1-14{\cdot}7a)}{x^2}-0{\cdot}19_2a(1-18{\cdot}2a)(1-8{\cdot}8a)x^2-\ldots. \quad . \quad . \quad . \quad (8)$$

while, if we ignore anharmonicity so that our differential equation reads

$$y=\frac{1}{x^{10}}-\frac{1}{x^6}+a\left(\frac{d^2y}{dx^2}\right)^{1/2} \quad . \quad . \quad . \quad . \quad . \quad (9)$$

the corresponding solution is

$$y=\frac{1}{x^{10}}-\frac{1-10{\cdot}5a}{x^6}-\frac{2a(1-10{\cdot}5a)}{x^2}-0{\cdot}19_2a(1-10{\cdot}5a)(1-7{\cdot}5a)x^2-\ldots. \quad . \; . \; . \quad (10)$$

For sufficiently small a (the case of the heavier gases) it matters little which series we adopt. On the other hand, for values of a approaching 0·1 (as in the case of the hydrogen isotopes and helium) it becomes difficult to assess the convergence of the series and the influence of anharmonicity becomes increasingly significant, so that even further anharmonic terms (with coefficients of higher powers of a) would be necessary in the original differential equation. Consequently it appears necessary to look for some approximate solution of the problem in closed form, which will yield the appropriate initial terms in the series above and on the other hand enable us to appreciate directly its range of convergence for *all* values of a to be discussed.

Rewriting eqn. (9) in the form

$$z^2=\frac{a^2d^2z}{dx^2}+\frac{110a^2}{x^{12}}-\frac{42a^2}{x^8} \quad . \; . \; . \; . \; . \; . \; . \quad (11)$$

$$\left(\text{where } z=y-\frac{1}{x^{10}}+\frac{1}{x^6}\right)$$

we have

$$z=\frac{10{\cdot}5a}{x^6}\left\{1-\frac{21}{55}\left(1-\frac{1}{42}z''x^8\right)x^4\right\}^{1/2} \quad . \; . \; . \; . \; . \quad (12)$$

If we then set $z\approx(10{\cdot}5a/x^6)$ (and therefore $z''\approx[42(10{\cdot}5a)]/x^8$) as an approximation in the right-hand side this gives

$$y=\frac{1}{x^{10}}-\left\{1-10{\cdot}5a\left[1-\frac{21}{55}(1-10{\cdot}5a)x^4\right]^{1/2}\right\}\Big/x^6 \quad . \; . \quad (13)$$

which on expansion yields

$$y=\frac{1}{x^{10}}-\frac{1-10{\cdot}5a}{x^6}-\frac{2a(1-10{\cdot}5a)}{x^2}-0{\cdot}19_2a(1-10{\cdot}5a)^2x^2-\ldots. \quad . \; . \quad (14)$$

Comparing with eqns. (10) and (8) above, this appears a very reasonable ' solution ' and it follows immediately from (13) that the solution always exists for

$$x^4\leqslant\frac{55}{21(1-10{\cdot}5a)}. \quad . \; . \; . \; . \; . \; . \; . \; . \quad (15)$$

It may then be shown that for values of a up to $\sim$0·08 (the value appropriate to ^{4}He) the minimum value of y, given by (15) occurs rather accurately for

$$x_0{}^4=\frac{5}{3(1-10a)}. \quad . \; . \; . \; . \; . \; . \; . \; . \quad (16)$$

and this, from (15), always lies within the range of existence of (13). It should perhaps be noted that the value of (13) as an overall solution of the problem in closed form is enhanced by the fact that when $10{\cdot}5a=1$ eqn. (13) gives $y=(1/x^{10})$ which is indeed the exact solution of (9) in this particular case.

From eqn. (2) we have

$$k\theta/\epsilon=(8\cdot9)a(d^2y/dx^2)^{1/2}$$

which from (13) yields

$$\left(\frac{k\theta}{\epsilon}\right)^2=\left(\frac{8}{9}a\right)^2\left\{\frac{110}{x^{12}}-\frac{42}{x^6}-\frac{21a}{x^6}(1-Ax^4)^{-3/2}(21-33Ax^4+10A^2x^8)\right\} \quad (17)$$

where $A=\frac{21}{55}(1-10\cdot5a)$ and for very small values of a we find for $x=x_0$ (i.e. equilibrium under $p=0$)

$$k\theta/\epsilon=2\cdot61a(1-9\cdot6a). \quad . \quad . \quad . \quad . \quad . \quad . \quad . \quad . \quad (18)$$

We now choose a (and hence β—cf. eqn. (2)) to make θ agree with the experimental value for Xenon, yielding $\beta=1\cdot17$, and it should be noted that this is the only adjustable constant in the theory.

Table 1

Element	V_0 calc. cm^3	V_0 exp. cm^3 (Est. at 0°K)	E_0 calc. cals/mole	E_0 exp. cals/mole	θ calc. °K	θ exp. °K
Xe	34	33	3790	3778	55	55
Kr	28	26·3	2710	2678	63·6	63
A	23	23·5	1880	1850	79	80
Ne (Normal)	13·4	13·9	435	448	59	64
D_2 (Normal)	20	19·6	290	276	80	97
H_2	25	22·6	172	183	70	105
He*	31	21·2	7·3	12	11·3	21

* Under approximately 25 atm. pressure.

We then compute from the foregoing equations the atomic volume, the latent heat of vaporization and the characteristic temperature for Xe, Kr, A, Ne, D_2, H_2 and ^{4}He, all at zero temperature and pressure. The theoretical and experimental values are presented in table 1.

Although in the present work the correspondence of the theoretical values with experiment is less close for the lighter elements, it is seen that even for helium the numerical agreement is fair. Other calculations of these thermodynamic quantities such as that of de Boer (1948) (cf. also Corner 1939) have proved feasible only for the heavier elements (Xe to Ne).

§ 4. Zero-Point Energy and the Law of Corresponding States

From the leading terms of eqns. (8), (10) or (14) we see that as a first approximation the reduced energy at absolute zero is given by

$$y\approx\left(\frac{1}{x^{10}}\right)-\left(\frac{1-10\cdot5a}{x^6}\right). \quad . \quad . \quad . \quad . \quad . \quad . \quad (19)$$

This expression yields immediately

$$x_0^4 = \frac{5}{3(1-10{\cdot}5a)} \quad . \quad . \quad . \quad . \quad . \quad . \quad . \quad . \quad . \quad (20)$$

(cf. eqn. (16)) and

$$k\theta/\epsilon = 2{\cdot}61a(1-10{\cdot}5a)^{3/2} \quad . \quad . \quad . \quad . \quad . \quad . \quad . \quad (21)$$

(cf. eqn. (18)).

Now eqn. (19) for y is still in the Lennard-Jones form and hence immediately implies the existence of a law of corresponding states for the solid phase even in the presence of zero-point energy. The continued existence of such a law is shown in the following ways :

(*a*) If a law of corresponding states exists, the quantity $M\theta^2 V_0^{2/3}/E_0$ should be a constant† (cf. Dugdale 1951). (Here M is the molar mass, V_0 and E_0 are the molar volume and energy at absolute zero.) Table 2 shows indeed how well this prediction is obeyed, although the rather precise agreement must be regarded as fortuitous in the case of helium.

Table 2

Substance	θ_0(°K)	E_0 (cals/mole)	V_0 (cm³/mole)	M (g/mole)	$\frac{M\theta_0^2 V_0^{2/3}}{E_0}$
Xe	55	3778	33·0	131·3	$1{\cdot}08\times10^3$
Kr	63	2678	26·3	83·7	$1{\cdot}10\times10^3$
A	80	1850	23·5	39·9	$1{\cdot}14\times10^3$
Ne	64	448	13·9	20·2	$1{\cdot}07\times10^3$
He	21*	12	21·2	4·00	$1{\cdot}12\times10^3$

* Extrapolated value for a molar volume of 21·2 cm³, corresponding to 25 atm. pressure.

Moreover, using (19), (20) and (21), we have

$$\frac{M\theta^2 V_0^{2/3}}{E_0} = \frac{6ON^{2/3}\beta^2\hbar^2}{2^{1/3}4\pi^2 k^2} = 1{\cdot}14\times10^3$$

in the same units as table 2. (N is Avogadro's number.)

(*b*) Another consequence of the law of corresponding states would be the existence of a reduced melting-curve on the assumption (cf. e.g. Herzfeld and Goeppert-Mayer 1934) that the onset of melting is determined by the characteristics of the solid. That such a reduced melting curve does indeed exist for the low boiling-point substances was first shown by Simon (Simon and Glatzel 1929, Simon, Ruhemann and Edwards 1929, Simon 1937).

The melting curve proposed by Simon reads

$$\frac{p}{a} = \left(\frac{T}{T_0}\right)^c - 1 \quad . \quad . \quad . \quad . \quad . \quad . \quad . \quad . \quad (22a)$$

† This follows from dimensional considerations.

in which p and T are the pressure and temperature of melting, T_0 is effectively the triple-point temperature and a is a pressure characteristic of each substance. For the low boiling-point substances c is found to lie between about 1·5 and 1·9. Thus, regarding c as strictly constant for these elements, we have the reduced equation

$$\pi = \tau^c - 1. \qquad (22\,b)$$

Simon related a to the quantity $(L-RT)/V$, where L is the molar latent heat of vaporization of the liquid and V its volume at the boiling-point. On the basis of the present considerations, a should be proportional to E_0/V_0. Numerically, either relationship gives reasonable agreement with the experimental data (Dugdale 1951).

We are grateful to Dr. G. Herzberg, F.R.S. for commenting on the manuscript.

References

de Boer, J., 1948, *Physica*, **14,** 139.
de Boer, J., and Michels, A., 1938, *Physica*, **5,** 945.
Corner, J., 1939, *Trans. Faraday Soc.*, **35,** 711.
Domb, C., 1952, *Changements de Phases* (Paris : Soc. de Chim. Physique), p. 338.
Domb, C., and Salter, L., 1952, *Phil. Mag.*, **43,** 1083.
Dugdale, J. S., 1951, " Properties of Helium at Low Temperatures and High Pressures ", *Thesis*, Oxford University.
Dugdale, J. S., and Simon, F. E., 1953, *Proc. Roy. Soc.* A, **218,** 291.
Herzfeld, K. F., and Goeppert-Mayer, M., 1934, *Phys. Rev.*, **46,** 995.
Lennard-Jones, J. E., 1924, *Proc. Roy. Soc.* A, **106,** 441.
Lennard-Jones, J. E., and Ingham, A. E., 1925, *Proc. Roy. Soc.* A, **107,** 636.
London, F., 1937, *Trans. Faraday Soc.*, **33,** 8.
Pauling, L., and Wilson, E. B., 1935, *Introduction to Quantum Mechanics* (New York and London : McGraw-Hill).
Simon, F. E., 1934, *Nature, Lond.*, **133,** 529 ; 1937, *Trans. Faraday Soc.*, **33,** 65.
Simon, F. E., and Glatzel, G., 1929, *Z. Anorg. Chem.*, **178,** 309.
Simon, F. E., Ruhemann, M., and Edwards, W. A. M., 1929, *Z. Phys. Chem.* B, **6, 331.**

XCI. *An Extended Use of Perturbation Theory*

By R. N. Gould
H. H. Wills Physical Laboratory, University of Bristol
and
A. Cunliffe
University College of Hull *

[Received May 14, 1954]

Summary

It is shown that the unique solution of a partial differential equation

$$(H+U)\phi=0, \quad . \quad . \quad . \quad . \quad . \quad . \quad . \quad . \quad (1)$$

can be determined in terms of the unique solution of the partial differential equation

$$H\theta=0, \quad . \quad . \quad . \quad . \quad . \quad . \quad . \quad . \quad (2)$$

and the eigen-functions of the equation

$$H\psi=\lambda\psi. \quad . \quad . \quad . \quad . \quad . \quad . \quad . \quad . \quad (3)$$

In (1), (2) and (3), ϕ, θ and ψ denote functions of one or more variables, H and U are operators, and λ is an eigen-value. The equations are to be satisfied throughout a volume D bounded by a surface S which is the same for all three equations. (1) and (2) are subject to precisely the same boundary conditions, ϕ and θ being specified at every point of S and being identical with each other over S. (3) is subject to the boundary condition $\psi=0$ at all points of S, and the solutions ψ_i are assumed to form a complete set.

By reference to the one dimensional case it is shown that the use of eqn. (3) is not always necessary. Thus, in the particular case where ϕ is a function of one variable x, only, $H=(d^2/dx^2)+$a constant, and $U=f(x)$, the solution can be derived from equations which can be integrated directly.

§ 1. Introduction

Let a quantity ϕ satisfy the partial differential equation

$$(H+U)\phi=0 \quad . \quad . \quad . \quad . \quad . \quad . \quad . \quad . \quad (1)$$

throughout a volume D bounded by a surface S. Let (1) have a unique solution when ϕ is specified at every point of S. It is required to find this solution when the solutions of the following equations are known :

$$H\theta=0, \quad . \quad . \quad . \quad . \quad . \quad . \quad . \quad . \quad (2)$$

$$H\psi=\gamma\psi. \quad . \quad . \quad . \quad . \quad . \quad . \quad . \quad . \quad (3)$$

* Communicated by the Authors.

(2) and (3) are to be satisfied throughout the same volume D bounded by the same surface S as in (1). (2) is subject to exactly the same boundary conditions as (1), that is θ must be equal to ϕ at each point of S. θ is assumed to be the unique solution of (2). In (3), λ is a constant, and ψ is subject to the boundary condition $\psi=0$ at all points of S. It is assumed that the solutions of (3) subject to this boundary condition give rise to an infinite number of eigen-values λ_i with associated eigen-functions ψ_i, and that the ψ_i form a complete set in terms of which an arbitrary function can be expanded in the volume D.

§ 2. General Derivation

Let U be expressed in the form

$$U=\sum_k \alpha_k U_k \quad . \quad . \quad . \quad . \quad . \quad . \quad . \quad . \quad . \quad . \quad (4)$$

where the U_k are operators, and the α_k are constants independent of position and are to be regarded as independent parameters. Under these conditions ϕ of (1) may be considered to be a function of the α_k as well as of position. It will be assumed that ϕ can be expanded in a Taylor series

$$\phi=\theta+\sum_k \alpha_k\phi_k+\sum_{k,s}^{k\geqslant s} \alpha_k\alpha_s\phi_{ks}+\ldots \text{etc.}, \quad . \quad . \quad . \quad . \quad . \quad (5)$$

where ϕ_k, ϕ_{ks}, etc. are functions of position which vanish at all points of S. If the α_k's all vanish, (1) reduces to (2), and so ϕ reduces to θ in accordance with (5).

Substituting for ϕ from (5) into (1)

$$\{H\theta\}+\{\sum_k \alpha_k(H\phi_k+U_k\theta)\} + \left\{\sum_{k,s}^{k\geqslant s} \alpha_k\alpha_s(H\phi_{ks}+U_k\phi_s+U_s\phi_k)\right\}+\text{etc.}=0. \quad . \quad (6)$$

Since the α_k's are independent parameters, the coefficients of the α_k's, α_{ks}'s, etc., may be equated to zero and hence,

$$\left.\begin{aligned} H\theta&=0,\\ H\phi_k&=-U_k\theta,\\ H\phi_{ks}&=-U_k\phi_s-U_s\phi_k\ldots\text{etc.}\end{aligned}\right\} \quad . \quad . \quad . \quad . \quad . \quad . \quad (7)$$

The first of these equations is automatically satisfied because of (2). The other equations are subject to the boundary conditions that the ϕ_k's, ϕ_{ks}'s etc., vanish at all points of S. These functions can therefore be expanded in terms of the ψ_i of (3), and by the use of (7),

$$\begin{aligned}\phi_k&=-\sum_i\left(\int_D \psi_i^*U_k\theta d\tau\right)\psi_i/\lambda_i,\\ \phi_{ks}&=\sum_i\left[\int_D \psi_i^*\sum_j\left\{U_k\left(\int_D \psi_j^*U_s\theta d\tau\right)\right.\right.\\ &\qquad\left.\left.+U_s\left(\int_D \psi_j^*U_k\theta d\tau\right)\right\}\left(\psi_j/\lambda_j\right)d\tau\right]\psi_i/\lambda_i \quad . \quad . \quad . \quad (8)\end{aligned}$$

where the integrals $\int_D d\tau$ are taken throughout the whole volume τ of D, and the ψ_i's have been taken to be normalized according to the equation

$$\int_D \psi_i^* \psi_j d\tau = \delta_{ij}.$$

Subject to the series being convergent, the solution of (1) is given by (5) through (8). In the particular case where U can be expressed in terms of a single parameter t according to the equation $U = tU_1 + t^2U_2 + t^3U_3 + \ldots$ i.e. $\alpha_k = t^k$, the solution of (1) becomes

$$\phi = \theta - t\sum_i \left(\int_D \psi_i^* U_1 \theta d\tau\right)\psi_i/\lambda_i + t^2 \sum_i \left[\int_D \psi_i^* \sum_j \left\{U_1\left(\int_D \psi_j^* U_1 \theta d\tau\right)\psi_j/\lambda_j\right\} d\tau - \int_D \psi_i^* U_2 \theta d\tau\right](\psi_i/\lambda_i) + O(t^3).$$

§3. The Second Order Linear Ordinary Differential Equation

The technique may be applied to the ordinary differential equation

$$\frac{d^2\phi}{dx^2} + f\phi = 0. \quad \ldots\ldots\ldots \quad (9)$$

In (9), f is a function of the independent variable x, and it will be supposed that it is required to find the solution of (9) in the interval $(0, \pi)$ given that $\phi = P_0$ at $x = 0$ and $\phi = P_1$ at $x = \pi$.

The solution of the equation

$$\frac{d^2\theta}{dx^2} + a^2\theta = 0 \quad \ldots\ldots\ldots \quad (10)$$

where a is a constant in the interval $[0, \pi]$, subject to the same boundary conditions as (9), and the solutions of

$$\frac{d^2\psi}{dx^2} + a^2\psi = \lambda\psi \quad \ldots\ldots\ldots \quad (11)$$

subject to the boundary conditions $\psi(0) = 0 = \psi(\pi)$ are directly determinable. Thus

$$\theta = P_2 \sin ax + P_0 \cos ax, \quad P_2 = (P_1 - P_0 \cos a\pi)/\sin a\pi,$$
$$\psi_i = (2/\pi)^{1/2} \sin ix, \quad \lambda_i = a^2 - i^2.$$

If $f - a^2$ can be expanded as a Fourier half range sine series in the open interval $(0, \pi)$

$$f - a^2 = \sum_k \alpha_k \psi_k = \sum_k \left(\int_0^\pi (f - a^2) \sin kx\, dx\right)(2/\pi) \sin kx.$$

By putting $\psi_k = U_k$, and using (5) and (8), successive approximations to ϕ can be obtained. Thus to first order,

$$\phi = \theta - \sum_k \left[(2/\pi)^2 \int_0^\pi (f - a^2) \sin kx\, dx \times \sum_i \left\{\int_0^\pi \sin ix \sin kx (P_2 \sin ax + P_0 \cos ax) dx\right\} \{\sin ix/(a^2 - i^2)\}\right].$$

In the one dimensional case, however, using either a Fourier expansion of $f-a^2$, or a power series development of f, equations (7) always yield direct integrals ; that is, they can always be solved by the usual operator methods without recourse to eigen-function expansion. In the case of the Fourier development of $f-a^2$, ϕ may be written to first order,

$$\phi=\theta+\sum_k \alpha_k \left[A_k \sin ax+B_k \cos ax-\left\{ P_2 \left[\frac{\cos (a-k)x}{2ak-k^2}+\frac{\cos (a+k)x}{2ak+k^2} \right] \right.\right.$$
$$\left.\left. +P_0 \left[\frac{\sin (a-k)x}{k^2-2ak}-\frac{\sin (a+k)x}{2ak+k^2} \right] \right\} \Big/ (2\pi)^{1/2} \right]$$

where

$$A_k=4aP_2 \cot a\pi/(2\pi)^{1/2}(k^2-4a^2)+\{\operatorname{cosec} a\pi/(2\pi)^{1/2}\}$$
$$\times\left\{ P_2 \left[\frac{\cos (a-k)\pi}{2ak-k^2}+\frac{\cos (a+k)\pi}{2ak+k^2} \right]+P_0 \left[\frac{\sin (a-k)\pi}{k^2-2ak}-\frac{\sin (a+k)\pi}{k^2+2ak} \right] \right\}$$

$$B_k=4aP_2/(2\pi)^{1/2}(4a^2-k^2)$$

$$\alpha_k=\int_0^\pi (f-a^2)(2/\pi)^{1/2} \sin kx\, dx.$$

In the particular cases $a=u/2$; $u=0, 1, 2, \ldots$, modified first order approximations can be obtained along similar lines.

§ 4. Discussion

The application of Fourier expansions to the solution of boundary value problems is well known (Churchill 1941) ; such methods, however, approach the problem in a different way from that concerned here. For the present method eigen-function expansions are required, if at all, for the solution of eqns. (7). In the one dimensional case the Fourier expansion of $f-a^2$ is to be regarded as merely a particular choice of the quantities U_k. The boundary conditions on ϕ can be satisfied providing it is possible to obtain the solution θ of (2), where θ also satisfies the same boundary conditions. Initially one is thus lead to a simplified boundary value problem. In the subsequent calculation of the perturbation terms the functions derived are all to vanish at the boundary. Expansion in terms of the ψ_i automatically ensures that this boundary condition will hold. Although the general application of the method as presented here appeals to eigen-function expansion for the solution of eqns. (7), it is interesting to note that this is not invariably a feature. For instance in the one dimensional case, if f is developed as a power series in its argument, the equations involved may all be solved by the usual methods. In general the method may be expected to be appropriate when U is ' small '. There is some scope in the choice of the expansion of U, and in a particular case this can affect the computation involved. If the f of § 3 varies only slightly about a^2, f may be replaced by $a^2+\alpha(f-a^2)$, α should then be taken as the parameter and put equal to unity in the final solution. The case where f varies only slightly about a^2 is just that for

which the W.K.B. method (Wentzel 1926) is useful, and in certain cases it can be shown that the first order results obtained by the present method are in agreement with the W.K.B. approximations.

Acknowledgments

The authors wish to express their thanks to Prof. L. S. Palmer for his generous help and interest, and also to Drs. D. Polder and A. F. Devonshire for some comments.

References

Brillouin, 1926, *C. R. Acad. Sci., Paris*, **183**, 24.
Churchill, 1941, *Fourier Series and Boundary Value Problems* (New York : McGraw-Hill Book Co. Inc.).
Kramers, 1926, *Z. Phys.*, **39**, 828.
Wentzel, 1926, *Z. Phys.*, **38**, 518.

XCII. *Relations between the Elastic Moduli and the Plastic Properties of Polycrystalline Pure Metals*

By S. F. Pugh
Atomic Energy Research Establishment, Harwell*

[Received May 14, 1954]

Abstract

Relations between the elastic and plastic properties of pure polycrystalline metals are discussed and a systematic relation between shear modulus, Burgers vector and plastic shear strength of metals possessing the same lattice structure is proposed. In addition reasons are given for believing that in a limited temperature range malleability is related to Poisson's ratio.

§ 1. Introduction

In this report it is intended to discuss some empirical relations between the elastic moduli and plastic properties of pure metals. The properties which will be related to the elastic moduli are the hardness, tensile strength, elongation in tension and fracture stress. In the past, brittleness of beryllium has been variously attributed to the presence of impurities (Sloman 1932), which are admittedly difficult to remove, or to its low axial ratio (Raynor 1946), while the malleability of titanium has been attributed to the profuseness of its slip and twin modes (Rosi, Dube and Alexander 1953). The analysis contained in this report was undertaken in order to discover whether these large differences in plasticity at room temperature could be due to differences in those characteristics of the force fields between the atoms in the lattice which are revealed by the elastic constants.

Three empirical relations between the elastic and plastic properties of pure metals will be discussed :—

(1) The resistance to plastic deformation is proportional to the elastic shear modulus, G, and the Burgers vector, b, for metals at all temperatures below one-third of the melting point.

(2) Fracture strength for all pure metals is proportional to the bulk modulus, K, and a lattice parameter, a.

(3) The quotient, K/G, is an indication of the extent of the plastic range for a pure metal, so that a high value of K/G is associated with malleability and a low value with brittleness.

* Communicated by the Author.

§ 2. Elastic and Plastic Shear

2.1. *Dislocation Theory*

It has been shown (Nabarro 1952) that the dominating term in the calculated energy of a dislocation is almost independent of the assumption made about the nature of the law relating shear stress and shear strain for large strains when neighbouring planes are moving cooperatively over each other. The energy of a dislocation per unit length in an isotropic elastic medium is proportional to $Gb^2/(1-n)$ for an edge dislocation, and Gb^2 for a screw dislocation (Nabarro 1952), where G is the elastic shear modulus of the material, b is the Burgers vector of the dislocation and n is Poisson's ratio. These values for the energy are different if the dislocation has dissociated, but the correlation is unaffected if the decrease due to dissociation is by the same proportional amount for each metal of the same structure.

General dislocations are of mixed edge and screw character, with energy per unit length lying between Gb^2 and $Gb^2/(1-n)$. Since the relative amounts of the two components are not known, Gb^2 will be used as the energy of any unspecified type of dislocation. Discrepancies due to neglect of n are small since it normally lies between $\frac{1}{4}$ and $\frac{1}{2}$ except for beryllium.

Assuming that the plastic flow stress is determined by the necessity for operating Frank–Read sources of length l, then the flow stress, s, is given by $s \propto Gb/l$ (Frank and Read 1950). Identation hardness values provide a convenient measure of the resistance to plastic flow at a strain well beyond the yield point. l can be assumed to be either constant in absolute length from metal to metal, or constant in the number of atom diameters constituting its length. Since the atomic diameters do not vary greatly from metal to metal, it is not important here to distinguish between these alternatives. Assuming the former to be true, it follows that if B is the hardness,

$$1/B=c/G\,.\,b, \qquad \ldots\ldots\ldots \quad (1)$$

where c is a constant for all metals of the same structure. The relation between hardnes and flow stress is discussed later.

2.2. *Thermally Activated Processes*

The 'softness' $1/B$, of a metal can be considered to consist of two components : the first, due to movement of dislocations, is a function only of elastic moduli and lattice dimensions and has already been discussed ; the second due to thermally activated processes is a function of temperature and rate of straining. Since diffusion of vacancies can also play a part in plastic deformation (Mott 1951), the hardness calculated by considering the elastic shear modulus alone would be too high when relaxation is occurring and therefore, an extra term must be included in the expression (1) above.

Since room temperature represents a different ' reduced ' temperature for each metal the contribution of thermally activated processes to the mechanical properties at room temperature will differ for each and will be a function of melting temperature, being larger for metals of low melting point.

Thus $$1/B=(c/Gb)+f(T/Tm, t), \quad . \quad . \quad . \quad . \quad . \quad . \quad (2)$$

where $f(T/Tm, t)$ is a function of testing temperature T, melting point Tm, and time of stressing, t.

For room temperature stressing of metals melting above 1000°C, $f(T/Tm, t)\simeq 0$ and the value of c for these metals can be calculated. The constancy of c from these computations is a check on the validity of the original assumptions. An indication of the function $f(T/Tm, t)$ has been obtained by plotting Gb/B against Tm for all metals of the same lattice type. These curves reproduced in figs. 1–3 are horizontal for high Tm, but rise rapidly with decreasing Tm for $Tm<1000$°C.

2.3. *Computations*

Values obtained by Köster (1948 a) for the shear moduli of the polycrystalline pure metals are reproduced in tables 1, 2 and 3. Since doubt has been cast on the value for zirconium this has been replaced by the results of the later work of Reynolds (1952). Köster's value for Young's modulus of platinum has also been questioned, and therefore the value for the rigidity modulus is in doubt. A value of the rigidity modulus of platinum has been calculated from the value of Young's modulus quoted in *Metals Handbook* (1948) and from Bridgman's (1952) value for the bulk modulus.

The sources of the hardness values used in the correlations are indicated in the tables by the letters following the numbers. Values were taken mainly from *Metals Handbook* 1948 (M). In those cases where hardness values for the pure metal were not quoted in *Metals Handbook*, the values from Tabor 1951 (T), or *Metals Reference Book* (S), are taken. The value for vanadium was taken from a recent paper by Nash, Ogden, Durtschi and Campbell 1953 (R). The remaining values were determined at A.E.R.E. (A), by Hancock and others using specpure rods reduced about 80% by rolling followed by annealing to give a fine grain size.

The values of Gb/B for the face centred cubic metals are shown in table 1 and are plotted against melting temperatures in fig. 1. For these metals with melting points above 900°C (except platinum and thorium), Gb/B is constant to $\pm 8\%$. This constancy is surprising and very significant in view of the large range of values (table 1) that the rigidity modulus G, and the hardness B, cover individually. The curve obtained, fig. 1, rises steeply for metals melting below 900°C. Lead and aluminium lie on this part of the curve, and it is deduced that thermally activated processes play a part in plastic deformation of these metals at room temperature. This is obviously the case for lead, but not so for aluminium which does

Table 1. Rigidity Modulus and Hardness of f.c.c. Metals

Face centred cubic metals	Lattice parameter a Å	Burgers vector b Å	Rigidity modulus G kg/mm²	Force to move dislocations $G.b$	Brinell hardness B	Gb/B	Melting point °C	Predicted hardness
Calcium	5·57	3·94	750	2960	17 M	474	850	9
Strontium	6·05	4·28	620	2650			757	7
Aluminium	4·04	2·86	2720	7780	17 M	458	660	
Thorium	5·08	3·60	3160	11380	39 A	290	1850	34
Nickel	3·52	2·49	7500	18660	60 A	310	1455	
Rhodium	3·79	2·68	15300	41000	122 M	335	1966	
Iridium	3·83	2·70	21400	58000	170 M	340	2454	
Palladium	3·88	2·74	4450	12280	38 M	320	1555	
Platinum	3·92	2·77	5300	17240	40 M	430	1773	
Copper	3·61	2·56	4640	11840	≃ 33 A	360	1083	
Silver	4·08	2·88	2940	8480	25 M	340	960	
Gold	4·07	2·88	2820	8120	25 M	320	1063	
Lead	4·94	3·49	570	2000	4 M	500	327	

not creep at a measurable rate at room temperature. It is known however, that vacancies can diffuse rapidly in aluminium at room temperature (Molenaar and Aarts 1950).

The points for platinum and calcium do not lie on the curve. The value of Gb/B for calcium which is difficult to purify is about half of the expected value. It is suggested that a value of 9 Brinell is more likely for the hardness of pure calcium. Gb/B for platinum is 30% above the expected value. The errors may arise from a marked anisotropy in platinum. Further experiments have not so far resolved this anomaly.

Fig. 1

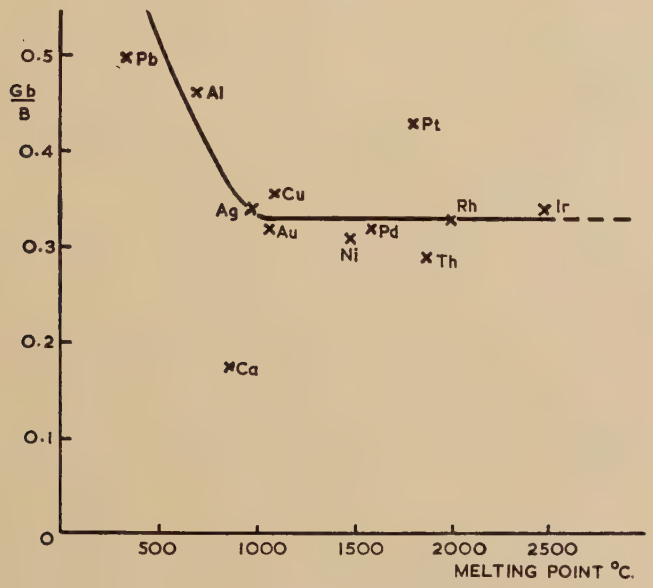

Face-centred-cubic metals.

The body centred cubic metals can be divided into two subgroups. The first consists of those metals with low melting points including lithium and the sodium group, in which the temperature dependent term is dominant in the expression for hardness. In the second subgroup of which iron has the lowest melting point (1535°C) it can safely be assumed that thermally activated processes play little part in plastic deformation. Excluding tungsten, the metals in the latter group give values of Gb/B constant to $\pm 10\%$; see table 2 and fig. 2. The quoted hardness of tungsten is much too high to give a good agreement and a value of 151 Brinell is indicated for the pure metal from the curve of fig. 2.

The curve Gb/B against melting point for the hexagonal metals, fig. 3, is the same in form as the two previous curves, consisting of a horizontal section for metals melting above 900°C, and a steeply rising section for metals with lower melting points. From this it is inferred as above, that, since Gb/B is constant for the high melting point metals, thermally activated processes play no appreciable part in their deformation but increase

Table 2. Rigidity Modulus and Hardness of b.c.c. Metals

Body centred cubic metals	Lattice parameter a Å	Burgers vector b Å	Rigidity modulus G kg/mm²	Force to move dislocations $G.b$	Brinell hardness B	Gb/B	Melting point °C	Predicted hardness
Lithium	3·50	3·03	430	1300	≏ 0·5 M	2600	180	
Sodium	4·28	3·70	340	1260	0·07 M	18000	98	
Potassium	5·31	4·60	130	600	0·037 T	16000	64	
Barium	5·01	4·34	500	2170	—	—	710	8
Vanadium	3·03	2·62	5500	14400	64 R	225	1700	52
Niobium	3·29	2·85	6000	17100	70 A	240	2500	
Tantalum	3·30	2·86	7000	20000	70 T	286	2850	
Chromium	2·88	2·50	7300	18300	70 M	260	1920	
Molybdenum	3·14	2·72	12200	33200	156 M	213	2620	121
Tungsten	3·16	2·74	15140	41500	260 T	143	3382	151
Iron	2·86	2·48	8280	20500	70	293	1535	

Table 3. Rigidity Modulus and Hardness of h.c.p. Metals

Hexagonal close packed metals	Lattice parameter $a=b$ Å	Rigidity modulus G kg/mm²	Force to move dislocations $G.b$	Brinell hardness B	$G.b/B$	Melting point °C	Predicted hardness
Beryllium	2·28	13500	30800	98 M	314	1300	200
Magnesium	3·20	1700	5660	30 M	189	650	
Lanthanum	3·75	1500	5630	37 T	152	885	
Titanium	2·95	3870	11400	75 A	152	1800	
Zirconium	3·23	3540	11500	73 A	157	1860	
Hafnium	3·20	3100	9900			2200	64
Cobalt	2·50	7630	19100	125 M 48 S	153 398	1478	125
Rhenium	2·76	21000	58000			3167	374
Ruthenium	2·70	17600	47500	220 M	215	2500	306
Osmium	2·73	22800	62300	400±10%M	155	2700	
Zinc	2·66	3790	10000	30 T	333	419	
Cadmium	2·97	2460	7300	22 M	332	321	
Thallium	3·45	280	970	5	200	449	4

the ease of plastic shear in the lower melting point metals, magnesium, thallium, cadmium and zinc.

Dealing now with the discrepancies ; thallium is so soft that a change in the quoted hardness value of one point Brinell is sufficient to provide a value of Gb/B lying on the curve. There is little published work on the

Fig. 2

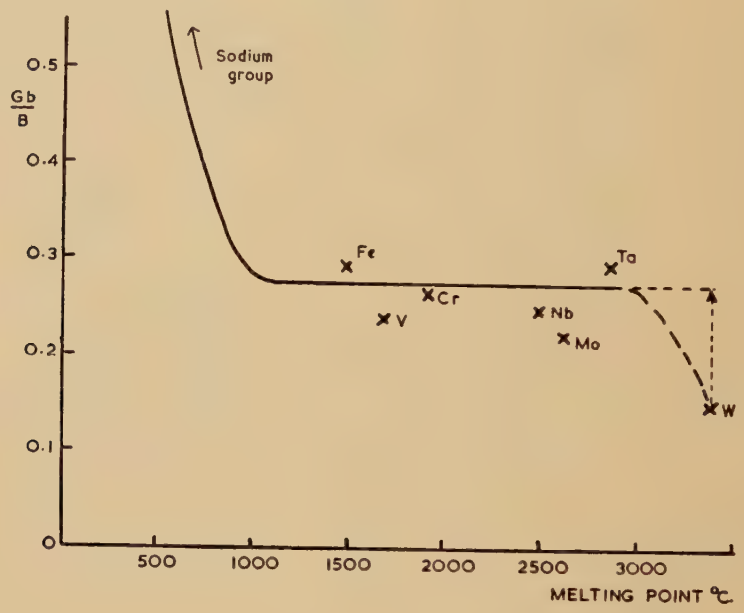

Body-centred-cubic metals

Fig. 3

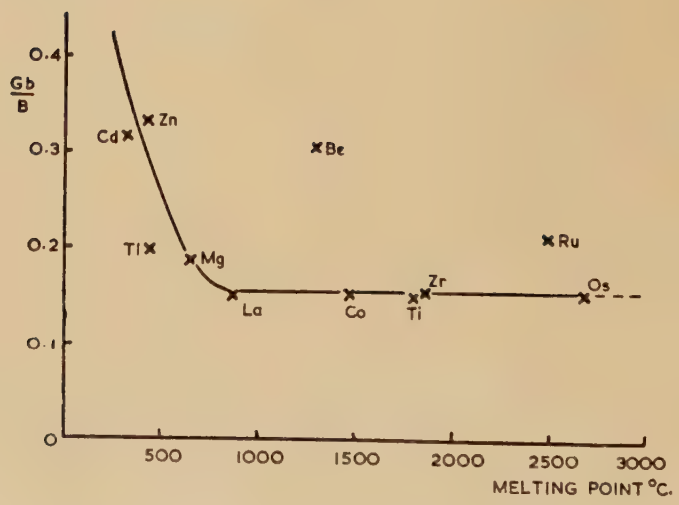

Hexagonal metals.

mechanical properties of ruthenium and the value of 220 for its hardness in table 2 is considerably lower than the predicted value of 306 points Brinell. Also contrary to expectation the predicted hardness of beryllium is double the hardness of the best vacuum cast ingot of the purest material now available. The predicted hardness is based on the behaviour of dislocations and their movements in slip processes, and if slip were the main mode of deformation then it should have the predicted hardness of 200 points Brinell. In fact beryllium deforms mainly by twinning (Lee and Brick 1952) and since in this metal twinning appears to be easier than slip, the measured hardness is below that predicted. Two consequences follow from this result. The first is that the stress for slip in beryllium is very high indeed (Brick, Lee and Greenewald 1951) and further purification is not likely to reduce it to a value low enough for slip to occur in preference to twinning. Secondly, since the amount of deformation that can occur by twinning is limited, beryllium at room temperature even when pure will not be capable of undergoing large amounts of plastic deformation. The low observed hardness of ruthenium may also arise from the ease of twinning.

2.4. *Relevance of Testing Temperature in the Proposed Correlation*

Köster (1948 b) has shown that the variation in the elastic moduli with temperature is the same for most metals at the same homologous temperature and that the moduli diminish linearly with temperature from absolute zero to about one-third of the melting temperature in degrees absolute. If curves of elastic moduli plotted against homologous temperature for different metals are fitted for values of the modulus at liquid air temperature they also fit at $Tm/3$. In this low temperature range the hardness of metals also diminishes slowly with increasing temperature (Druyvesteyn 1947). Direct evidence is however lacking since measurements at only a few temperatures have been made. The relation between shear modulus and hardness discussed above is valid over a range of temperatures including room temperature, if the change in hardness with temperature is entirely due to a change in the shear modulus for temperatures below $Tm/3$. The measurements of hardness at liquid air temperatures reported by Druyvesteyn (1947) indicate that at liquid air temperatures the hardness has increased by about 20%, i.e. twice as much as would be predicted. This is probably due to the difference in mobility of vacancies produced during deformation. For b.c.c. metals the increase is an order of magnitude greater than the predicted increase. Nabarro (1948) has explained the latter increase in terms of the locking of dislocations by interstitial solute atoms. This hardening effect is the probable cause of the poor correlation at very low temperatures, and among the b.c.c. metals. The high value for the hardness of tungsten at room temperature may also be due to this dislocation locking phenomenon.

In the higher temperature range in which relaxation effects exist, the value of shear modulus and hardness obtained will depend on the rate of

straining during testing. For given conditions of determination of elastic and plastic properties correlation between G and B can still be obtained by introducing the extra term in the expression which is dependent on reduced temperature. Altering the experimental conditions under which the mechanical properties are determined will result in curves similar to those in figs. 1–3 but the rising part will be of different slope.

The hardness of metals at high temperatures neglecting relaxation processes can now be predicted by substituting the correlation factor c, and the value of G at the appropriate temperature in the formula $B=Gb/c$. The value of hardness so obtained indicates the behaviour of the metal under shock loading at temperatures above $Tm/3$, since $f(T/Tm, t)$ will also be zero when t is zero or very small.

2.5. *Discussion of* § 2

Relaxation processes at room temperature can be neglected for all metals with melting points above about 900°C so that for these metals Gb/B is constant to $\pm 10\%$ in each group of metals of the same structure. The factor c for the hexagonal metals has an average value one-half of the average value for the cubic metals. This is to be expected from the lack of slip modes (Taylor 1938) in single crystals of hexagonal metals to which must be attributed an effective doubling of the intrinsic hardness of these metals in polycrystalline form.

Since the forces to move dislocations also depend on the distribution of widths of Frank–Read sources, it must be concluded that this distribution is in fact the same for all metals of the same structure, an assumption made in arriving at the function relating elastic shear modulus and plastic shear strength.

The elastic constants of metals are not markedly affected by impurities, for example Köster and Rauscher (1948) found that in many binary alloy systems including Mo–W, Co–Pt, and Cu–Ni the modulus of the alloys was a linear function of composition between the values of those of the constitutents. Thus when 1% iron is added to gold the modulus is raised 1%, while 1% tin diminishes the modulus by 2%. Ten per cent palladium raises the modulus of silver by 20%; this was the largest increase measured for any alloying addition to silver.

The most serious source of error in determination of elastic properties of polycrystalline metals arises from the presence of preferred orientation in the samples on which measurements are made (Köster 1948 b). Since the individual crystals of many metals are elastically anisotropic, the values obtained for the elastic constants will vary markedly with the type of preferred orientation in the samples examined. For instance values of the modulus of torsion of an iron single crystal about a [100] and a [111] axis differ by a factor of two (Barrett 1953). It is assumed that the values quoted are those for samples in which the crystal orientation is random, but this may not always be the case.

Plastic properties of metals are structure sensitive and are modified by impurities, inclusions and defects in the lattice. Sachs and Weerts (1930) have shown that a 5% addition of silver to gold, an addition which changes the elastic moduli by a few per cent, will increase the yield stress by a factor of two, while Greenland (1937) has shown that the yield stress of mercury at −60°C decreases when the impurity content decreases from 10^{-5} to 10^{-8}. The mechanical properties discussed in this report, namely elongation, hardness and tensile strength, while structure sensitive are less so than yield point, since they involve a large amount of deformation which itself introduces structural faults into the lattice. It seems probable that these properties are not altered appreciably by impurities present in amounts less than 10^{-4}, except in the case of interstitial atoms in a b.c.c. metal. Since it is assumed that metal of such purity is displaying properties unaffected by the small amount of impurity remaining, these mechanical properties are defined as the ' intrinsic ' properties of the metal. It is also assumed in conformity with the above definition that most elastic properties quoted in the tables are the ' intrinsic ' properties of the metals, since they are for annealed metals of 99·99% purity.

§ 3. Relation of Bulk Modulus to Fracture Stress

Fracture Theory

To complete the description of the plastic behaviour of polycrystalline pure metals under given stressing conditions a knowledge of the rate of work hardening and the true fracture stress is required in addition to the resistance to plastic shear which has been derived in the previous section from the elastic shear modulus. It would then be possible to correlate the tensile stress–strain curves for all metals.

None of the metals dealt with here fails by truly brittle fracture under uniaxial tensile stress, but some of the results of study of brittle fracture can usefully be employed in this discussion. In fact, some metals do not fracture at all in tensile testing but neck down to a point. Speculation on the fracture strength of these materials is however important since it might explain why plastic deformation occurs in preference to fracture. The ease of fracture in part determines the stage in work hardening at which fracture occurs.

The stress concentrations occurring near the roots of cracks have been calculated by Inglis (1913). Just beyond the root of a crack a triaxial stress field is set up when an overall uniaxial tensile stress is applied. The local stress here has at least one tensile component greater than the applied stress and into this region the crack penetrates, if the applied stress is sufficiently great. The elastic strain in this region will depend on the bulk modulus of the material.

The work done during fracture is converted partly into the energy of plastic deformation, partly into elastic energy and partly into surface energy (Griffiths 1920). The proportion of the energy absorbed by plastic

deformation will be greater the greater the ease of plastic deformation in relation to ease of fracture. The elastic energy is in part recoverable during fracture, although much is dissipated.

Since the work expended in causing fracture must be converted partly to surface energy of the freshly created surfaces (Obreimoff 1930), then true fracture stress should be related to surface energy, provided the law of force for lattice separation is the same for all metals considered. Values for the surface energy of metals are not known and it is therefore useful to employ here the correlation of surface energy and elastic constants previously suggested by Elliot (1947). In fig. 4 the force between those neighbouring atomic planes which are separated by the fracture surface is plotted against the separation in excess of the equilibrium separation in the absence of applied stress. When a stress is applied large enough to cause crack propagation the work done in separating the two planes will be proportional to the area under the curve and since none of this work is recoverable, it will be entirely converted to surface energy.

Fig. 4

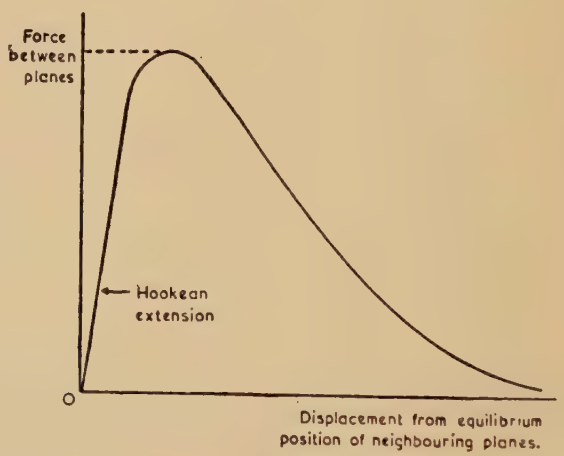

Relation between force and separation of neighbouring planes.

The force-displacement curve, fig. 4, is assumed to be of the same form for all metals of the same structure, and the abscissa scale is assumed to be proportional to the lattice parameter. The ordinate scale will depend on an elastic modulus relevant to the relation between uniaxial tension and linear extension with the normal directions constrained to remain constant. This modulus will therefore lie between the bulk modulus and Young's modulus, and for convenience here the value of the bulk modulus will be used in the correlations. The curve, fig. 4, relating stress to atomic separation shows an initial linear increase following Hooke's Law, the rate of increase then falling off until the stress decreases with increasing separation and falls to a negligible value. The conditions just beyond the root of the crack are here being considered, where, due to the triaxial

stress concentration, the shear stress is small, and the dilatational elastic strains can rise to much greater values than are usually obtained before plastic shear relaxes the stresses. The maximum of the curve, fig. 4, can be considered to be the true ultimate fracture stress. Since it has been assumed that this one curve will apply to all metals of the same structure if the vertical values are divided by the bulk modulus and the horizontal values by the lattice parameter, it follows that for each group of metals the surface energy per unit area, given by the area under the curve will also be proportional to the product of the bulk modulus and the lattice parameter. The magnitude of this product will therefore be used as a criterion of the intrinsic fracture stress in each group of metals of the same structure, so that intrinsic fracture stress $\sigma \propto Ka$ (3).

In relating the intrinsic fracture stress to the true stress at fracture it is necessary to take into account the stress concentration factor, which is a function of the shape and sharpness of the crack. Since the crack will become less sharp when plastic flow occurs, it follows that the stress concentration will decrease as the plastic shear stress decreases. Thus true fracture stress

$$\tau \propto Ka/f(Gb/K). \quad . \quad . \quad . \quad . \quad . \quad . \quad . \quad (4)$$

For most pure metals the stress concentration factor will not be large and the variation of this factor from metal to metal will be small, therefore $f(Gb/K)$ in expression (4) above is sufficiently constant to be neglected in first order of magnitude calculations, so that $\tau \propto Ka$.

It seems unlikely that temperature will have any effect on fracture stress other than through its small effect on the bulk modulus. In the high temperature range, on the other hand, failure is more likely to be entirely plastic by necking, so that in this range of temperature, fracture by crack propagation is of practical interest, only where conditions of shock loading exist.

§ 4. Elastic Constants and Malleability of Pure Metals

4.1. *The Stress–Strain Curve*

If certain assumptions are made concerning the shape of stress–strain curves in the plastic range, the relative malleability of individual metals in a group can be related to the size of the gap between the stress required to produce a given small strain and the true fracture stress ; alternatively, malleability can be related to the difference between ease of plastic shear and ease of fracture. Since both the latter quantities have been related to the elastic constants, the correlation can be extended to include malleability. The actual shape of the stress–strain curve is not being considered here, and therefore ductility will not be discussed, since it is related to the uniform elongation which in turn is related to the shape of the stress–strain curve. The quantity related to the elastic constants will be the local strain at the neck of a tensile test piece after fracture.

To discuss the correlation of elastic properties and malleability, it is proposed to introduce the assumption that stress is the same function of strain for all pure metals with the same lattice structure. The stress–strain curves will then differ only in the stress scale and the point at which the curve is terminated at fracture. In other words, for metals of a given lattice structure, it is assumed that the true stress–true strain curves can be made to superpose merely by multiplying stress by a different factor for each metal. This is only approximately true for metals of high melting point ; low melting point metals can not be included in this correlation at all because they have work hardening curves of an entirely different form.

Once the stress–strain curve for one metal in a group has been determined, the curve for any other metal in the group can be constructed from a knowledge of one point on the latter curve, since the curves differ only in the stress scale. The measured hardness will provide such a point since it represents a certain average strain produced by a given stress system (Tabor 1951). For high melting point metals hardness has been correlated with the elastic shear modulus and Burgers vector, so that these quantities can be used to fix the multiplying factor required to construct the stress–strain curve for any metal in a given group.

Fig. 5

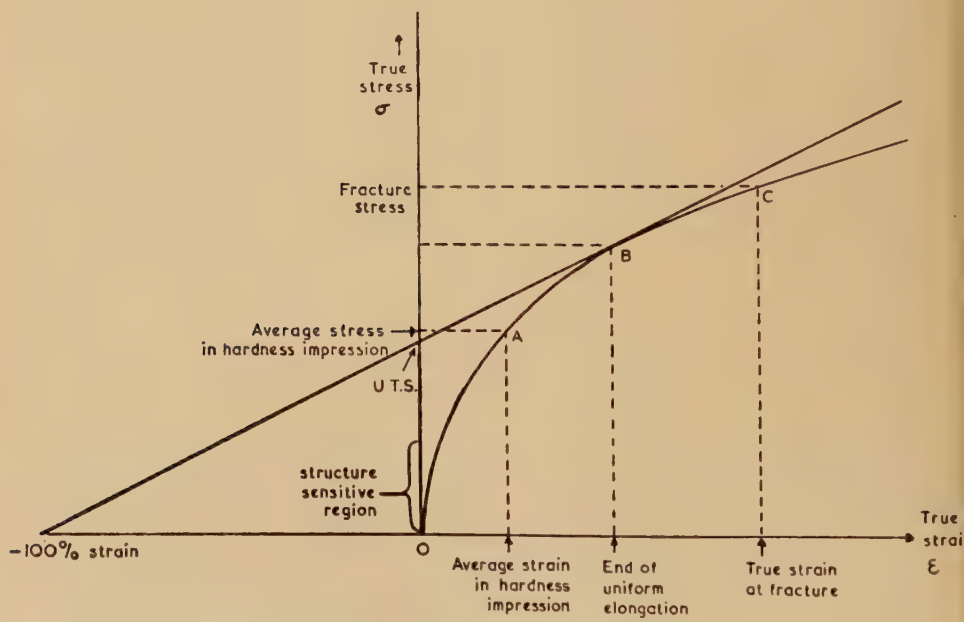

True stress–true strain curve OABC.

The curve OABC, fig. 5, is a true stress–true strain curve for a group of metals with the same lattice. The point A is fixed from a knowledge of the Brinell hardness. In this group of metals the abscissa of A, being the average strain in the hardness impression, will be the same for all metals, while the ordinate will be proportional to the hardness number, which in

turn, can be derived from the elastic shear modulus. Thus the vertical scale of the stress–strain curve can be fixed using the shear modulus G and Burgers vector, b. The stress for any given strain is therefore given by the product Gbg and the work hardening function, where g is constant within each group of metals.

From the analysis of Sachs and Fick (1926) the point B at which the tangent from -100% strain touches the curve, fig. 5, corresponds to the point at which necking begins, and is thus the point of maximum load. The tangent touches the curve at a point whose abscissa is independent of the vertical scale of the curve, so that the strain at the beginning of necking must also be constant in the group of metals considered. It therefore follows that the ultimate tensile strengths of metals of high melting point in this group will also be proportional to Gb.

4.2. *The Strain at Fracture*

Having related the stress scale of the curve OAB to Gbg it is now necessary to fix the point C at which fracture occurs. In the previous section reasons were given for believing that the true fracture stress was proportional to the bulk modulus and lattice parameter in a group of metals of the same lattice structure. Thus the ordinate of the point C is fixed, and this fixes the abscissa for the true strain at fracture. Whereas the true fracture stress is rarely measured, the true strain at fracture or its equivalent the reduction in area is measured and is an indication of malleability. It follows immediately that the malleability will be greater, the greater the fracture stress. The strain at fracture will decrease as the vertical scale of the curve is increased, that is as Gb increases. If the true stress–true strain curve is defined by $\epsilon=f(\sigma/Gb)$ and the intrinsic fracture stress is $\sigma_F=Kad$, where d is a constant, then the strain at fracture is $\epsilon_F=f(Kad/Gb)$. Thus if $\epsilon\propto\sigma^2$ then $\epsilon_F\propto(Kad/Gb)^2$. In a group of metals with the same lattice structure a/b is constant, so that $\epsilon_F=\phi(K/G)$. In the hexagonal group differences in axial ratio do cause small differences in the ratio a/b, but these can be neglected.

The reduction in area indicates the extent of the local strain in the region of fracture and is thus the best indication of malleability ; however figures are available for few pure metals and therefore the correlation will be based on the total elongation at fracture, which includes for each metal a different proportion, though constant amount, of uniform elongation. In view of the lack of suitable experimental data it is not intended to press the correlation too far, but merely to put metals in order of malleability and to note whether very brittle and very malleable metals have the expected values of K/G and Poisson's ratio.

In materials with low K/G, which are expected to be brittle, the stress concentration at the root of a crack will be high since plastic flow is relatively difficult. This adds to the brittleness of these materials deduced from the value of K/G. Thus brittleness is a co-operative phenomenon, and will appear fairly sharply below a given value of K/G in pure metals.

The modulus ratio K/G is related to Poisson's ratio n.

For $$\frac{K}{G}=\frac{2(1+n)}{3(1-2n)} \text{ or } n=\frac{3K/G-2}{6K/G+2}.$$

Thus malleability should also correlate with Poisson's ratio.

4.3. *Comparison of the Parameter K/G and Elongation at Room Temperature*

(*a*) *High Melting Point Metals*

The metals are again separated into groups, according to their lattice structure, f.c.c., b.c.c., and h.c.p. Values for the parameter K/G and elongation values of pure samples where available are shown in table 4. Among the f.c.c. metals of high melting point in table 4, K/G varies from 1·74 for iridium to 6·14 for gold indicating on the present proposed correlation that pure gold is the most malleable f.c.c. metal and iridium the least malleable. This prediction would appear to be correct since gold can be beaten into leaf which is translucent, while iridium is only worked above 1500°c. Copper, silver, palladium and platinum all have high values of K/G indicating good malleability when pure, and this is in agreement with their observed behaviour. The values of K/G would indicate that thorium and rhodium should have low elongations at room temperature.

In the hexagonal group the lack of slip modes causes these metals to be generally more brittle than the cubic metals but there is still a wide range of malleability. Again comparing values of K/G with malleability, titanium, zirconium and hafnium all have high K/G values in agreement with the observation that these are the hexagonal metals which will withstand the greatest amount of cold work before fracture. Cobalt and magnesium have intermediate K/G values as would be expected. Rhenium, ruthenium and osmium all have low values of K/G and of these osmium is known to be brittle. Beryllium has the lowest value of K/G or Poisson's ratio for any metal ; it is therefore deduced that the lack of malleability of this metal is an inherent property of the pure metal, and is not merely due to impurities in solution, oxide films or other inclusions, although the latter will still have a deleterious effect.

The b.c.c. metals all have approximately the same values of K/G and Poisson's ratio. The high melting point metals would on this basis all be expected to have equal malleability and this appears to be the case for all metals except tungsten, which on the previous correlation also was suspected of being hardened by impurity.

The remaining metals have various lattice structures, and a large range of K/G values. The K/G value for manganese is low, but this must not be correlated with its brittleness, since the main reason must be the lack of an easy slip mode in the complex lattice of α manganese (Bradley and Thewlis 1927). Quenched γ manganese is plastic and presumably must have very different elastic properties. The brittleness of antimony, bismuth, silicon and germanium must also be ascribed to the lack of

straight close-packed rows of atoms in the crystal lattice. Uranium is a borderline case since the slip modes are more restricted than those in hexagonal metals (Cahn 1953) and confer only a limited malleability. The very malleable metals in this group all have low melting points.

Table 4. Criterion K/G and Elongation of f.c.c. and h.c.p. Metals

F.c.c.	Rigidity modulus G kg/mm^2	Bulk modulus K kg/mm^2	K/G	Poisson's ratio	Elongation %	Purity %
Calcium	750	1750	2·33	0·31	60	
Strontium	620	1220	1·97	0·28		
Aluminium	2720	7460	2·74	0·34	50	99·99
Thorium	3160	5500	1·74	0·26		
Nickel	7500	18900	2·52	0·32	30	99·95 (Ni+Co)
Rhodium	15300	27000	1·77	0·26	Small	
Iridium	21400	37300	1·74	0·26	Small	
Palladium	4450	19000	4·27	0·39	40	99·9+
Platinum	5300	27800	5·25	0·44	40	
Copper	4640	13900	3·00	0·35	60	99·99
Silver	2940	10100	3·44	0·37	60	99·99
Gold	2820	17300	6·14	0·42	50	99·99
Lead	570	4200	7·37	0·44	64	99·99
H.c.p.						
Beryllium	13500	11700	0·867	0·08	1	
Magnesium	1770	3390	1·915	0·28	16	99·98
Lanthanum	1500	2840	1·90	0·28		
Titanium	3870	12500	3·23	0·36	37	
Zirconium	3540	9100	2·58	0·33	40	
Hafnium	3100	11100	3·58	0·37		
Cobalt	7630	18500	2·43	0·31		
Rhenium	21000	37000	1·76	0·26		
Ruthenium	17600	29000	1·65	0·25		
Osmium	22800	38000	1·67	0·25	0	
Zinc	3790	6000	1·59	0·27	25	99·99
Cadmium	2460	5000	2·03	0·29	50	99·99
Thallium	280	2900	10·3	0·45	Large	

(b) Plasticity at Low Temperatures

From the above survey it is concluded that qualitatively K/G and Poisson's ratio correlate with malleability in the way which was expected from the argument developed earlier.

The discussion so far has been concerned with the properties of metals at room temperature mainly because more data for room temperature properties are available. The effect of low temperature on the mechanical properties of a particular metal will depend in the first place on whether deformation at room temperature involves relaxation processes. In the earlier discussion it was concluded that relaxation processes would cause a large drop in hardness but not in fracture stress, so that the malleability for a given value of K/G should be much greater in low melting point metals. This is found for example in zinc and cadmium which have greater elongation values than magnesium although the values of K/G are about the same. At liquid air temperature zinc is fairly brittle, as would be expected assuming K/G is not greatly different at the lower temperature, while there is much smaller increase in the brittleness of magnesium at the lower temperature (Druyvesteyn 1947). The lithium and sodium group of metals also have enhanced malleability arising from the occurrence of relaxation processes at room temperature.

For metals in which relaxation effects do not occur appreciably during deformation at room temperature, the plastic shear strength at lower temperatures will change in proportion with the shear modulus, both increasing as the temperature is diminished. The change in malleability with decreasing temperature will depend on the relative rates of change of the shear and fracture strength that is of G and K. In general these appear to change at the same rate, so that malleability is independent of temperature until relaxation processes begin to occur. Thus for zirconium the elongation changes little with temperature from $-196°$ to room temperature (Rosi and Perkins 1952). Iron begins to twin rather than slip and becomes more brittle at low temperatures, and a new phenomenon is assumed to affect deformation by slip at low temperatures, due to the presence of interstitial solute atoms of carbon or nitrogen. Most body centred cubic metals become brittle and increase in hardness in much higher proportion than the expected increase in shear modulus when tested at liquid air temperatures. This increase in hardness can be correlated with an increase in steepness of the stress–strain curve which was previously assumed to have the same shape for all metals of the same structure. In contrast sodium becomes more malleable at $-253°$C. The reason for the increased or diminished work hardening rate at very low temperatures is difficult to seek. Tungsten is the metal of highest melting point, and so for tungsten room temperature represents a low homologous temperature ; the mechanical properties of tungsten show a significant divergence from the correlation with the elastic constants at room temperature being both harder and more brittle than would be predicted, in the same way that other b.c.c. metals behave at lower temperatures.

In face centred cubic metals the increase in hardness on cooling to $-183°$C is about 20% while the change in shear modulus is more likely to be 10%. For a metal melting at 1000°C this change in temperature

is, however, larger in terms of the homologous temperature than the difference of homologous temperature between this metal and one melting at 2500°C, both considered at room temperature. There is no sign that iridium (melting at 2545°C), tantalum (melting at 2850°C) or osmium (melting at 2700°C) diverge from the proposed correlations by more than 10%. The change in mobility of vacancies with temperature therefore has only a small effect on the stress–strain curve in the temperature range below $Tm/3$ and for strains below about 20%.

4.4. *Other Parameters for Malleability*

In addition to the elastic constants, it has been shown that the lattice structure also has to be considered in predicting the plastic properties of pure metals, since it determines the deformation modes. Hardness, brittleness or malleability do not directly correlate with melting point or axial ratio, as can best be seen in the hexagonal group of metals. Zirconium and titanium are both malleable and yet lie between beryllium and osmium in melting point, and between beryllium and magnesium in axial ratio, all these metals being less malleable than zirconium and titanium. Even in this group hardness and malleability correlate with elastic moduli in the manner discussed previously, and it is suggested that the increase of hardness with melting point (to which beryllium is an exception), occurs only because, in general, shear modulus can be correlated both with hardness on the one hand and melting point on the other.

4.5. *Anisotropy*

In correlating shear modulus with ease of slip it would be preferable to take the modulus for shear on the slip plane in the slip direction rather than the average shear modulus, but these values are not available for most metals. Since in general slip occurs on systems for which the relevant shear modulus is below the average value in metals possessing elastic anisotropy, it follows that the average shear modulus for these anisotropic metals will indicate too high a slip stress for these metals. Since single crystal anisotropy will in general result not only in planes of easy slip but also in planes of easy cleavage, its resultant effect on malleability may be only small. In the same way occurrence of cleavage is not necessarily an indication of brittleness, since it is likely to be accompanied by a plane of low critical shear stress in the single crystal.

The other result of anisotropy has already been mentioned namely that which results in an incorrect average value for elastic constants due to the presence of preferred orientation in the samples tested.

4.6. *The Periodic Law and Plastic Properties of Metals*

Köster (1948 b) noticed that the value of the elastic constants of metals is a function of their position in the periodic table. The value of Young's modulus varies periodically with atomic number, while in each sub-group Poisson's ratio is constant within narrow limits and the lattice structure

of all elements in a given sub-group is usually the same. Since it has also been shown that the plastic properties are a function of the elastic properties of the elements of the same lattice it follows that the plastic properties of metals will be functions of their position in the periodic table. These correlations arise, of course, from the fact that the electronic structure and atomic volume and hence type of binding in the lattice determines the position of an element in the periodic table. Thus in sub-group IVA zirconium, titanium and hafnium are hexagonal metals with Poisson's ratio 0·36 and these metals are the most malleable hexagonal metals ; in group IB, copper, silver and gold are f.c.c. metals, their Poisson's ratio is 0·35–0·42 and they are very malleable ; in sub-group IIB magnesium, zinc, and cadmium are hexagonal with small malleability. Beryllium has a special position in the periodic table consistent with its possession of unusual properties.

§ 5. Conclusions

Assuming that pure metals of any given lattice will have the same work hardening mechanism it has been shown that the room temperature hardness, tensile strength, and intrinsic fracture strength can be related to the elastic constants for metals with melting points above 900°c. Thermally activated processes take place during deformation at room temperature in metals with melting points below 900°c, modifying the plastic behaviour. In these metals plasticity at low temperature can be predicted.

The above correlations are consistent with the conclusion reached in dislocation theory, that most of the energy of a dislocation is stored outside the core, in that part of the lattice in which the strains are Hookean.

Acknowledgments

The author wishes to thank Dr. W. M. Lomer and Dr. J. W. Glen for invaluable discussions during the preparation of this report and Dr. H. M. Finniston for his continued help and encouragement.

References

American Society for Metals, 1948, *Metals Handbook.*
Barrett, C. S., 1953, *Structure of Metals* (New York : McGraw-Hill), p. 533.
Bradley, A. J., and Thewlis, J., 1927, *Proc. Roy. Soc.* A, **115,** 456.
Brick, R. M., Lee, H. T., and Greenewald, H., 1951, *U.S.A.E.C. Report N.P.* 3112.
Bridgman, P. W., 1952, *Studies in Large Plastic Flow and Fracture* (New York : McGraw-Hill).
Cahn, R. W., 1953, *Acta Met.*, **1,** 49.
Druyvesteyn, M. J., 1947, *Appl. Sci. Res.* A, **1,** 66.
Elliot, H. A., 1947, *Proc. Phys. Soc.*, **59,** 208.
Frank, F. C., and Read, W. T., 1950, *Phys. Rev.*, **79,** 722.
Greenland, K. M., 1937, *Proc. Roy. Soc.* A, **163,** 34.
Griffiths, A. A., 1920, *Phil. Trans. Roy. Soc.* A, **221,** 180.

Inglis, C., 1913, *Proc. Inst. Nav. Archit.*, **219**.
Köster, W., 1948 a, *F.I.A.T. Review of German Science, General Metallurgy*, p. 41 ; 1948 b, *Zeit. f. Metallkde.*, **39,** 145.
Köster, W., and Rauscher, W., 1948, *Zeit. f. Metallkde.*, **39,** 111.
Lee, H. T., and Brick, R. M., 1952, *J. Metals*, **4,** 147.
Molenaar, J. C., and Aarts, W. H., 1950, *Nature, Lond.*, **166,** 690.
Mott, N. F., 1951, *Proc. Phys. Soc.* B, **64,** 729.
Nabarro, F. R. N., 1948, *Rep. Conf. Strength of Solids* (London : Physical Society), p. 38 ; 1952, *Advances in Physics*, **1,** 269.
Nash, J. W., Ogden, H. R., Durtschi, R. E., and Campbell, I. E., 1953, *J. Electrochem. Soc.*, **100** (6), 272.
Obreimoff, J. W., 1930, *Proc. Roy. Soc.* A, **127,** 290.
Raynor, G. V., 1946, *J. Roy. Aeronaut. Soc.*, **50,** 390.
Reynolds, M. B., 1952, *U.S.A.E.C. Report A.E.C.U.*—1894 and 1953, *Trans. A.S.M.*, **45,** 839.
Rosi, F. D., Dube, C. A., and Alexander, B. H., 1953, *Trans. A.I.M.E.*, **197** (*J. Metals*, **5**), 257.
Rosi, F. D., and Perkins, F. C., 1952, *U.S.A.E.C. Report SEP*-87.
Sachs, G., and Fick, G., 1926, *Der Zugversuch* (Leipzig).
Sachs, G., and Weerts, J., 1930, *Zeit. Phys.*, **62,** 473.
Sloman, H. A., 1932, *J. Inst. Metals*, **44,** 365.
Tabor, D., 1951, *The Hardness of Metals* (Oxford : Clarendon Press).
Taylor, G. I., 1938, *J. Inst. Metals*, **62,** 307.

XCIII. *The Hardness Properties of Cube Faces of Diamond*

By E. M. Wilks and J. Wilks
Clarendon Laboratory, Oxford*

[Received March 23, 1954]

Summary

Experiments have been made on the abrasion hardness properties of polished cube faces of diamond in directions parallel to the crystallographic axes. Provided the faces coincide with the lattice planes, a four fold symmetry of hardness is observed. However, a misorientation of the face with respect to the lattice of more than 30 min produces an asymmetry in the hardness values. This may well explain why diamond polishers have seldom found the four-fold symmetry on cube planes, for it is very difficult to grind a face on a substance as hard as diamond to within a few minutes.

§ 1. Introduction

It has long been known that the abrasion properties of diamond are very varied, that certain faces are harder than others, and that not all directions on a given face are equally easy to abrade or polish ; there have also been several attempts to relate these variations in hardness with the underlying structure of the diamond (Tolkowsky 1920, Stott 1931, Kraus and Slawson 1939). Although none of these treatments is entirely satisfactory, they all lead to hardness properties which exhibit the full symmetry of the diamond, as indeed might be expected from any theory. However, it has often been mentioned (e.g. Grodzinski 1952) that diamond polishers do not observe complete symmetry, and we have therefore investigated this point in some detail by a study of the hardness properties of cube planes.

The hardness of the cube plane, as determined by its resistance to abrasion or polish, is very dependent on the direction of abrasion. Such a face is comparatively easy to grind in directions parallel to the crystallographic axes, but becomes extremely hard in directions at 45° to the axes. This great variation in hardness is itself an interesting problem, but here we are concerned only with the question of whether it is equally easy to abrade the face in each of the four directions parallel to the crystallographic axes. A certain amount of experimental evidence is available, but it is rather inconclusive. Tolkowsky (*loc. cit.*) found that the four directions parallel to the axes were not equally easy to polish, but on the other hand, he was not able to obtain facets that corresponded

* Communicated by Professor Sir Francis Simon, F.R.S.

exactly with the cube planes. However, Tolkowsky surmised that had he abraded true cube planes, then the four-fold symmetry would have been observed ; therefore he averaged his results to show this symmetry. Later it was shown (Wilks, E. M. 1952) that a striking feature of the asymmetry was the difference in hardness between parallel but opposite directions. She also found that the asymmetry could be reduced, but not eliminated, if the faces to be ground were oriented by means of x-rays. Finally Denning (1953) has reported that it is possible to realize the four-fold symmetry by tilting the plane of the facet until the effect is obtained ; apart from this symmetry, however, there seems to be no evidence that the effect was observed on true cube planes. Denning also showed that very small changes in orientation produced large changes in the symmetry properties. Thus although it appeared that the effect reported by polishers was quite consistent with their not having worked on true cube planes, there was no conclusive evidence. Indeed it has been suggested (Grodzinski *loc. cit.*) that the effect was a manifestation of the lower tetrahedral symmetry for diamond which has been proposed by various authors (Eppler and Rose 1925, Raman 1944, Raman and Ramaseshan 1946), even though it now seems that this symmetry is inconsistent with x-ray data (Lonsdale 1945).

§ 2. The Experiments

In order to make a detailed investigation of the abrasion properties, we obtained a cube of diamond cut from a natural octahedron ; it was claimed that two adjacent faces had been located to within $\pm$ 30 min by means of x-rays and the remainder oriented with respect to them. The abrasions on each face were made parallel to the edges of the cube, which were assumed to be parallel to the crystallographic axes. The abrasions were made using the Grodzinski micro-abrasion tester (see for example Grodzinski 1952), and the criterion of hardness taken to be the reciprocal of the depth of cut which was determined by multiple beam interferometry with an accuracy of $\pm$ 0·1 $\lambda/2$ (Wilks, E. M., *loc. cit.*).

It was known from previous work that the depth of abrasion was inevitably affected by variations in the process of abrasion, in particular by the amount of diamond powder on the wheel, and the degree of blunting of the wheel during the tests. To allow for these effects, 10 cuts were made on each face, four cuts parallel to one edge and two cuts parallel to each of the other three edges. The first three cuts were made in the same direction ; the stone was then rotated through successive angles of 90°, and one cut made after each rotation. An analysis of the results from the 6 faces showed that the depth of cut was reproducible to about 10% ; this figure sets the limit to the accuracy of the experiment.

As the edges of the diamond cube were only 2·5 mm long, the size of cut had to be reduced from that of previous experiments ; we used $\frac{1}{2}$ inch diameter cast iron wheels which gave cuts about 5×10^{-2} cm long. As we were not concerned with a direct comparison of hardness

between faces, we replaced the wheel when it showed signs of becoming blunted. However, a given wheel made all 10 cuts on a given face, being recharged with diamond powder of 0–1 micron size after 5 runs on each face.

§ 3. Experimental Results

Table 1 shows the average depths of the abrasions on each of the faces,

Table 1

Face	Direction of Abrasion	[00$\bar{1}$]	[001]	[010]	[0$\bar{1}$0]
($\bar{1}$00)	Depth : units of $\lambda/2$	15·4	14·8	14·2	12·3
(100)		14·4	15·4	16·7	14·4
Face	**Direction of Abrasion**	[$\bar{1}$00]	[100]	[001]	[00$\bar{1}$]
(010)	Depth : units of $\lambda/2$	13·1	8·1	4·6	15·3
(0$\bar{1}$0)		7·8	11·1	11·9	5·7
Face	**Direction of Abrasion**	[$\bar{1}$00]	[100]	[0$\bar{1}$0]	[010]
(001)	Depth : units of $\lambda/2$	18·2	12·6	11·6	18·5
(00$\bar{1}$)		7·2	19·0	16·9	5·9

which are labelled crystallographically. The direction in which each abrasion was made is given by the appropriate crystallographic axis ; this axis indicates the direction in which that part of the wheel in contact with the stone was moving. (The layout of cuts on a typical face, together with their directions, is shown in fig. 1.) On four faces there is a marked asymmetry between the depths of cut in the axial directions, with a noticeable difference between parallel but opposite directions of abrasion ; in one case the ratio between the depths of cut in opposite directions is greater than 3 : 1. On the remaining two faces, however, there is no difference in depth of cut between the four directions, and within the experimental limits these two faces therefore exhibit a four fold symmetry.

As the complete symmetry on the cube was not observed, we decided to check the orientations of all the polished faces by optical and x-ray goniometry. X-ray measurements on three faces gave results consistent with the optical observations to within 15 minutes, this limit being set by the x-ray technique.

The results of these measurements are shown in table 2. As the stone is approximately a cube, we may suppose to a first approximation that two independent rotations, about two of the cubic axes, will translate the plane of a given facet into the corresponding lattice plane. The results

Fig. 1

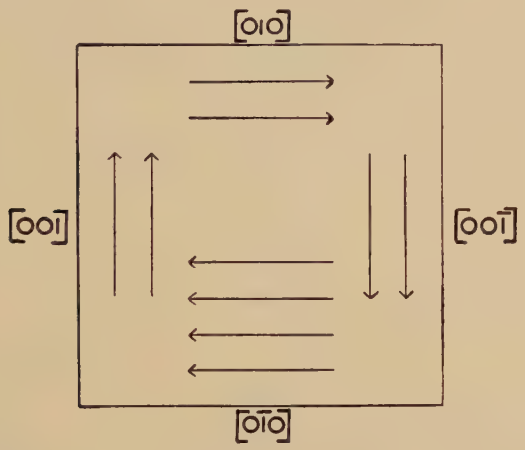

The layout of the abrasions on a typical face (100).

of the goniometer measurements are therefore expressed (in table 2) as the angles and directions through which the plane of a facet must be rotated in order for it to coincide with the lattice. (The direction of rotation is indicated by the plane towards which the rotation is to be made.) It is seen that while two faces are parallel to the lattice to within the accuracy of our measurements, the others are not truly aligned, and one is misoriented by as much as 135 min.

Table 2

Cube Face	($\bar{1}$00)		(100)		(010)		(0$\bar{1}$0)		(001)		(00$\bar{1}$)	
Angle from facet to lattice	2′	9′	2′	21′	61′	135′	43′	80′	37′	73′	65′	125′
Direction of Rotation	(00$\bar{1}$)	(0$\bar{1}$0)	(010)	(001)	(100)	(001)	($\bar{1}$00)	(00$\bar{1}$)	(100)	(0$\bar{1}$0)	($\bar{1}$00)	(010)

We now consider the effects of this misorientation. One result is that the edges of the cube will not be exactly parallel to the crystal axes. As the directions of the abrasions were made parallel to an adjacent edge, these too will not be quite parallel to an axis. However, a series of subsidiary tests confirmed earlier observations that at an azimuthal angle of as much as 5° off true, the depth of cut was reduced by no more

than about 10%. Thus to the accuracy of our measurements, this particular effect may be ignored. The essential point seems to be the alignment of the facet with respect to the crystal lattice. First of all, this may result in the plane of the wheel not being perpendicular to the lattice planes. There is however no obvious correlation between such misorientation and the depths of the cuts, and any such effect is probably small. The main effect seems to be associated with a misorientation of the facet of the type shown in figs. 2 (*a*) and 2 (*b*). From tables 1 and 2 it may be seen that for two cuts on a given face, parallel and anti-parallel to a cubic axis, the deeper cut always occurs when the abrasion is as in fig. 2 (*a*), and the lesser cut as in fig. 2 (*b*). Moreover in fig. 3 we display

Fig. 2

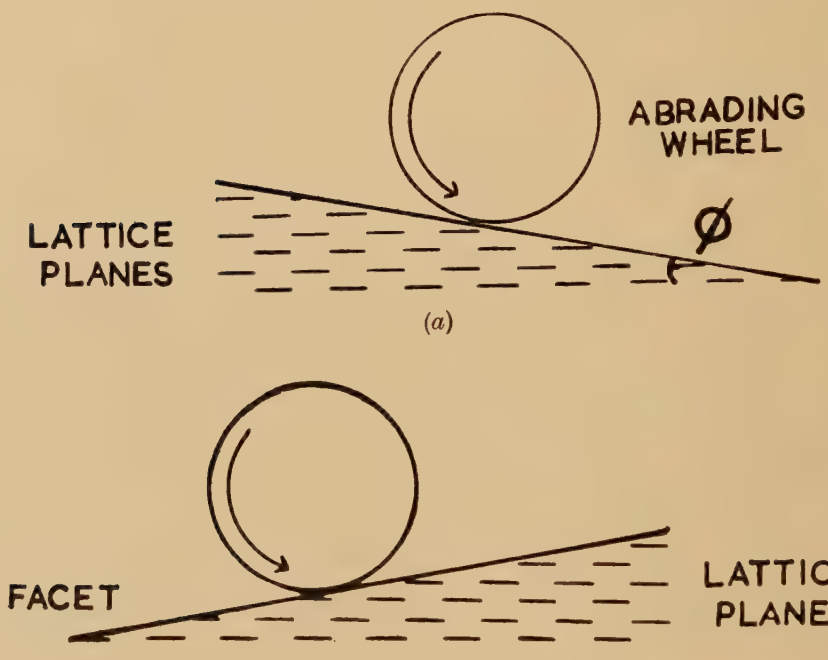

Diagrams to show possible orientations of the facets with respect to the cubic lattice planes. (Not to scale.)

these results by plotting the ratio of the depths of opposite cuts against the angle ϕ of fig. 2 (*a*), and it is clear that the asymmetry tends to vanish as ϕ approaches zero. That is to say, the asymmetry is due to the misorientation of the facets. Although it is clear that such misorientation will result in the abrading wheel striking the diamond asymmetrically with respect to the cleavage planes, we do not at present have sufficient data to discuss the underlying mechanism in detail. Further investigations are now in progress.

Finally we note that it is somewhat more difficult to correlate the depths of cuts made at right angles to each other on a given face with the misorientation of the face. However, it may be seen from table 1 that abrasions perpendicular to each other have appreciably different depths only when there are also considerable differences between parallel and anti-parallel cuts on the face. In particular, on the two faces that were approximately correctly aligned, the cuts on all four directions were of equal depths to within the experimental error.

Fig. 3

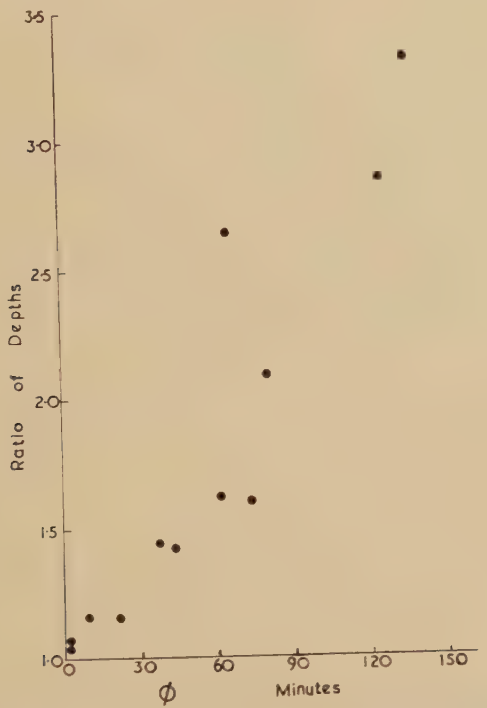

The ratio of the depths of parallel but opposite abrasions on a given face plotted against the angular misorientation of the face.

§ 4. Conclusions

It appears from these results that the hardness properties of cube faces of diamond exhibit the full cubic symmetry, but that these properties are very sensitive to any misorientation of the faces. Thus the inconclusive results of previous workers may be accounted for by the difficulty of obtaining facets coinciding exactly with the crystallographic planes. The use of x-rays to orientate the specimen therefore seems to be essential when investigating the hardness and related properties of diamond. (For example, we may mention that a nominal dodecahedron face was reported by Bowden and Kenyon (1953) to be as much as 6° to 8° off

true.) It must also be remembered that even if x-rays are used the diamond is so hard that it is still difficult to grind a facet to within ± 30 min.

Acknowledgments

We are most grateful to Mr. H. M. Powell, F.R.S., for providing us with facilities to make the goniometry measurements; to Mr. P. Grodzinski for the use of his micro-abrasion tester; and to Sir Francis Simon, F.R.S., for the interest he has shown in the work. We also wish to thank Industrial Distributors for a maintenance grant (E. M. W.) and I.C.I. for a Research Fellowship (J. W.).

References

Bowden, F. P., and Kenyon, D. M., 1953, private communication.
Denning, R. M., 1953, *Amer. Min.*, **38,** 108.
Eppler, W. F., and Rose, H., 1925, *Cent. f. Min.* A, 251.
Grodzinski, P., 1952, *Diamond Technology* (London : N.A.G. Press).
Kraus, E. H., and Slawson, C. B., 1939, *Amer. Min.*, **24,** 661.
Lonsdale, K., 1945, *Nature, Lond.*, **155,** 144.
Raman, C. V., 1944, *Proc. Ind. Acad. Sci.* A, **20,** 189.
Raman, C. V., and Ramaseshan, S., 1946, *Proc. Ind. Acad. Sci.* A, **24,** 1.
Stott, V., 1931, *N.P.L. Collected Researches*, **24,** 1.
Tolkowsky, M., 1920, *D.Sc. Thesis*, London.
Wilks, E. M., 1952, *Phil. Mag.*, **43,** 1140.

XCIV. *The Specific Heat of Graphite below* 90°K

By U. Bergenlid*, R. W. Hill, F. J. Webb and J. Wilks
The Clarendon Laboratory, Oxford†

[Received March 26, 1954]

Abstract

Values are given of the specific heat of graphite between 1·5°K and 90°K. Below about 12° the specific heat varies with temperature as $T^{2\cdot4}$; this is inconsistent with the work of several authors who, on theoretical grounds, have predicted a T^2 temperature dependence.

§ 1. Introduction

Several years ago two of us measured the specific heat of graphite in the temperature range 8 to 90°K in order to establish the absolute value of the entropy. At that time satisfactory specific heat measurements had only been made at temperatures above 90°K (Jacobs and Parks 1934), and therefore the value of the entropy had to be based on an extrapolation of the specific heat to lower temperatures. Although some results below 90°K had been obtained previously by Nernst (1911), they were too few and too inaccurate to give more than a rough indication of how the extrapolation should be made, so further measurements were deemed advisable. The results of these measurements entirely confirmed the accepted entropy values (Jacobs and Parks) and were therefore not published. Recently, however, considerable interest has been shown in anisotropic materials, and several authors have presented theoretical treatments of the specific heat of graphite. In addition de Sorbo and Tyler (1953) have given experimental values which are not in complete agreement with our own. Therefore, it seems worth while to publish these results, and also some recent values obtained at helium temperatures.

§ 2. Experimental Method for the Range 8 to 90°K (Bergenlid and Hill)

There are two difficulties which complicate the measurement of the low temperature specific heat of graphite. Firstly, owing to its small specific heat, the heat capacity of a specimen is rather small compared with that of a suitable calorimeter. The second difficulty is that graphite is a powerful adsorbent for gases, whose relative heat capacity may be considerable at low temperatures. By using a block specimen on to which thermometers and heaters can be wound directly, the use of a calorimeter may be avoided. Some provision must however be made for cooling the

* Now at the Royal Technical High School, Stockholm.
† Communicated by the Authors.

specimen and calibrating the thermometers without using exchange gas at low temperatures. A copper vessel of about 1 cm^3 capacity was therefore attached to the block. Two copper wires held the vessel in place and a layer of bakelite varnish helped to establish thermal contact between it and the block: the same varnish was used to mount the constantan heater and the constantan and platinum thermometers.

The assembly was mounted in a cryostat which incorporated a Simon helium liquefier and has been described elsewhere (Hill 1953). Cooling of the specimen was effected by condensing oxygen, hydrogen or helium gas under pressure in a tube leading to the copper vessel. Gentle pumping on a second tube helped the liquid to run into the vessel, but the procedure was always rather slow when the specimen was appreciably warmer than the boiling point of the liquid concerned. The thermometers could conveniently be calibrated against the vapour pressures of these liquids: in addition the platinum thermometer was calibrated at the ice point.

The specimen was cooled to about 1°K by the evaporation of liquid helium from the copper vessel, and the last of the liquid was removed by simultaneous heating and pumping: this left the specimen at about 2°K. At this temperature the heat generated by the constantan thermometer warmed up the specimen at too great a rate to permit the accurate measurement of the heat capacity. A warming curve was therefore taken up to about 7°K above which temperature the heat capacity was reasonably large, and also the resistance–temperature relation for the constantan thermometer was effectively linear. Thus, although the true specific heat was not obtained below about 8°K, it was observed that the specific heat increased smoothly from 2°K upwards.

Forty-eight points were taken in the range 7·7 to 90°K; over most of this range an accuracy of $\pm 1\%$ can be claimed, but below 15°K the accuracy decreases, reaching about $\pm 5\%$ at 8°K.

§ 3. Experimental Method below 4°K (Webb and Wilks)

The measurements at helium temperatures were made on a cylindrical block of graphite (weighing 160 g) hung up by nylon threads inside a double-walled cryostat. Although helium exchange gas was used to cool the specimen down to 20°, it was removed by pumping for two or three hours at hydrogen temperatures. Cooling to lower temperatures was then brought about by making a mechanical contact between the specimen and the helium cryostat; the details of this 'heat switch' will be given in a later paper. In this way, we ensured that the quantity of gas adsorbed on the specimen was negligible, and also that a very high degree of thermal insulation was obtained at helium temperatures.

The heater, a length of constantan wire, was wound on a thin copper former attached to a light copper ring, and the thermometer, an Allen and Bradley 1 4 watt 56 ohm resistor, was soldered to a similar ring. These two units were clamped firmly to the block of graphite, one at each end. The two rings were constructed so that they could be screwed together and a direct determination made of the combined heat capacities

of the heater and thermometer units. We thus avoided uncertain corrections due to the heat capacities of the varnish, solder and carbon resistor, which in the helium region are of the order of 10% of the total heat capacity. The thermometer was calibrated against the vapour pressure of the helium in the cryostat ; in calculating the specific heats, the calibration curve was differentiated graphically, as this procedure was found more convenient than trying to fit an analytical expression to the calibration points. Thirty specific heat values were obtained between 4·1° and 1·5°K (the lowest temperature at which the thermometer

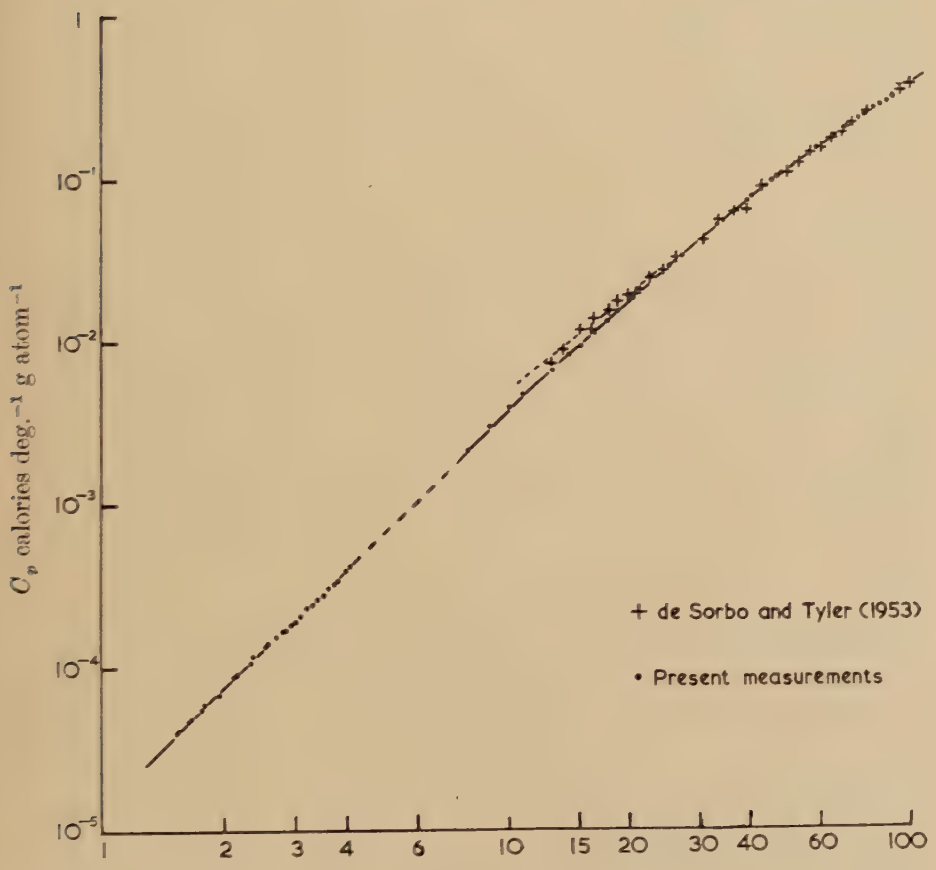

The specific heat of graphite.

could be calibrated conveniently) and the accuracy of the final curve should be better than ±2%. We made some measurements above 4°K, but these are less reliable (being based on an interpolated calibration curve) and are not given ; above 8°K they join up smoothly with the earlier measurements.

§ 4. Discussion

Our results are plotted logarithmically in the figure, together with recent values by de Sorbo and Tyler (1953). It is seen that our values agree with de Sorbo's above 25°K, but below that temperature our values are smaller than his. This disagreement may be due to de Sorbo's use of exchange gas at low temperatures ; some of this gas would inevitably be adsorbed on the specimen and its progressive desorption as the temperature is raised could cause the measured values to be too high. It is difficult, however, to estimate even the order of magnitude of the correction. So far as the thermodynamic functions are concerned the discrepancy is too small and occurs at too low a temperature to affect the accepted values for temperatures above 90°K.

If we attempt to fit the specific heat to an expression of the form T^n we find that at about 90°K n equals 1·8, and that it increases to a value of 2·4 at the lowest temperatures. Thus the T^2 dependence found by de Sorbo appears to be valid only over a limited temperature range. Our results are inconsistent with the treatments of Komatsu and Nagamiya (1951), Gurney (1952), and Rosenstock (1953), as these all lead to a T^2 dependence at the lowest temperatures. The most promising theoretical approach appears to be that of Krumhansl and Brooks (1953) ; these authors predict a T^2 law at the higher temperatures changing to T^3 at sufficiently low temperatures. However, our values do not give very good agreement with this treatment either, for they do not show any suggestion of a transition to a T^3 region at lower temperatures. We may also note that the temperature dependence of the specific heat is now nearer to that deduced by Berman (1952) from his measurements of the thermal conductivity of several specimens of graphite.

Acknowledgments

We wish to thank A.E.R.E. Harwell for supplying the graphite and Sir Francis Simon for his interest in the experiments. Two of us (R. W. H., J. W.) wish to acknowledge the award of I.C.I. fellowships, and F. J. W. the award of a Nuffield fellowship.

References

Berman, R., 1952, *Proc. Phys. Soc.* A, **65,** 1029.
de Sorbo, W., and Tyler, W. W., 1953, *J. Chem. Phys.*, **21,** 1660.
Gurney, R. W., 1952, *Phys. Rev.*, **88,**, 465.
Hill, R. W., 1953, *J. Sci. Instrum.*, **30,** 331.
Jacobs, C. J., and Parks, G. S., 1934, *J. Amer. Chem. Soc.*, **56,** 1513.
Komatsu, K., and Nagamiya, T., 1951, *J. Phys. Soc. (Japan)*, **6,** 438.
Krumhansl, J. A., and Brooks, H., 1953, *J. Chem. Phys.*, **21,** 1663.
Nernst, W., 1911, *Ann. Physik*, **36,** 395.
Rosenstock, H. B., 1953, *J. Chem. Phys.*, **21,** 2064.

XCV. *Observations on the Associated Production of Heavy Mesons and Hyperons*

By C. Dahanayake,* P. E. Francois, Y. Fujimoto,† P. Iredale, C. J. Waddington and M. Yasin
H. H. Wills Physical Laboratory, University of Bristol ‡

[Received June 8, 1954]

Abstract

In a systematic search for K-mesons and hyperons produced in emulsions, two events have been found which appear to be due to the reaction

$$\pi+\mathrm{N}\rightarrow \mathrm{Y}+\mathrm{K},\quad \text{where N represents a bound nucleon.}$$

The evidence suggests that such reactions play an important role in the production of heavy unstable particles.

§ 1. Introduction

Soon after the discovery of the heavy unstable particles—K-mesons and hyperons—there appeared to be a contradiction between their copious production in nuclear disintegrations and their long average lifetimes before decaying. It was therefore suggested that the particles are commonly produced in pairs (Nambu *et al.* 1951, Pais 1952). Until recently, however, there has been little evidence in support of this view. Experiments on cosmic radiation established the existence of several types of heavy mesons and showed that they can be directly produced in nuclear disintegrations, but they gave little evidence for the production of heavy particles in pairs. In 1953, however, Lal *et al.* found two events from each of which two heavy particles were emitted, and they suggested this evidence might be relevant to the question of the production of K-particles. A few similar observations were made with Wilson chambers (*Bagneres Report* 1953). At the time, it was difficult to estimate the significance of these observations, but it now appears probable that they were due to the associated production of heavy particles in nuclear interactions

The situation was radically changed by experiments in Brookhaven (Fowler *et al.* 1954) which established the existence of the associated production of heavy particles as a result of the interaction of fast π-mesons (1·5 Bev) with free protons. The reaction can be written in the general form $\pi^-+\mathrm{P}^+\rightarrow \mathrm{Y}+\mathrm{K}$, the heavy particles being either both neutral or oppositely charged :—

$$\pi^-+\mathrm{P}^+\rightarrow \Lambda^\circ+\theta^\circ\,;\quad \pi^-+\mathrm{P}^+\rightarrow \mathrm{Y}^-+\mathrm{K}^+.$$

* On leave of absence from the University of Ceylon.
† On leave of absence from the University of Kyoto.
‡ Communicated by Professor C. F. Powell, F.R.S.

In this note, we report two further examples of associated charged Y and K-particles emerging from high-energy disintegrations recorded in nuclear emulsions. The observations are consistent with the view that they arise in a reaction of the type $\pi+\mathbf{N}\rightarrow \mathrm{K}+\mathrm{Y}$, where $\mathbf{N}$ is a bound nucleon. Taken in conjunction with the results of other experimenters, it appears almost certain that such reactions play a very important role in the production of heavy particles in disintegrations of great energy.

§ 2. Experimental Details

During the past year, we have been engaged in a systematic study of the particles emitted from nuclear disintegrations produced by cosmic radiation, using photographic plates exposed at great altitudes. The principal purpose of the investigation is to measure the relative frequency of occurrence of different types of K-mesons and charged hyperons. The essential feature of the experiment is that we identify the heavy mesons by methods which do not depend upon observing characteristic secondary processes occurring at the end of the range. For this purpose, we determine the mass of those particles which are emitted from the disintegrations with velocities in a definite range of values, by measuring the grain-density and range of the tracks. The observations are being made with two stacks of stripped emulsions made up of 40 and 46 sheets, respectively. The measurements are sufficiently accurate to distinguish with high efficiency the particles of mass 1000 m_e, among the much larger numbers of protons, deuterons and π-mesons (see *Report of Padua Conference* 1954).

In making the measurements, it is convenient to confine attention to tracks which satisfy the following conditions :—

(*a*) They are associated with ' stars ' from which two or more secondary shower particles are emitted.

(*b*) The velocities of emission of the particles must be less than 0·57 *c*. The corresponding values of the grain-densities are greater than $2g^*$, where g^* is the ' plateau value '; the values of γ, the ratio of the total to the rest energy, are then less than 1·22.

(*c*) The ranges of the particles in the emulsion must be greater than 2 mm.

(*d*) The directions of emission of the particles satisfy certain geometrical criteria, designed to ensure that any K-mesons among the selected particles will have only a small probability of leaving the stack before being brought to rest.

Among 2500 particles which satisfy the above criteria, and of which the masses have been determined, there are 9 K-mesons of mass $\sim$1000 m_e and two charged hyperons. The latter have been recognized because they decayed in flight ; one of them was emitted from the same disintegration as one of the K-mesons.

In an attempt to obtain further evidence for an associated production of K and Y particles, the parent stars of all the observed heavy unstable

particles were examined in greater detail. For this purpose, all associated tracks with ionization greater than the plateau value were followed from emulsion to emulsion until the particles were found either to have left the stack or to have been brought to rest. In this examination, another K-meson was found, emitted from the parent star of the second of the Y particles. Details of the two events with associated Y and K-particles are given in tables 1 and 2.

More accurate determinations of the masses of the K-mesons in these events were made by other methods ; by measurements of range, scattering (R, $\bar{\alpha}$); blob density, scattering (b^*, $\bar{\alpha}$); and blob-density, range (b^*, R); the masses were deduced by a comparison with the results of similar measurements on the tracks of protons. Similar observations were also made on the tracks of the hyperons. These measurements allowed a reliable determination of the velocities of emission of the different particles.

Of the four secondary particles produced by the decay of the associated heavy mesons and hyperons, only that of one of the hyperons, Y_6, permitted accurate scattering measurements ; all the others were too steeply inclined to the plane of the emulsions. Grain-density measurements of sufficient precision were made, however, in the case of the secondaries of the heavy mesons, to prove that they do not represent the alternative mode of decay of the τ-meson $\tau^{\pm} \rightarrow \pi^{\pm}+\pi^{\circ}+\pi^{\circ}$ (Crussard *et al.* 1954). The velocities of the secondary charged particles were too great to be consistent with such an interpretation.

§ 3. Interpretation

The essential question posed by the above observations is whether the two particles forming a pair are produced in independent interactions within a single nucleus—which may conveniently be referred to as ' plural production '—or whether they result from a single interaction—' associated production '.

Plural Production

We assume that the production of one particle is independent of the other, and also independent of the type of the parent star. In the conditions of the experiment, the probability of observing two pairs of dissimilar heavy unstable particles due to chance coincidences is found to be only 0·12%. In making this estimate, it has been assumed that of those heavy particles emitted from the stars we have examined, which could have been identified by mass measurements or by the secondary effects they produced, only a quarter satisfied our selection criteria. This and other features of the assumptions on which our estimate is based will not be strictly valid, but the order of magnitude of the result is unlikely to be seriously in error.

The probability of observing two associated pairs, in the conditions of the experiment, is so small that it seems almost certain that we are dealing with associated production of heavy particles, each involving a heavy meson and a charged hyperon.

Table 1

Star type	Particle	Angle between tracks	γ of emission	length (mm)	Decay	$\bar{\alpha}-R$	Mass (in m_e) b^*-R	$\bar{\alpha}-b^*$
1. $19+3n$	K_{41}	$23°\pm0{\cdot}5°$	$1{\cdot}18\pm0{\cdot}01$	38·3	at rest	940 ± 160	965 ± 100	—
	Y_5		$1{\cdot}19\pm0{\cdot}02$	9·6	in flight	—	—	2350 ± 350
2. $19+3p$	K_{42}	$37°\pm0{\cdot}5°$	$1{\cdot}26\pm0{\cdot}01$	70·9	at rest	—	1020 ± 50†	900 ± 60
	Y_6		$1{\cdot}21\pm0{\cdot}02$	17·5	in flight	—	—	1850 ± 250

† Blobs, gaps, range.

Table 2. Secondaries

Particle	Length/plate mm	Ionization plateau	$p\beta$ Mev/c	Q‡ value of decay
K_{41}	1·2	~1·0	—	—
Y_5	0·85	~1·0	—	>8·5 Mev
K_{42}	0·9	~0·9	—	—
Y_6	5·0	$1{\cdot}02\pm0{\cdot}02$	190 ± 10	116 ± 15 Mev

‡ Assuming the mode of decay $Y^{\pm}\rightarrow\pi^{\pm}+n+Q$.

Multiple Production

Assuming an associated production, the two most plausible reactions are :—

(i) $\pi+N \rightarrow Y+K$,

(ii) $N+N \rightarrow Y+K+N$, where N is a nucleon.

Of these two reactions, only (i) has been observed experimentally ; it was established by the Brookhaven experiments with 1·5 Bev π-mesons. No examples of reaction (ii) have been reported, but it may be an important source of pairs in the events of high energy which are commonly met in studies with cosmic radiation In addition, there may be other reactions in which more than two particles are created, but these will require greater threshold energies, and, if they occur at all, they are probably much less frequent.

In a stack of photographic plates, the reactions leading to the production of heavy particles may be produced either by protons and π-mesons entering from outside, by similar particles produced in the stack, or by secondary particles which interact with other nucleons in the parent nucleus in which they are created. It is possible to estimate the relative proportions of such events :—

If the struck nucleon is assumed to be at rest, the threshold energies for reactions (i) and (ii) are 0·93 Bev and 1·85 Bev, respectively. From these values, and the data of Camerini *et al.* (1950) on the stars observed in plates exposed to cosmic rays at high altitudes, we can calculate the numbers of particles capable of producing these reactions which are associated with the stars which have been examined.

Since there was very little local matter around the stack during exposure, the flux of high energy π-mesons entering it must have been negligible compared with that of the nucleons. Further, about 1500 secondary π-mesons are estimated to have been produced in the observed disintegrations with energies greater than the threshold for reaction (i), but only about 100 secondary nucleons with energies greater than the threshold for reaction (ii). Thus, if we assume that the cross section for reaction (ii) is not appreciably greater than that for (i), it appears reasonable to neglect production by secondary nucleons compared with that due to secondary π-mesons.

Of the 3000 stars we have examined, about 2000 were due to a primary nucleon with sufficient energy to produce two or more shower particles and a pair of heavy unstable particles. It appears therefore that in the stars we have examined there were approximately equal numbers of π-mesons and nucleons capable of producing associated pairs of heavy particles.

It is reasonable to suppose that, whatever the reaction by which they are formed, some of the heavy particles constituting the pairs will be uncharged. For example, in the Brookhaven experiments, four of the five pairs observed were neutral. It is probable therefore, that an appreciable number of heavy particles produced in our experiments will be neutral, and will thus almost certainly be lost to observation.

It must also be emphasized that if they are to be detected in the present experiment, both of the heavy unstable particles must be ejected with non-relativistic velocities, and one of them with a value of γ less than 1·22. Owing to the much higher velocity of the C-system, the probability that both of a pair of charged heavy unstable particles formed in reaction (ii) shall have a sufficiently low energy to be observed, is less than that for reaction (i), unless there is a strong correlation in the directions of emission of the secondary particles. These considerations suggest that in the stars examined, only a few examples of charged pairs produced by either reaction could have been expected, and the probability of finding two is considerably less if they are due to reaction (ii) than if they arise from reaction (i). It is therefore reasonable to assume, tentatively, that the two observed events are due to reaction (i), although other possibilities cannot be excluded. We have therefore analysed both events in terms of this reaction.

For this purpose, we have calculated the energies of the particles produced in the reaction $\pi + N \rightarrow K + Y$, for different values of the kinetic

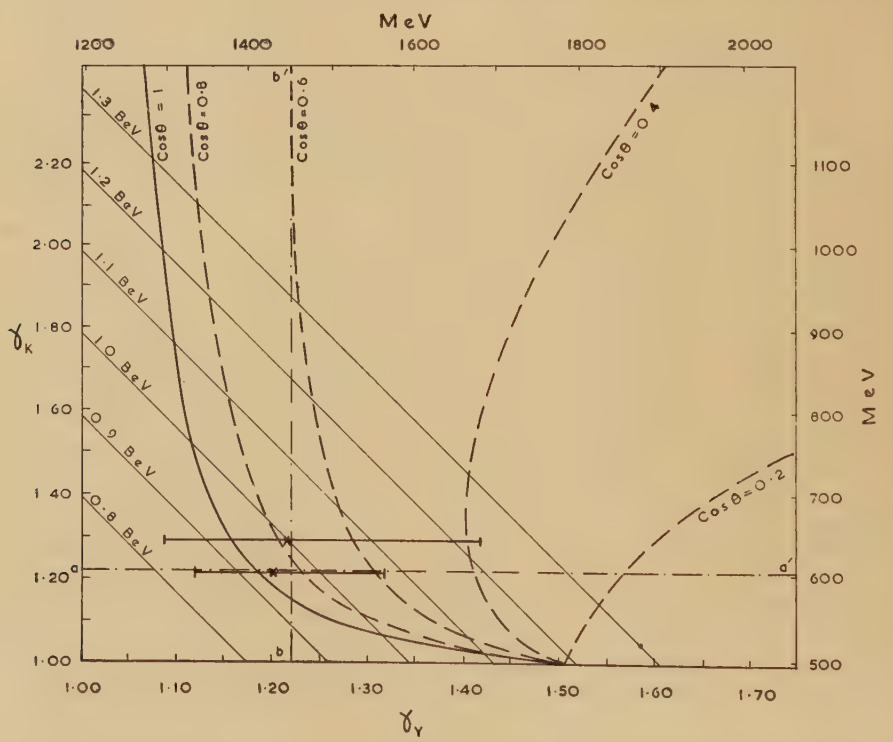

Relation between γ_K and γ_Y for various values of θ. Lines of constant kinetic energy, E_π, are also shown. Points representing the two observed events are plotted, together with the maximum uncertainties due to the Fermi energy of the nucleon. Lines corresponding to the upper limits of γ accepted in the systematic search are indicated by the broken lines aa′ and bb′.

energy, E_π, of the π-meson, and of the angle θ, between the directions of emission of the heavy particles, assuming the struck nucleon to be at rest.

The figure shows the variation of γ_K with γ_Y for different values of θ. If the finite Fermi energy of motion of the nucleon in the nucleus is taken into account, the significance of a point representing an experimental observation, when plotted on this diagram, will be uncertain by an amount which depends on the maximum possible energy of the struck nucleon. The points corresponding to the two events described are shown with limits due to the effect of a Fermi momentum equal to ± 100 Mev/c. They indicate that each event is consistent with the assumed reaction. While not decisive, this consistency provides support for the correctness of the assumption, and for the view that in each case the two charged heavy particles escaped from the parent nucleus without further interactions. If so, the observed energies and directions of motion of the two particles define the energy of the primary π-meson. The result in event (i) is $E_\pi = 0{\cdot}94$ Bev, and in (ii), $E_\pi = 0{\cdot}99$ Bev.

Fowler *et al.* have suggested that there may be a correlation in each event, between the plane of the decay of the Y-particle, and the plane defined by the directions of motion of the two associated heavy particles. Owing to the possibility of interactions of the particles in escaping from the nucleus, and to the difficulty of defining accurately the planes in an emulsion because of the scattering of the particles, it may be questioned whether any such correlation would be preserved. In our events, the angles between the planes were 48° and 18° respectively.

§ 4. Conclusions

Events of the type we have observed are unlikely to be due to chance coincidence, and can best be interpreted as examples of the reaction

$$\pi + \mathrm{N} \rightarrow \mathrm{K} + \mathrm{Y}, \quad \text{where N is a nucleon.}$$

It appears that a considerable proportion of the slow Y and K particles created in high energy nuclear disintegrations are produced in association. A more detailed analysis must await the accumulation of observations of greater statistical weight.

Acknowledgments

We wish to thank Dr. D. H. Perkins for making the mass measurements on K_{42}, and Mrs. D. M. Ford, Miss S. Lawrence, and Miss B. J. Bolt, for assistance in the examination of plates. We are deeply indebted to Professor C. F. Powell, F.R.S., for his continued interest and encouragement.

This work has been carried out as part of a programme of research supported by the Department of Scientific and Industrial Research to whom three of us, (P. E. F., P. I., and C. J. W.) are indebted for maintenance grants.

C. D. wishes to thank the Government of Ceylon; Y. F. the British Council, and M.Y. the Government of India and the Muslim University of Aligarh, for maintenance grants.

References

Camerini, U., Fowler, P. H., Lock, W. O., and Muirhead, H., 1950, *Phil. Mag.*, **41**, 413.

Crussard, J., Kaplon, M. F., Klarmann, J., and Noon, J. H., 1954, *Phys. Rev.*, **93**, 253.

Fowler, W. B., Shutt, R. P., Thorndike, A. M., and Whittemore, W. L., 1954, *Phys. Rev.*, **93**, 861.

Lal, D. Yash Pal, and Peters, B., 1953, *Proc. Ind. Acad. Sci.*, **38**, 398.

Nambu, Y., Nishijima, K., and Yamaguchi, Y., 1951, *Prog. Theo. Phys.*, **6**, 615.

Pais, A., 1952, *Phys. Rev.*, **86**, 663.

XCVI. *A New Estimate of the Lifetime of Λ^0-Particles*

By D. I. Page
The Physical Laboratories, The University, Manchester*

[Received March 24, 1954]

Abstract

A further estimate of the mean lifetime of Λ^0-particles has been made from measurements on 23 decay events. V-events have been selected in which the positive secondary particle can be identified as a proton from its momentum and ionization. The decay scheme for these events is assumed to be

$$\Lambda^0 \rightarrow P^+ + \pi^- + 37 \text{ MeV}.$$

The result of the analysis of the events is a mean lifetime of

$$(3{\cdot}6^{+1{\cdot}1}_{-0{\cdot}7}) \times 10^{-10} \text{ sec.}$$

The weighted mean of all the published results is now

$$\tau = (3{\cdot}7^{+0{\cdot}6}_{-0{\cdot}5}) \times 10^{-10} \text{ sec.}$$

§ 1. Introduction

Among 357 neutral V-events observed in an experiment at the Jungfraujoch (Astbury *et al.* 1952, Page and Newth 1954) 25 gave positive secondary particles which were heavily-ionizing. By combining the estimate of the ionization in the track with the measured momentum of a particle it is possible to estimate its mass. In this way Λ^0-decays have been separated from other types of neutral V-events since Λ^0-particles disintegrate according to the scheme

$$\Lambda^0 \rightarrow P^+ + \pi^- + 37 \text{ MeV}, \quad . \quad . \quad . \quad . \quad . \quad . \quad (1)$$

while other neutral V-events have light mesons as their secondary particles. Using the momentum–ionization method it is very easy to distinguish light mesons from protons.

From the distribution of the identified Λ^0-decays in the cloud chamber the mean lifetime of Λ^0-particles has been estimated.

§ 2. Selection of Events

The following requirements were considered necessary to enable a V-event to be identified as a Λ^0-decay from measurements of the track of the positive secondary particle :

(*a*) the projection of the positive secondary track on the plane of the cloud chamber should be at least 5 cm long for adequate measurement of momentum and ionization to be made, and

* Communicated by Professor P. M. S. Blackett, F.R.S.

(*b*) the corresponding projection of the negative track should be at least 1·0 cm long for the decay to be recognized and reconstructed stereoscopically in space. This requirement is essential as, in several cases, the negative particle's momentum was calculated from that of the positive particle and the angle (ϕ) between the two tracks, using the decay scheme (1).

V-events which fulfilled the conditions (*a*) and (*b*) were selected from the original sample of 357 events and the ionization density in the tracks of the positive secondary particles were estimated by four observers. In 25 cases the particles were found to be heavily-ionizing by all four observers.

For these 25 events the positive particle's momentum was measured and the result combined with the estimate of ionization to determine the mass of the particle. In 23 cases the result was consistent with the particle being a proton and inconsistent with its being a light meson while in one case the converse was true.

The identification of the 23 events as Λ^0-decays was checked by ensuring that the two secondary momenta (p_+, p_-) and the angle (ϕ) were consistent with the decay scheme (1); where possible the method of identification used by Gaythor (1954), which uses only measurements of angles, was also applied as a check.

§ 3. Measurements and Analysis

From the measurements of p_+, p_- and ϕ for each event the momentum (P) of the primary Λ^0-particle was found. In 9 events only one of the secondary momenta could be accurately measured and decay scheme (1) was used to find the other. In four events (marked with an asterisk in table 1) the ionization of the proton provided the best estimate of its momentum.

The line of flight of the primary particle was found from p_+ and p_- and the path length (l) before decay was measured. The potential path length (L) of each particle was also measured, allowing for the identification criteria given in § 2 (Page and Newth 1954). The values of P, l, and L are given for the 23 events in table 1. The times (t and T) listed in the table are the proper times of flight corresponding to the distances l and L.

Column 7 of table 1 shows the ' information ' that each particle provides for the lifetime estimate expressed as a fraction of what could be obtained in a chamber of unlimited size. This fraction is a function of T/τ and its significance has been discussed by Bartlett (1953) and by Alford and Leighton (1953). The total information contained in the 23 events is equivalent to what would be obtained from about 18 events with an infinite potential path length. By contrast, the 26 events of Page and Newth (1954) only gave as much information as 4 complete, unlimited observations. This difference arises from the fact that Page and Newth used faster Λ^0-particles in their analysis and the values of T were much smaller than those in table 1.

The procedure devised by Bartlett (1953) has been used to estimate the decay constant $(1/\tau)$ from the values of t and T listed in the table. The result is

$$1/\tau=(0{\cdot}275\pm0{\cdot}064)\times10^{10}\ \text{sec}^{-1},$$

$$\tau=(3{\cdot}6^{+1{\cdot}1}_{-0{\cdot}7})\times10^{-10}\ \text{sec},$$

where the error is only that due to the small number of events.

Table 1. Time of Flight Measurements on 23 Λ^0-Particles

Event	P (10^8 ev/c)	l (cm)	L (cm)	t (10^{-10} sec)	T (10^{-10} sec)	Information per particle
PG 229	5·9	2·1	28	1·3	18	0·78
QF 136	2·1	3·1	33	5·5	58	1·00
QG 388	5·6	0·8	28	0·5	19	0·82
QQ 759	5·1	2·8	19	2·0	14	0·63
QR 275	5·4*	1·5	27	1·0	19	0·82
QU 50	4·1	9·6	15	8·7	14	0·63
QW 293	10·6	5·7	40	2·0	14	0·63
QX 679	1·9	3·0	40	5·9	79	1·00
QZ 889	8·2	4·5	36	2·0	16	0·72
RC 3	2·7	0·9	11	1·2	15	0·67
RC 11	3·1	11·9	36	14·3	43	0·99
RD 347	9·0	8·8	34	3·6	14	0·63
RD 494	4·9*	1·5	1·5	1·1	1	0·00
RG 700	2·7	3·6	16	4·9	22	0·89
RG 855	4·7	5·0	44	3·9	35	0·98
RH 576	4·5	0·2	18	0·2	15	0·67
RH 722	5·3*	5·1	32	3·6	22	0·89
RH 840	6·2	6·3	35	3·8	21	0·87
RJ 272	3·8	0·9	19	0·9	19	0·82
RJ 653	7·7*	11·2	37	5·4	18	0·79
RK 415	6·3	7·6	38	4·5	22	0·89
RK 550	5·7	0·4	24	0·3	16	0·72
RM 423	4·0	1·2	25	1·1	23	0·91
				$\bar{t}=3{\cdot}4$		Total 17·7

* The values of the momenta marked with an asterisk are those derived from the estimate of the ionization of the proton secondary particle.

Event QX 679 was reported by Millar and Page (1953) and events RH 840 and RK 415 are reproduced in Plate 25 (*a* and *b*).

§ 4. Non-Statistical Errors

In discussing the effect of non-statistical errors it is helpful to express τ in the form used by Bridge *et al.* (1953).

$$\tau=\tau'+\tau'',$$

where

$$\tau'=\bar{t}=\frac{1}{N}\sum_{i=1}^{N}t_i=\frac{M}{Nc}\sum_{i=1}^{N}\left(\frac{l}{P}\right)_i$$

and N is the number of events analysed and M is the mass of the Λ^0-particle. τ' is the mean *observed* lifetime. This differs from the *true* mean lifetime by an amount τ'' which depends upon the limited times T for which the particles could be observed. Thus

$$\tau''=f(T_i, \tau)=F(L_i, P_i, \tau).$$

For the analysis made in this paper we have

$$\tau'=3{\cdot}4\times 10^{-10}\text{ sec}, \quad \tau''=0{\cdot}2\times 10^{-10}\text{ sec}.$$

(*a*) *Errors in L*

An error in L affects τ'' only and from the small size of τ'' we see that any reasonable error in L has a negligible effect on τ.

(*b*) *Errors in M*

The most accurate determination of the mass of the Λ^0-particle is that made by Friedlander *et al.* (1954) using events observed in photographic emulsion. They find a value of $(2182\pm 2)m_e$, the error being largely due to the uncertainty in the assumed mass of the π-meson. This uncertainty gives rise to a proportional uncertainty (0·1%) in the value of τ.

(*c*) *Errors in l*

Any systematic error in l, such as measuring distances from an incorrect boundary of the illuminated volume of the cloud chamber, will probably be constant, independent of l. To find the effect of such an error on the value of τ the values of l were all decreased by 0·2 cm and the value of τ' recalculated (τ'' is not appreciably altered). The result was to decrease τ' by $0{\cdot}2\times 10^{-10}$ sec. There is a random error in measuring l which is estimated to be about 0·2 cm. This produces an error of about 2% in τ.

(*d*) *Errors in P*

Any random or systematic error in P is likely to arise from a curvature measurement and will be roughly proportional to P^2. Thus the slow particles which contribute most information to the lifetime estimate are those whose momenta are most accurately known. The average random error in P is estimated to be about 15%; this leads to an error of 3% in τ.

(*e*) *Discussion of Errors*

From these individual errors in measurement it is estimated that the effect on τ of random errors is about 4% as compared with the statistical error (due to the small number of events) of 25%. The most likely source of a systematic error is in the measurement of l and could give rise to an error in τ of as much as 10%.

To estimate the mean lifetime to better than *ca.* 5% slow Λ^0-decays do not appear to be the best events to analyse. For slow particles the values of l are necessarily small and the error introduced in measuring l is large.

The effect of any systematic error can be lessened by using events for which l is larger (i.e. Λ^0-particles with higher momenta). With these events the values of T are small and the statistical ' information ' from each event is reduced. Many more events are therefore needed to reduce the statistical error.

The analysis of slow particles such as those reported here is a reasonably rapid method of estimating the lifetime to within about 10% but any more accurate determination will be a long and laborious task.

§ 5. Conclusions

Estimates of the mean lifetime of Λ^0-particles made by other workers have been summarized in an earlier paper (Page and Newth 1954). The weighted mean value of the lifetime was given there as

$$1/\tau=(0{\cdot}27\pm0{\cdot}05)\times10^{10}\ \text{sec}^{-1}.$$

Taking into account the present result, the new weighted mean value is

$$1/\tau=(0{\cdot}272\pm0{\cdot}039)\times10^{10}\ \text{sec}^{-1},$$

$$\tau=(3{\cdot}7^{+0{\cdot}6}_{-0{\cdot}5})\times10^{-10}\ \text{sec}.$$

It is interesting to consider how many events are needed to bring the statistical error down to the size of the measurement error. To have a 10% statistical error, 100 ' complete ' observations (events with infinite values of T) would be needed. If all events that are used give approximately the same information as those reported here, about 110 more events are needed before the total amount of information reaches that from 100 unbiassed observations. At the present rate of collection of events in the Jungfraujoch experiment another 18 months of operating time are needed. To determine the mean lifetime to even finer limits will, as we saw in § 4, take very much longer.

Acknowledgments

The Administration of the Jungfraujoch Research Station and its manager, Mr. Hans Wiederkehr, provided facilities for work at the Jungfraujoch and the International Council of Scientific Unions made a grant towards the running costs of the experiment there. I have received a grant from the Department of Scientific and Industrial Research during the course of my work.

I have had the benefit of discussions with Mr. J. A. Newth and other colleagues in Manchester in preparing this paper and I am particularly indebted to Miss P. M. Miles who made a large number of the measurements reported here.

The Jungfraujoch experiment has received continued support from Professor P. M. S. Blackett and I am grateful to him for his guidance.

References

Alford, W. L., and Leighton, R. B., 1953, *Phys. Rev.*, **90,** 622.
Astbury, J. P., Chippindale, P., Millar, D. D., Newth, J. A., Page, D. I., Rytz, A., and Sahiar, A. B., 1952, *Phil. Mag.*, **43,** 1283.
Bartlett, M. S., 1953, *Phil. Mag.*, **44,** 249.
Bridge, H. S., Peyrou, C., Rossi, B., and Safford, R., 1953, *Phys. Rev.*, **91,** 362.
Friedlander, M. W., Keefe, D., Menon, M. G. K., and Merlin, M., 1954, *Phil. Mag.*, **45,** 533.
Gaythér, D. B., 1954, *Phil. Mag.*, **45,** 570.
Millar, D. D., and Page, D. I., 1953, *Phil. Mag.*, **44,** 1049.
Page, D. I., and Newth, J. A., 1954, *Phil. Mag.*, **45,** 38.

(*a*) Event RH 840. From the measurements on this event the energy release in the disintegration is found to be (34 ± 7) MEV, consistent with a Λ^0-decay.

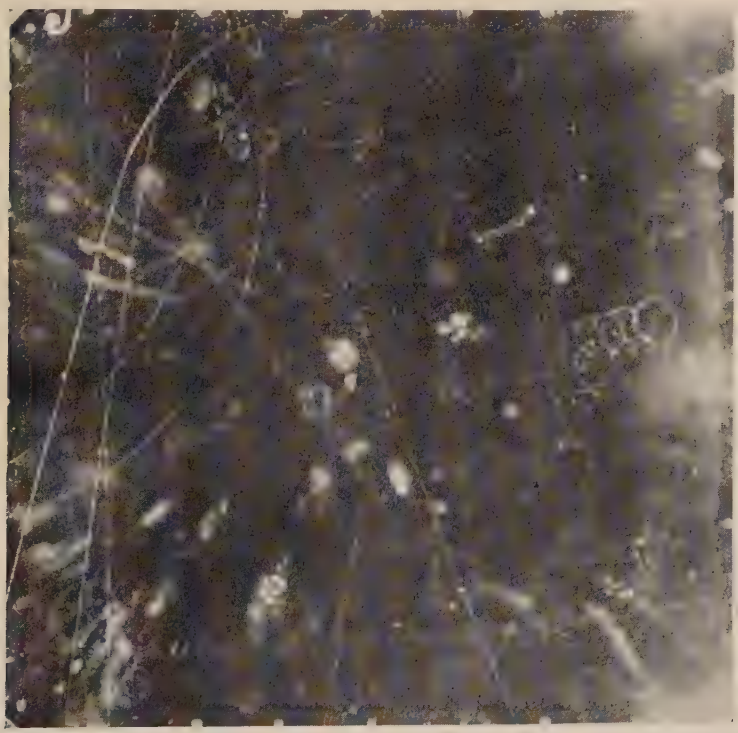

(*b*) Event RK 415. The decay occurs in the top left hand corner of the cloud chamber. The proton travels downwards, following the direction of the Λ^0-particle. The heavily ionizing π-meson moves upwards and backwards in the chamber. Multiple Coulomb scattering prevents an accurate measurement of the π-meson's momentum but the event is consistent with a Λ^0-decay.

XCVII. *The Elastic Scattering of Neutrons by Alpha Particles*

By B. H. Bransden and J. S. C. McKee
Department of Physics, Queen's University of Belfast*

[Received March 17, 1954]

Abstract

The theory of the scattering of neutrons by alpha particles is formulated using the variational method. It is assumed that the five-body wave function can be written in the Wheeler resonating group form and allowance is made for possible two-body spin orbit coupling.

Detailed numerical calculations of the S-wave phase shifts for incident neutrons below 7 Mev, and of the zero energy cross section, are presented for two-body potentials having the exchange properties of an ordinary, a Majorana–Heisenberg exchange, a symmetrical exchange and a Serber interaction. Comparison of the theoretical results with experimental data strongly favours forces of the Majorana–Heisenberg or symmetrical exchange type against those of the ordinary and Serber types.

§1. Introduction

Theoretical studies, based on conventional two-body nuclear potentials, of the elastic scattering of nucleons by deuterons, tritons and ^{3}He, have achieved reasonable agreement with experiment, at incident energies below 14 Mev (Buckingham, Hubbard and Massey 1952, Christian and Gammel 1953, Swan 1953 a, b). Throughout these calculations, it has been assumed that the wave function can be written in the Wheeler resonating group form and that the tensor component of the two-body potential can be represented by an equivalent central interaction. It is therefore of great interest to find whether calculations, based on similar assumptions, can interpret successfully the experimental data for the elastic collision of neutrons with alpha particles.

The total cross section for n–α scattering exhibits a maximum near 1 Mev, attributed to resonance scattering through the P ground state of the ^{5}He compound nucleus. Analysis of angular distribution measurements reveals that this level is split into a widely spaced inverted $P_{\frac{3}{2}}$—$P_{\frac{1}{2}}$ doublet, the separation of the characteristic energies being ~ 5 Mev (Adair 1952, Huber and Baldinger 1952, Dodder and Gammel 1952). Feingold and Wigner (1952) have shown that this doublet separation is an order of magnitude greater than that expected from the two-body tensor interaction, so it appears that either specifically many-body potentials are responsible, or that the two-body potential contains a spin orbit coupling term of the type $\mathbf{L}.\mathbf{S}$. The latter possibility has

* Communicated by the Authors.

been invoked by Case and Pias (1950) to explain the high energy p–p and n–p scattering, but apparently the required sign of the spin orbit coupling term is the opposite to that postulated in the nuclear shell model by Mayer (1949) and Haxel *et al.* (1949). However, it is still possible that the two-body potential contains spin orbit terms of the correct sign for the Mayer theory, having little effect on n–p and p–p scattering. For example, if these terms have exchange properties of the Serber type, they will vanish identically for p–p scattering and will only effect n–p scattering in even triplet states with $l \geqslant 2$.

In the present paper, formulae are obtained for the calculation of the n–α collision phase shifts by variational methods, including the case in which the two-body potential contains **L . S** coupling terms. It is assumed that the wave function can be written in the Wheeler group form, and that the non-central tensor two-body potential can be represented by an equivalent central potential. Detailed numerical calculations for the S-wave phases for energies up to 7 MeV are presented, assuming two-body potentials with exchange properties of the ordinary, Majorana–Heisenberg, symmetrical and Serber types. For S-wave scattering, the discussion is somewhat simplified by the absence of an S-level of ^{5}He (Dodder and Gammel 1952, Adair 1952) and by the vanishing of the **L . S** interaction. Further calculations for the $P_{\frac{3}{2}}$ and $P_{\frac{1}{2}}$ phase shifts, giving information as to the size of the postulated **L . S** interaction are in progress, and will be reported at a later date.

§2. The Wave Function

The resonating group structure wave function of the five-body system can be written in the form

$$\Psi(1234, 5)=(1-P_{15}-P_{25})\chi(1234)\sigma(1234)\mathscr{F}(5), \quad . \; . \quad (1)$$

where P is the operator exchanging both space and spin coordinates. Neutrons 1 and 2, protons 3 and 4 form the alpha particle, with space wave function $\chi(1234)$ and spin wave function $\sigma(1234)$ and $\mathscr{F}(5)$ represents the motion of neutron 5 relative to the centre of mass of the alpha group. The alpha particle, on the central field approximation, is in a pure S-state, symmetric in all four particles, with the appropriate singlet spin function

$$\sigma(1234)=\tfrac{1}{2}(\alpha_1\beta_2-\beta_1\alpha_2)(\alpha_3\beta_4-\beta_3\alpha_4). \quad . \; . \; . \; . \quad (2)$$

Introducing position vectors $\mathbf{r}_1$, $\mathbf{r}_2$, $\mathbf{r}_3$, $\mathbf{r}_4$, $\mathbf{r}_5$ for nucleons 1, 2, 3, 4, 5 respectively, and defining

$$\mathbf{r}=-\mathbf{r}_5+\tfrac{1}{4}(\mathbf{r}_1+\mathbf{r}_2+\mathbf{r}_3+\mathbf{r}_4),$$

the spin and angular dependence of $\mathscr{F}(5)$ can be exhibited as

$$\mathscr{F}(5)=\sum_{l=0}^{\infty}\sum_{j=l-\frac{1}{2}}^{l+\frac{1}{2}} F_j(r)\mathscr{A}_l\mathscr{Y}^{(m)}_{j,l,\frac{1}{2}}(5), \quad . \; . \; . \; . \; . \quad (3)$$

where $$\mathscr{Y}^{(m)}_{j,l,\frac{1}{2}}(5)=c_1(l,j)Y_{l,m-\frac{1}{2}}(\theta,\phi)\alpha_5+c_2(l,j)Y_{l,m+\frac{1}{2}}(\theta,\phi)\beta_5.$$

Here $Y_{l,m}$ are normalized surface harmonics and the Clebsch–Gordan coefficients $c_{1,2}(l, j)$ are defined by

$$\left.\begin{aligned} &j=l+\tfrac{1}{2} \\ &\quad c_1=(l+m+\tfrac{1}{2})^{\frac{1}{2}}(2l+1)^{-\frac{1}{2}}, \quad c_2=-(l-m+\tfrac{1}{2})^{\frac{1}{2}}(2l+1)^{-\frac{1}{2}} \\ &j=l-\tfrac{1}{2} \\ &\quad c_1=(l-m+\tfrac{1}{2})^{\frac{1}{2}}(2l+1)^{-\frac{1}{2}}, \quad c_2=(l+m+\tfrac{1}{2})^{\frac{1}{2}}(2l+1)^{-\frac{1}{2}}. \end{aligned}\right\} . \quad (4)$$

The asymptotic form of the radial function $F_j(r)$ is required to be

$$F_j(r) \sim r^{-1}\{k^{-1} \sin (kr-\tfrac{1}{2}l\pi)+a_j \cos (kr-\tfrac{1}{2}l\pi)\}, \quad . \quad . \quad (5)$$

where aj is related to the phase δ_j by

$$a_j=k^{-1} \tan \delta_j$$

and where k is the wave number of the incident neutron. If the normalizing coefficients $\mathscr{A}_l$ are written

$$\mathscr{A}_l=2i^l(2l+1)^{\frac{1}{2}}(1+k^2a_j^2)^{-\frac{1}{2}}\sqrt{\pi} \exp (i\delta j)$$

the differential cross section for elastic scattering into an element of solid angle $d\Omega$, direction (θ, ϕ) becomes

$$\begin{aligned} k^2\sigma(\theta)\, d\Omega= &\left| \sum_{l=0}^{\infty} \{(l+1) \exp (i\delta_{l+\frac{1}{2}}) \sin \delta_{l+\frac{1}{2}}+l \exp (i\delta_{l-\frac{1}{2}}) \sin \delta_{l-\frac{1}{2}}\}P_l(\cos \theta)\right|^2 \\ &+\left| \sum_{l=0}^{\infty} \{\exp (i\delta_{l+\frac{1}{2}}) \sin \delta_{l+\frac{1}{2}}-\exp (-i\delta_{l+\frac{1}{2}}) \sin \delta_{l-\frac{1}{2}}\}P_l'(\cos \theta)\right|^2 . \quad (6) \end{aligned}$$

§3. The Evaluation of the Phase Shifts δ_j

The phase shifts δ_j can be determined by the variational procedures introduced by Hulthén (1945, 1948) and Kohn (1948). The wave function $\Psi(1234, 5)$ satisfies the Schrödinger equation

$$\left.\begin{aligned} &(\mathscr{H}-E)\Psi=0, \\ &(\mathscr{H}-E)\equiv (T_0+T_\alpha+\tfrac{1}{2}\sum_{\substack{i=1 \\ (i\neq j)}}^{5}\sum_{j=1}^{5} \mathscr{V}(ij)-E_0-E_\alpha). \end{aligned}\right\} . \quad . \quad . \quad (7)$$

E_α is the alpha particle binding energy, E_0 the energy of relative motion of the neutron and alpha particle, and T_α, T_0 are the kinetic energy operators for the alpha group and the incident neutron respectively.

Then $E_0=\hbar^2/(2M')k^2$, M' the reduced mass is $M'=4M/5$, M being the nucleonic mass. The interaction between two nucleons may be written

$$\begin{aligned} \mathscr{V}(12)=&(mM_{12}+hH_{12}+bB_{12}+w)V(12) \\ &+(m'M_{12}+w')\mathbf{L}(12) \,.\, (\boldsymbol{\sigma}_1+\boldsymbol{\sigma}_2)U(12). \quad . \quad . \quad . \quad (8) \end{aligned}$$

Here M is the space exchange and B the spin exchange operator, and H is an operator exchanging both space and spin coordinates ; $\mathbf{L}(12)$ is the relative angular momentum operator and $\boldsymbol{\sigma}_1$, $\boldsymbol{\sigma}_2$ are the Pauli spin

operators for nucleons 1 and 2. The constants m, h, b, w; m', w' are normalized so that

$$m+h+b+w=1\ ;\ m'+w'=1,$$

in which case $x=m-h-b+w$ is the ratio between the singlet and triplet potentials in even states.

The stationary expression I_j is defined as

$$I_j=-\frac{2M'}{\hbar^2}\sum_{\text{spin}}\int \mathscr{A}_l^{-1}F_j^*(r)\mathcal{Y}^{(m)*}_{j,l,\frac{1}{2}}(5)\sigma(1234)\chi(1234)(\mathscr{H}-E)\Psi(1234,5)\,d\tau_{12345}, \quad . \quad . \quad . \quad . \quad (9)$$

the integration and summation being over the space and spin coordinates of nucleons 1 to 5. If I_j is constructed from trial functions $F_j^t(r)$, having the correct asymptotic form† (5) and depending on n constants $c_1, c_2, \ldots, c_n$, then the phase shifts δ_j can be found from the system of equations (Hulthén 1945)

$$\left.\begin{aligned}\frac{\partial I_j}{\partial c_m}&=0, \qquad m=1,2,\ldots,n,\\ I_j(a_j)&=0, \qquad \delta_j=\text{arc tan}\,(ka_j),\end{aligned}\right\}. \quad . \quad . \quad . \quad . \quad (10)$$

or from the alternative set (Hulthén 1948, Kohn 1948),

$$\left.\begin{aligned}\frac{\partial I_j}{\partial c_m}&=0, \qquad m=1,2,\ldots,n,\\ \frac{\partial I_j}{\partial a_j}&=-1, \quad \delta_j=\text{arc tan}\,(ka_j+I_j(a_j)).\end{aligned}\right\}. \quad . \quad . \quad . \quad . \quad (11)$$

Using the fact that the alpha wave function $\chi(1234)$ satisfies the equation

$$(T_\alpha+\tfrac{1}{2}\sum_{\substack{i=1\\(i\neq j)}}^{4}\sum_{j=1}^{4}\mathcal{V}(ij)-E_\alpha)\chi(1234)\sigma(1234)=0, \quad . \quad . \quad . \quad (12)$$

the spin summations and angular integrations in the integral (9) can be performed giving

$$\begin{aligned}I_j=&\int_0^\infty f_j(r)\left\{\frac{d^2}{dr^2}+k^2-\frac{l(l+1)}{r^2}+\alpha u(r)+\alpha' u'(r)\right\}f_j(r)\,dr\\ &+\int_0^\infty\int_0^\infty f_j(r)\left\{\beta q_l(r,r')+\beta' q_l'(r,r')+\gamma p_l(r,r')+\gamma' p_l'(r,r'),\right.\\ &\left.+n_l(r,r')\left(\frac{d^2}{dr'^2}+k^2-\frac{l(l+1)}{r'^2}\right)\right\}f_j(r')\,dr\,dr', \quad . \quad . \quad . \quad . \quad . \quad (13)\end{aligned}$$

where $f_j(r)=r^{-1}F_j^t(r)$ and $\mathbf{r}'=M_{15}\mathbf{r}=-\mathbf{r}_1+\frac{1}{4}(\mathbf{r}_5+\mathbf{r}_2+\mathbf{r}_3+\mathbf{r}_4)$.

† When considering resonance scattering through a level of the compound nucleus He^5, terms $c_m\phi_j(5)$ can be added to $F_j^t(r)$ (c_m being a variational parameter) with asymptotic form $\phi_j\sim 0$, so that $\chi(1234)\phi_j(5)\mathcal{Y}^{(m)}_{j,l,\frac{1}{2}}(5)\sigma(1234)$ represents the wave function of the appropriate level.

Introducing coordinates $\mathbf{r}''$, $\mathbf{r}'''$, where $\mathbf{r}''=M_{25}\mathbf{r}$, $\mathbf{r}'''=M_{35}\mathbf{r}$ and normalizing $\chi(1234)$ so that

$$\iiint \chi^2(1234)\, d\mathbf{r}'\, d\mathbf{r}''\, d\mathbf{r}'''=1 \quad . \quad . \quad . \quad . \quad . \quad (14)$$

we have

$$U(r)=-\frac{2M'}{\hbar^2}\iiint \chi^2(1234)V(15)\, d\mathbf{r}'\, d\mathbf{r}''\, d\mathbf{r}''', \quad . \quad . \quad (15)$$

and

$$\left.\begin{matrix} q_l(r,r') \\ P_l(r,r') \\ n_l(r,r') \end{matrix}\right\} =2\pi rr'\int_{-1}^{+1} P_l(\mu)\, d\mu \left\{\begin{matrix} Q(r,r') \\ P(r,r') \\ N(r,r') \end{matrix}\right.$$

where $\mu=\mathbf{r}\,.\,\mathbf{r}'/rr'$ and

$$\left.\begin{aligned} Q(r,r')&=-\frac{2M'}{\hbar^2}\iint \chi(1234)\chi(5234)V(15)\, d\mathbf{r}''d\mathbf{r}''', \\ P(r,r')&=-\frac{2M'}{\hbar^2}\iint \chi(1234)\chi(5234)V(14)d\mathbf{r}''d\mathbf{r}''', \\ N(r,r')&=-\iint \chi(1234)\chi(5234)\, d\mathbf{r}''\, d\mathbf{r}''', \end{aligned}\right\} \quad . \quad . \quad (16)$$

u', q_l', p_l' are obtained by replacing $V(ij)$ by $u(ij)$ in expressions* (16).

The constants α, β, γ ; α', β', γ' depend on the exchange character of the potential and are given by

$$\left.\begin{aligned} \alpha&=(4w-2m-2h+2b) & \alpha'&=\tfrac{5}{8}\Lambda(4w'-2m') \\ \beta&=(4m-2w-2b+2h) & \beta'&=\tfrac{1}{2}\Lambda(4m'-2w') \\ \gamma&=-3(w+m) & \gamma'&=-2\Lambda(w'+m') \end{aligned}\right\} \quad . \quad . \quad (17)$$

where $\Lambda=l$ if $j=l+\frac{1}{2}$ and

$$\Lambda=\begin{cases} -(l+1) & \text{if } j=l-\frac{1}{2}, \\ 0 & \text{if } l=0. \end{cases}$$

---

* As with the corresponding four- and three-body systems (Buckingham and Massey 1942, Swan 1953 a, b) the double integration over r and r' in (13) can be expressed in the symmetrical form

$$\int_0^\infty \int_0^\infty f_j(r)K(r,r')f_j(r')\, dr\, dr' \; ; \;\; K(r,r')=K(r',r)$$

provided $\chi(1234)$ satisfies (12). However, it is unnecessary to effect such a transformation, as it can be shown that the eqns. (10) still hold for a possibly incorrect function $\chi_t(1234)$ and eqns. (11) also hold provided

$$\int \chi_t(\chi_t-\chi)\, d\tau_{1234}$$

is small compared with unity.

§4. The S-Wave Phase : Potentials and Wave Functions

To determine the phase for S-wave scattering only the central potential $V(12)$ need be specified. In order that (13) may be evaluated analytically it is convenient to use Gaussian radial functions for both the potential and the alpha particle wave function,

$$V(r)=-V_0 \exp(-\mu r^2) \quad . \quad . \quad . \quad . \quad . \quad . \quad (18)$$

with the standard parameters (Rosenfeld 1948), $V_0=43{\cdot}7$ Mev, $\mu^{-\frac{1}{2}}=1{\cdot}9\times10^{-13}$ cm and $x=(w-h-b+m)=0{\cdot}62$, and

$$\chi(1234)=N \exp(-\lambda\Sigma r_{ij}^2), \quad . \quad . \quad . \quad . \quad . \quad . \quad (19)$$

with the variationally determined parameter $\lambda=0{\cdot}0751\times10^{26}$ cm^{-2}, and where N is chosen so that $\chi(1234)$ is normalized in $\mathbf{r}'$, $\mathbf{r}''$, $\mathbf{r}'''$ space according to (14). Then

$$N^2=\left(\frac{4}{5}\right)^9\left(\frac{2\alpha}{\pi}\right)^{\frac{9}{2}}2^{12}.$$

Four types of force with differing exchange characteristics were considered.

I Ordinary potential : $m=h=0$; $w=\frac{1}{2}(1+x)$; $b=\frac{1}{2}(1-x)$.

II Majorana–Heisenberg potential :

$$w=b=0 \; ; \quad m=\tfrac{1}{2}(1+x) \; ; \quad h=\tfrac{1}{2}(1-x).$$

III Symmetrical potential : $m=2b=\frac{1}{3}(1+3x)$; $h=2w=\frac{1}{3}(1-3x)$.

IV Serber potential : $m=w=\frac{1}{4}(1+x)$; $h=b=\frac{1}{4}(1-x)$.

With these constants the parameters α, β, γ take the values :

Force Type	α	β	γ
I	3·62	−1·19	−2·43
II	−1·19	3·62	−2·43
III	0	2·43	−2·43
IV	+1·215	1·215	−2·43

§5. The S-Wave Phase Shift : Numerical Calculations

Using the potential (18) and wave function (19) the potential functions U, q_l, p_l, n_l are readily evaluated in closed form (cf. Swan 1953 a),

$$\left.\begin{aligned} U(r)&=A_0 \exp(-\gamma_0 r^2), \\ q_l(r,r')&=A_1 \exp\{-\gamma_1(r^2+r'^2)\}\mathscr{I}_{l+\frac{1}{2}}(\kappa_1 rr'), \\ P_l(r,r')&=A_3 \exp\{-\gamma_2 r^2-\gamma_3 r'^2\}\mathscr{I}_{l+\frac{1}{2}}(\kappa_2 rr'), \\ n_l(r,r')&=A_4 \exp\{-\gamma_4(r^2+r'^2)\}\mathscr{I}_{l+\frac{1}{2}}(\kappa_3 rr'), \end{aligned}\right\} \quad . \quad . \quad . \quad (21)$$

where

$$i^{l+\frac{1}{2}}\mathscr{I}_{l+\frac{1}{2}}(x)\equiv(\pi x/2)^{\frac{1}{2}}J_{l+\frac{1}{2}}(ix) \quad . \quad . \quad . \quad . \quad . \quad . \quad (22)$$

and

$$A_0=\left(+\frac{2M'V_0}{\hbar^2}\right)\left(\frac{16\lambda}{16\lambda+3\mu}\right)^{\frac{3}{2}}; \qquad \gamma_0=\frac{8\lambda\mu(32\lambda+3\mu)}{(16\lambda+\mu)(16\lambda+3\mu)}.$$

$$A_1=\left(+\frac{2M'V_0}{\hbar^2}\right)\left(\frac{4}{5}\right)^3\left(\frac{32\lambda}{3\pi}\right)^{\frac{5}{2}}; \qquad \gamma_1=\left(\frac{4}{5}\right)^2\left(\frac{17}{3}\lambda+\mu\right),$$

$$\kappa_1=\left(\frac{4}{5}\right)^2\left(\frac{16}{3}\lambda-2\mu\right).$$

$$A_2=\left(+\frac{2M'V_0}{\hbar^2}\right)\left(\frac{4}{5}\right)^3\left(\frac{128\lambda}{\pi}\right)^{\frac{3}{2}}\left(\frac{\lambda}{12\lambda+\mu}\right)^{\frac{3}{2}}; \quad \gamma_2=\left(\frac{4}{5}\right)^2\frac{68\lambda^2+7\lambda\mu}{12\lambda+\mu},$$

$$\gamma_3=\left(\frac{4}{5}\right)^2\frac{68\lambda^2+27\lambda\mu}{12\lambda+\mu},$$

$$\kappa_2=\left(\frac{4}{5}\right)^2\frac{16\lambda(4\lambda+\mu)}{12\lambda+\mu}.$$

$$A_3=\left(\frac{4}{5}\right)^3\left(\frac{32\lambda}{3\pi}\right)^{\frac{3}{2}}; \qquad \gamma_4=\left(\frac{4}{5}\right)^2\frac{17}{3}\lambda,$$

$$\kappa_3=\left(\frac{4}{5}\right)^2\frac{16}{3}\lambda.$$

To complete the evaluation of the integral I_0 a suitable trial function $f_0(r)$ must be chosen. This must satisfy the condition

$$f_0(r)\sim k^{-1}\sin(kr)+a_0\cos(kr), \qquad \ldots \quad (23)$$

and preferably be such that the final integrations over r, r' may be performed analytically. A function satisfying these conditions and similar to those previously employed in discussion of n–d and n–T scattering (Troesch and Verde 1949, Clemental 1950, Swan 1953 a, b) was adopted

$$f_0(r)=k^{-1}\sin(kr)\{1+c_1\exp(-\lambda r^2)\}$$
$$+\cos(kr)\{a+c_2\exp(-\lambda r^2)\}\{1-\exp(-\lambda r^2)\}. \qquad (24)$$

With this form of $f_0(r)$, all integrals occurring in (13) can be evaluated in closed form (Watson 1948), with the exception of those arising from the kernel $n_l(r, r')$; but these terms are readily expressed as rapidly converging series containing confluent hypergeometric functions of type ${}_1F_1(n, m; x)$. Convenient tables of these functions covering the required range are available (*Brit. Assoc.*, 1926, 1927).

In addition to the phase parameter a_0, the trial function contains the two parameters c_1, c_2. Following a suggestion of Swan (1953 a), phases are calculated for each energy value and each type of potential by both the Hulthén and the Hulthén–Kohn methods for the combinations

(*a*) $c_1=c_2=0$, (*b*) $c_1\neq0$, $c_2=0$, (*c*) $c_1=0$, $c_2\neq0$, (*d*) $c_1\neq0$, $c_2\neq0$,

then the best choice of trial function is given by that combination for which the phases obtained by the two methods agree most closely.

The parameter a_0 satisfies the integral equation

$$ka_0=\alpha\int_0^\infty \sin(kr)U(r)f_0(r)\,dr+\int_0^\infty\int_0^\infty \sin(kr) \times\left\{\beta q_0(r,r')+\gamma p_0(r,r')+n_0(r,r')\left(\frac{d^2}{dr'^2}+k^2\right)\right\}f_0(r')\,dr\,dr'. \quad (25)$$

An additional test of the accuracy of the phase parameter a_0 determined by Hulthén's method, is provided by comparing the calculated a_0 with that obtained by substituting the Hulthén trial function into the right hand side of (25). This procedure provides no test for the phases calculated by the Hulthén–Kohn method, as in this case the calculated $f_0(r)$ and a_0, automatically satisfy (25).

§6. Results and Discussion

Values of the phase parameter a_0 have been calculated for each of the potentials I to IV by both the Hulthén and Hulthén–Kohn methods. at k=0·0, 0·15, 0·30 and 0·45.* These values are shown in table 1

Table 1. The Phase Parameters a_0 derived by the Hulthén and Hulthén–Kohn Variation Methods

(a_0 in units of 10^{-13} cm)

Wave number of incident neutron (in 10^{13} cm^{-1}) k	Force type					
	I			II		
	H	HK	*I*	H	HK	*I*
0	+7·30	7·31	7·07	−2·41	−2·41	−2·47
0·15	6·36	6·58	5·76	−2·52	−2·52	−2·55
0·30	2·83	3·45†	2·42	−2·94	−2·81	−3·05
0·45	0·99	1·00	1·19	−3·58	−3·63	−3·81
	III			IV		
	H	HK	*I*	H	HK	*I*
0	−2·00	−2·00	2·06	−1·22	−1·21	−1·28
0·15	−2·07	−2·07	−2·10	−1·34	−1·32	−1·41
0·30	−2·31	−2·22	−2·38	−1·45	−1·50	−1·40
0·45	−2·74	−2·44†	−2·64	−1·57	−2·90†	−1·50

H=Hulthén's method; HK=Hulthén–Kohn method; I=Value of a_0 obtained from integral eqn. (25) using the Hulthén wave function.

† Hulthén–Kohn values marked thus are less reliable: see text.

* In units 10^{13} cm^{-1}.

together with those obtained by employing the Hulthén wave function on the right hand side of the integral eqn. (25). The corresponding phase shifts δ_0 are given in table 2, together with additional values at $k=0{\cdot}075$, $0{\cdot}225$, $0{\cdot}375$ obtained by the interpolation of $a_0^{-1} \equiv k \cot \delta_0$. Excellent agreement is obtained between phases calculated by the Hulthén and Hulthén–Kohn methods, except in certain cases at the higher energies. Where disagreement does occur, it appears that the

Table 2. Calculated Phase Shifts*

Wave number of incident neutron, k (units 10^{13} cm^{-1})	Force type			
	I		II	
	H	KH	H	KH
0	0	0	0	0
0·075	0·492	0·495	−0·181	−0·180
0·150	0·762	0·778	−0·362	−0·360
0·225	0·810	0·870	−0·544	−0·523
0·300	0·705	0·803	−0·723	−0·700
0·375	0·542	0·594	−0·894	−0·861
0·450	0·420	0·421	−1·050	−0·913
	III		IV	
	H	KH	H	KH
0	0	0	0	0
0·075	−0·150	−0·150	−0·093	−0·093
0·150	−0·301	−0·301	−0·199	−0·196
0·225	−0·453	−0·451	−0·305	−0·318
0·300	−0·606	−0·587	−0·410	−0·466
0·375	−0·751	−0·715	−0·515	−0·663
0·450	−0·890	−0·833	−0·616	−0·918

H=Hulthén. HK=Hulthén–Kohn.

* All phases are in radians.

Hulthén phase is to be preferred, since it is found that the corrections, $I_0(a_0)$, to the Kohn–Hulthén phase parameters (cf. eqn. (11)) are not small, while, on the other hand, the Hulthén wave function still satisfies the integral eqn. (25) with reasonable accuracy.

The phase shifts calculated from a_0 by the relation $\delta_0 = \arctan(ka_0)$ are indeterminate to the extent $n\pi$, (n an integer), and in order to conform to the normalization of the phase shifts obtained from analysis of the experimental angular distributions, δ_0 has been chosen to vanish for zero incident energy. Using this normalization, the phases resulting

from the ordinary potential I are positive and those resulting from the exchange potentials are increasingly negative in the order IV, III, II. The wave functions $f_0(r)$ are compared in fig. 1 at $k=0{\cdot}0$; $0{\cdot}3$, for the extreme cases of the ordinary and Majorana–Heisenberg potentials.

Nogami (1942, 1946) has calculated the phase δ_0 for the type III exchange force at thermal energies, and also at incident neutron energies of 1·0 and 2·5 MeV. Gaussian wave functions and potentials similar to those of the present paper were used, but the phases were calculated by the Flügge (1937) method from the integro-differential equation for $f_0(r)$. Unfortunately, Nogami in obtaining his solution neglected the

Fig. 1

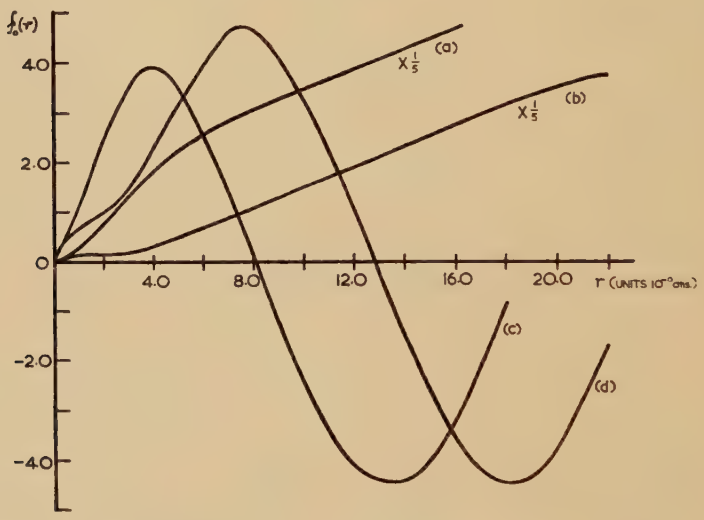

Calculated wave functions $f_0(r)$: (a) and (b) wave functions for ordinary and Majorana–Heisenberg exchange potentials at $k=0$, normalized so that $f_0(r) \sim r+a_0$; (c) and (d) wave functions for ordinary and Majorana–Heisenberg exchange potentials at $k=0{\cdot}3$ normalized so that

$$f_0(r) \sim k^{-1} \sin(kr)+a_0 \cos(kr).$$

kernels q_0 and n_0, which have an important effect on the calculated phase, so that his results, which are included in fig. 2 and table 3, are not strictly comparable with ours.

Our calculated zero energy cross sections are given in table 3, together with the experimental result, and in fig. 2 the calculated phases (given by Hulthén's method) are compared with the results of phase shift analyses of the experiment angular distributions (Huber and Baldinger 1952, Seagrave 1953). It is seen that the predictions of the ordinary and Serber potentials, I and IV, are in definite disagreement with the experiment data. The phases calculated using the Majorana–Heisenberg exchange potential are in close agreement with the results of Seagrave

(1953) and the corresponding zero energy cross section agrees remarkably well with the latest experimental value ; but it should be remembered that the results of a phase shift analysis are not necessarily unique and

Table 3. The Zero Energy Cross Section* Q_0

Force type	I	II	III	IV	Observed cross section‡
Q_0	6·69	0·73	0·50 [0·93†]	0·19	0·78

* Units of 10^{-24} cm^2.
† Nogami (1942).
‡ Hibdon and Muehlhause (1951).

Fig. 2

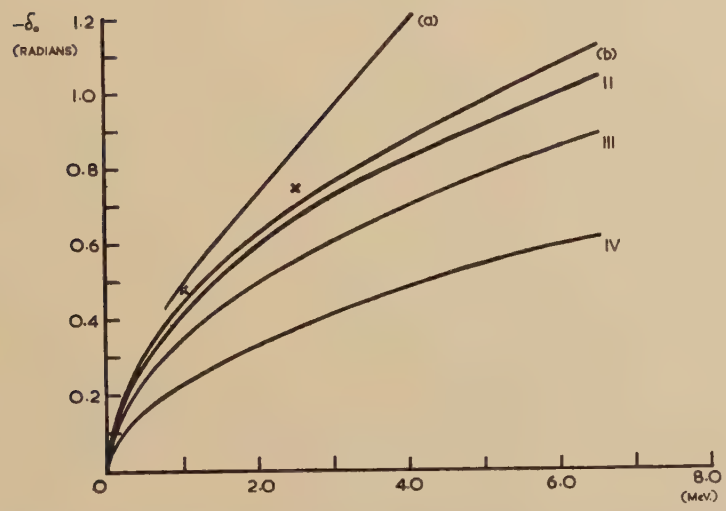

Calculated and experimental phase shifts δ_0 : II, III, IV, calculated Hulthén phases for the Majorana–Heisenberg exchange, symmetrical exchange, and Serber exchange interactions respectively.

(*a*) Experimental phases of Huber and Baldinger (1952).

(*b*) Experimental phases of Seagrave (1953).

For energies below 2·61 Mev Seagrave's curve summarizes phases inferred from p—α scattering experiments which have been analysed by Dodder and Gammel (1952).

$\times$ Phases calculated by Nogami (1942, 1946).

consequently the experimental phases may be in error by a few degrees, furthermore some error will be introduced into the theoretical calculations by the use of Gaussian wave functions for the alpha particle, so that little preference can be given to the results of the type II force over those of the

symmetrical exchange force III. It is in any case clear that the theoretical result strongly supports the phase shifts summarized by Seagrave (1953) and is in disagreement with those obtained by Huber and Baldinger (1952).

§7. Conclusions

The variational method applied to n–α elastic scattering, in conjunction with a resonating group wave function, appears to be capable of giving a correct description of S-wave scattering, at low energies, and it seems reasonable to hope that a similar calculation, of the higher phases, will determine whether the observed properties of the collision are consistent with the inclusion of spin orbit coupling in the two-body potential.

The numerical results strongly support saturated exchange forces of the Majorana–Heisenberg and symmetrical types against the unsaturated ordinary and Serber interactions, in agreement with the conclusions of Buckingham, Hubbard and Massey (1952) and Swan (1953 a, b), drawn from their studies of the n–d and n–T collisions.

References

Adair, R. K., 1952, *Phys. Rev.*, **86,** 155.

Brit. Assoc. Adv. Sci., Reports, 1926, 272 ; 1927, 220.

Buckingham, R. A., and Massey, H. S. W., 1941, *Proc. Roy. Soc.* A, **179,** 123.

Buckingham, R. A., Hubbard, S. J., and Massey, H. S. W., 1952, *Proc. Roy. Soc.* A, **211,** 183.

Case, K. M., and Pais, A., 1950, *Phys. Rev.*, **80,** 203.

Christian, R. S., and Gammel, J. L., 1953, *Phys. Rev.*, **91,** 100.

Clemental, E., 1951, *Nuovo Cim.*, **8,** 185.

Dodder, D. C., and Gammel, J. L., 1952, *Phys. Rev.*, **88,** 520.

Feingold, A. M., and Wigner, E. P., 1952 (quoted by Adair, 1952).

Flügge, S., 1937, *Z. f. Phys.*, **108,** 545.

Haxel, O., Jensen, J. H. D., and Suess, H. E., 1949, *Phys. Rev.*, **75,** 1766.

Hibdon, C. T., and Muehlhause, C. O., 1951, *Atomic Energy Commission Report*, ANL 4680.

Huber, P., and Baldinger, E., 1952, *Helv. Phys. Acta*, **25,** 435.

Hulthén, L., 1944, *K. Fysiogr. Sallsk. Lund, Forh.*, **14,** 1 ; 1948, *Ark. Mat. Astr. Fys.* A, **35,** 25.

Kohn, W., 1948, *Phys. Rev.*, **74,** 1763.

Mayer, M. G., 1949, *Phys. Rev.*, **75,** 1969.

Nogami, M., 1942, *Proc. Phys. Math. Soc. Japan*, **24,** 26 ; 1946, *J. Phys. Soc. Japan*, **1,** 11.

Rosenfeld, L., 1948, *Nuclear Forces* (Amsterdam : North-Holland Publishing Co.).

Seagrave, J. D., 1953, *Phys. Rev.*, **92,** 1222.

Swan, P., 1953 a, *Proc Phys. Soc.* A, **66,** 238 ; 1953 b, *Ibid.*, **66,** 740.

Troesch, A., and Verde, M., 1951, *Helv. Phys. Acta*, **24,** 39.

Watson, G. N., 1948, *Bessel Functions*, 2nd ed. (Cambridge : University Press).

XCVIII. CORRESPONDENCE

Thermoelectric Power of Monovalent Metals at High Temperature

By P. G. Klemens
Division of Physics, Commonwealth Scientific and Industrial Research Organization, Sydney

[Received May 19, 1954]

MacDonald and Roy (1953) have derived expressions for the absolute thermoelectric power of single band metals at high temperatures, and compared them with experimentally determined values of the monovalent metals. They concluded that while the results for most of these metals can be explained theoretically, the case of potassium is anomalous. These conclusions are based on values of the Fermi energy derived from the free electron model. The Fermi energy, however, may differ from the free electron value, and when this is taken into account the thermoelectric power of potassium need no longer be regarded as anomalous.

As shown by Mott and Jones (1936) the absolute thermoelectric power is in general given by

$$S=-\frac{\pi^2K^2T}{3e}\left(\frac{1}{\sigma}\frac{d\sigma}{dE}\right)_\zeta \qquad . \quad . \quad . \quad . \quad . \quad . \quad (1)$$

where ζ is the Fermi energy, and

$$\sigma(E)=\int\frac{\tau(\mathbf{k})}{\text{grad } E}\left(\frac{\partial E}{\partial k_x}\right)^2 dS. \qquad . \quad . \quad . \quad . \quad . \quad (2)$$

In the above τ is the relaxation time for state k, and the integration is over the energy-contour E in **k**-space. One can write

$$\left(\frac{1}{\sigma}\frac{d\sigma}{dE}\right)_\zeta=\frac{x}{\zeta} \qquad . \quad . \quad . \quad . \quad . \quad . \quad . \quad . \quad (3)$$

so that

$$x=\frac{d(\log\sigma)}{d(\log E)}. \qquad . \quad . \quad . \quad . \quad . \quad . \quad . \quad . \quad (4)$$

MacDonald and Roy have discussed the possible values of x for bands deviating from the quadratic dependence $E\propto k^2$, with the dependence of τ on E given by the Wigner–Seitz model, as used in the discussion of high-temperature scattering (Mott and Jones 1936). They deduced that x, defined by (4), cannot exceed $+3$, but can take smaller and even negative values.

If in (3) one uses values ζ' for the Fermi energy calculated on the free electron theory, values of x can be derived for the monovalent metals from the observed values of S which range from $+2{\cdot}2$ to $-6{\cdot}7$, with the

exception of potassium, for which $x=3{\cdot}8$. However, since ζ does not necessarily equal ζ' these experimental values of x should be compared, not with (4), as MacDonald and Roy have done, but with $(\zeta'/\sigma)(d\sigma/dE)$.

Assuming a band of spherical symmetry, we find from (2)

$$\frac{1}{\sigma}\frac{d\sigma}{dE}=\frac{2}{k}\frac{dk}{dE}+\frac{d^2E}{dk^2}\left(\frac{dk}{dE}\right)^2+\frac{1}{\tau}\frac{d\tau}{dE} \quad . \quad . \quad . \quad . \quad (5)$$

so that,

$$\frac{E'}{\sigma}\frac{d\sigma}{dE}=\frac{\hbar^2}{2m}\left[2k\frac{dk}{dE}+k^2\frac{d^2E}{dk^2}\left(\frac{dk}{dE}\right)^2+\left(\frac{k}{\tau}\frac{d\tau}{dk}\right)k\frac{dk}{dE}\right] \quad . \quad . \quad . \quad (6)$$

where $E'=\hbar^2k^2/2m$. For the free-electron model, the first term is $+1$ the second term $+1/2$ and the third term is $(k/\tau)(d\tau/dk)/2$, which cannot exceed $+3/2$. But for likely deviations from the free electron model, both the first and the third term will be larger than these free electron values, because dk/dE will be greater. The factors d^2E/dk^2 and $(dk/dE)^2$ will tend respectively to decrease and increase the second term, so that this term may be larger or smaller than the free electron value, depending on how E varies with k. A value of $3{\cdot}8$ for (6) is therefore possible for a suitable variation of E with k, such as, to quote the simplest but not the only example, a quadratic variation $E\propto k^2$ with an effective electron mass larger than the free mass. The observed thermoelectric power of potassium is thus not necessarily in disagreement with the band theory.

Near the zone boundary d^2E/dk^2 will be negative, and dk/dE will be large, so that the second term will be negative and numerically larger than the other terms. The fact that x is negative for the noble metals implies that there are, in these cases, strong deviations from the free electron theory, as is also borne out by a comparison of the electrical and thermal conductivities of these metals at low temperatures (Klemens 1954).

References

Klemens, P. G., 1954, *Proc. Phys. Soc.* A, **67,** 194 ; *Aust. J. Phys.*, **7,** in press.
MacDonald, D. K. C., and Roy, S. K., 1953, *Phil. Mag.*, **44,** 1364.
Mott, N. F., and Jones, H., 1936, *Properties of Metals and Alloys* (Oxford : Clarendon Press).

XCIX. *Notices of New Books and Periodicals received*

Progress in Nuclear Physics, Vol. 3. Edited by O. R. Frisch. [Pp. 279.] (London : Pergamon Press, Ltd.) Price 63*s*.

This book, like its predecessors, is a collection of review articles on subjects in Nuclear Physics. The success of such a book must depend to a great extent on the selection of subjects. Care must be taken not to choose subjects which have recently been reviewed elsewhere. This would seem to be the criterion which has kept all aspects of meson physics out of this and previous volumes. A middle course must be steered between experimental methods and techniques on the one hand and theoretical physics on the other. It is one of the regrettable features of nuclear physics today that workers in the experimental and theoretical fields seem to be getting more and more isolated from one another. This enhances the value of a series such as this which can serve as a bridge between the two fields.

The subjects chosen for this volume are well balanced between theory and experiment and are all very timely. Five of the articles deal with research tools : The diffusion cloud chamber, which is of use for the rapid detection of particles produced by high energy accelerators, has recently been highly developed and this review will serve as a welcome introduction to this new technique. The proportional counter is now an extremely accurate instrument for work at low energies and the construction and the mode of operation are fully discussed together with a review of recent experiments on β- and γ-ray spectra using this instrument. The subject of Čerenkov radiation is an interesting one in itself and its application for the detection of fast particles fully merits its inclusion in this volume. The articles on research tools are concluded by reviews of solid conduction counters which may be of use in the future, and of the production of intense ion beams for use in accelerators. The latter subject is one which has received little attention and in view of its importance for the successful and efficient running of accelerators the article should prove valuable.

The annihilation of positrons and the subject of positronium, the 'atom without a nucleus', are reviewed by the foremost pioneer in this field. The recent success of several experiments in aligning nuclei in paramagnetic salts at low temperatures has inspired an article on this subject which includes a discussion of the production and possible experimental uses of polarized beams of particles.

The volume ends with two semi-theoretical articles on stripping reactions and on the collisions of deuterons with nucleons. The former describes the theory behind the reactions which have been so successful in assigning spins and parities to many nuclear levels. A survey of the experimental work following the theoretical predictions of Butler is given. The article on the collisions of deuterons with nucleons includes a survey of the experimental results and deals with what can be learnt from them about the fundamental forces between nucleons. This is very welcome because of the wealth of experimental evidence which has been accumulating in recent years.

The typography and the reproduction of figures are very good. Mistakes are mercifully infrequent but the English could perhaps be a little less clumsy at times. It cannot be expected however, that in such a collection of articles the standard of English can be uniformly high.

All the articles have excellent bibliographies and they will be of great use to any physicist requiring more detailed knowledge than is given in the actual review. This series is becoming a very valuable work of reference in nuclear physics. The price is high but no higher than equivalent American publications.

D. J. P.

Nuclear Moments. By N. F. Ramsey. (New York: John Wiley & Sons, Inc.; London: Chapman & Hall, Ltd.) [Pp. 10+169.] Price 40*s*., $5.

Before 1945 the 'external' properties of the nucleus due to its magnetic dipole or electric quadrupole moment were mainly investigated by optical spectroscopy or molecular beam methods. Since then there has been a spectacular development in this borderline field between nuclear physics and solid state physics or physical chemistry. The application of microwave spectroscopy and nuclear magnetic resonance techniques has made possible a detailed investigation of a great variety of interesting effects, many of which provide solid state research with new tools. Ramsey's book is an excellent first introduction to the subject and contains 18 pages of references, tables of nuclear moments, shielding corrections and hyperfine interactions and an appendix on nuclear shell structure. D. P.

The Physics of Experimental Method. By H. J. J. Braddick. (Chapman & Hall.) [Pp. 404.] Price 35*s*.

It is a pleasure to review a book which will sit worthily on the bookshelves of most experimental physicists, next to Strong's classic of fifteen years ago. Dr. Braddick has brought into one compact volume, and described with a most attractive zest and clarity, a great deal of what the good experimentalist needs to know; and on almost every page manages to remind him of the combination of practical common-sense, critical thinking, and technical knowledge which he must develop. Throughout, the reviewer had two strong impressions: first, that the author had himself used the particular technique, material or method of computation he was describing, and so spoke from first-hand knowledge; second, that he had already successfully explained it to others, and had enjoyed doing so. There is a pleasing absence of vagueness; no words are wasted; and the moral is frequently pointed by illustration or numerical example.

The first fifty pages (errors and mathematical treatment of results) include a section by J. Maddox summarizing 'useful' mathematics (elimination, numerical integration, relaxation). Some ninety pages on mechanical construction and materials present admirably the point of view of one who has to initiate or supervise the construction of apparatus. There are shorter sections on vacuum technique, electrical measurements (small currents, electrometers), and electronics (briefly including pulse techniques). Sixty pages deal with optics and photography (illuminants, lenses, photometry), twenty with the 'natural limits of measurements' ('noise' in its various forms), and forty-five with 'some techniques of nuclear physics' (ionization and particle counting, cloud chambers, nuclear emulsions).

This book does not treat any techniques in the detail, which Strong, for example, gives to glass working or quartz fibres; and every specialist will wish that he had been able to read Dr. Braddick on his own subject at greater length. It is possible (though difficult) to find some subjects hardly mentioned at all—high pressures, low temperatures, short-wave technique, transistors, precision metrology for example. But the author's choice is admirable, and the standard he assumes in, and imparts to, the reader, both in general principle and in detailed knowledge, is kept at a consistent level; frequent references are made to more extended treatments where necessary.

The book is well printed and produced and there are few misprints. Some 200 references and an index follow the text, and the diagrams, while lacking the particular beauty of those in Strong's book, are clear and adequate. B. W. R.

Structure and Properties of Solid Surfaces. Edited by ROBERT GOMER and CYRIL STANLEY SMITH. (University of Chicago Press.) [Pp. 491+xvi.] Price 64*s*.

THERE have recently been in America a number of Conferences on subjects connected with the physics of the solid state, papers at which have been published in book form shortly afterwards. These books are extremely useful, giving as they do a series of summarizing articles and original contributions in a restricted field.

It would be impossible in a short review to write critically of any of the fourteen contributions in this volume; its nature will be best indicated by a list of papers contributed. These are :—

The Use of Classical Macroscopic Concepts in Surface-Energy Problems by Conyers Herring.
Atomic Theory of Surface Energy by P. P. Ewald and H. Juretschke.
The Mechanical Properties of Crystalline Metal Surfaces by A. J. Shaler.
Wetting of Solids as Influenced by the Polarizability of Surface Ions by W. A. Weyl.
The Study of Solid Surfaces by George P. Thomson.
The Adhesion of Solids by F. P. Bowden and D. Tabor.
Crystal Growth and Chemical Structure by A. F. Wells.
Some Remarks on Facts and Theories of Crystal Growth by H. E. Buckley.
Epitaxy by H. Seifert.
Physical Adsorption of Gases on Solids by Terrell L. Hill.
Surface Structure from the Standpoint of Chemisorption and Catalysis by M. Boudart.
Physical and Chemical Adsorption of Gases on Iron Synthetic Ammonia Catalysts by P. H. Emmett.
Chemisorption on Solid Surfaces by Ahlborn Wheeler.
The Catalytic Action of Spinels by G.-M. Schwab, E. Roth, Ch. Grintzos, and N. Mavrakis.

N. F. M.

The Electromagnetic Field in its Engineering Aspect. By G. W. CARTER. (Longmans, Green & Co. Ltd.) Price 35*s*.

IT is a commonplace that most physicists have lost interest in classical physics, and that their effort is concentrated on nuclear matters. None the less, it is classical electromagnetism which sustains the electrical industry, and there is scope for infinite skill in shaping the subject to fit the needs of electrical engineers.

Professor Carter's book is a notable exercise in this skill, and a good final honours student might well buy the book and keep it for his postgraduate days. The mathematics used is formally not beyond the first year of an honours course in mathematics, but it is used with greatest elegance and clarity; and the literary style of the book is quite exceptionally good.

There are a few respects in which the reviewer would differ from the auth or; notably where he treats the vector $\overline{E}$ as a flux, comparable to the vector $\overline{D}$, rather than as an 'electrizing force', to use Heaviside's phrase. Further, in a text on electromagnetism, as distinct from a treatise on electrical machinery, the unit of H should be the ampere per metre, rather than the ampere-turn per metre. But these are points of detail; and, over all, the book does excellently all that it sets out to do.

It is of interest to record that Professor Carter's father, the late Dr. F.W. Carter, F.R.S., was one of the first distinguished Cambridge mathematicians to devote himself to the needs of the electrical industry: he was, for a long period, consulting engineer to the British Thomson-Houston Co., Ltd., Rugby. History is repeating itself.

G. H. R.

Review of Occasional Notes of the Royal Astronomical Society. [Vol. 3, No. 15, Oct. 53.] Price 3*s*.

THIS issue of *Occasional Notes* contains an article by Dr. de Graaff-Hunter on " Heights and names of Mount Everest and other peaks ", and one by Ernest Tillotson on " The constitution of the earth to a depth of 750 kilometres ". Dr. Hunter arrives at the very satisfactory conclusion that Mount Everest can, without impropriety, be called Mount Everest. He discusses the observations made in 1852 and subsequently to determine its height and gives an interesting account of the uncertainties in such operations. The chief of these is the position of the datum level surface or geoid under the mountain. There seems no doubt that Everest, for which Dr. Hunter gives a height of 29,080 ft., is the highest mountain in the world, but there is some doubt whether K_2 (Mount Godwin-Austen 28,253 ft.) or Kanchenjunga (28,225 ft.) is the second.

Mr. Tillotson gives a general review of the structure of the outer parts of the earth. He discusses the information obtained from earthquakes, volcanos, gravity measurements, and determinations of heat flow, and relates it to the processes of mountain building described by geologists. E. C. B.

[*The Editors do not hold themselves responsible for the views expressed by their correspondents.*]